

*406-425
H-34
11/17/94*

**NASA
Technical
Paper
3487**

December 1994

Influence of Turbulence Parameters, Reynolds Number, and Body Shape on Stagnation-Region Heat Transfer

G. James Van Fossen,
Robert J. Simoneau,
and Chan Y. Ching

(NASA-TP-3487) INFLUENCE OF
TURBULENCE PARAMETERS, REYNOLDS
NUMBER, AND BODY SHAPE ON
STAGNATION-REGION HEAT TRANSFER
(NASA. Lewis Research Center) 48 p

N95-28719

Unclassified



National Aeronautics and
Space Administration

H1/34 0051747



**NASA
Technical
Paper
3487**

1994

**Influence of Turbulence Parameters, Reynolds
Number, and Body Shape on Stagnation-
Region Heat Transfer**

G. James Van Fossen and Robert J. Simoneau
*Lewis Research Center
Cleveland, Ohio*

Chan Y. Ching
*Syracuse University
Syracuse, New York*



National Aeronautics and
Space Administration
Office of Management
Scientific and Technical
Information Program
1994

Trade names or manufacturers' names are used in this report for identification only.
This usage does not constitute an official endorsement, either expressed or implied,
by the National Aeronautics and Space Administration.

Influence of Turbulence Parameters, Reynolds Number, and Body Shape on Stagnation-Region Heat Transfer

G. James Van Fossen and Robert J. Simoneau
National Aeronautics and Space Administration
Lewis Research Center
Cleveland, Ohio 44135

and

Chan Y. Ching
Syracuse University
Syracuse, New York

Summary

The purpose of the present work was threefold: (1) to determine if a free-stream turbulence length scale existed that would cause the greatest augmentation in stagnation-region heat transfer over laminar levels; (2) to investigate the effect of velocity gradient on stagnation-region heat transfer augmentation by free-stream turbulence; and (3) to develop a prediction tool for stagnation heat transfer in the presence of free-stream turbulence. Heat transfer was measured in the stagnation region of four models with elliptical leading edges that had ratios of major to minor axes of 1:1, 1.5:1, 2.25:1, and 3:1. Five turbulence-generating grids were fabricated; four were square mesh, biplane grids made from square bars. The fifth grid was an array of fine parallel wires that were perpendicular to the model spanwise direction.

Heat transfer data were taken at Reynolds numbers ranging from 37 000 to 228 000. Turbulence intensities were in the range of 1.1 to 15.9 percent while the ratio of integral length scale to leading-edge diameter ranged from 0.05 to 0.30. Stagnation-point velocity gradient was varied by nearly 50 percent.

Stagnation-region heat transfer augmentation was found to increase with decreasing length scale but no optimum length scale was found. Heat transfer augmentation due to turbulence was found to be unaffected by the velocity gradient near the leading edge. A correlation was developed that fit heat transfer data for the square-bar grids to within ± 4 percent.

Introduction

Heat transfer to a stagnation region is important in many engineering applications; none, however, is more critical than in the gas turbine where combustor exit temperatures often exceed the melting point of superalloy turbine airfoil materials. In most cases the highest heat transfer rate on a turbine

airfoil occurs at the stagnation point, which makes it critical for the design of cooling schemes to obtain an accurate prediction of heat transfer in this region.

For a laminar free stream, the stagnation region can be modeled as a circular or elliptical cylinder in crossflow and the heat transfer can be found if the pressure distribution is known (ref. 1). Free-stream turbulence can augment stagnation-region heat transfer; enhancement of 190 percent over laminar values has been measured (ref. 2). In a gas turbine the stream of combustion products that approaches an airfoil is not laminar; turbulence intensities of 11 and 15 percent were measured at the exit of combustors by Zimmerman (ref. 3) and Goebel et al., (ref. 4) respectively.

Stagnation-region heat transfer augmentation in the presence of free-stream turbulence is believed to be caused by vorticity amplification (see ref. 5 for a review). Free-stream turbulence can be viewed as a continuum of tangled, vortical filaments. As illustrated in figure 1, those filaments with components normal to the stagnation line and normal to the free-stream flow are convected into the stagnation region where they are stretched and tilted by the divergence of streamlines and acceleration around the bluff body. This stretching causes the vorticity to be intensified through conservation of angular momentum. Prior experimental and numerical results (refs. 6 to 8) show that vorticity in the stagnation region causes heat transfer to be increased while the boundary layer remains laminar.

Turbulent eddies that are very large relative to the size of the bluff body are not stretched and, thus, act only as mean flow variations, but eddies that are very small (approaching Kolmogorov scales) are destroyed by viscous dissipation before they can interact with the boundary layer. This leads to the hypothesis that somewhere between these two extremes there must be an optimum eddy size that causes the highest heat transfer augmentation.

By considering vorticity amplification theory, it seems reasonable that leading-edge velocity gradient would have an effect on stagnation heat transfer. Higher velocity gradients

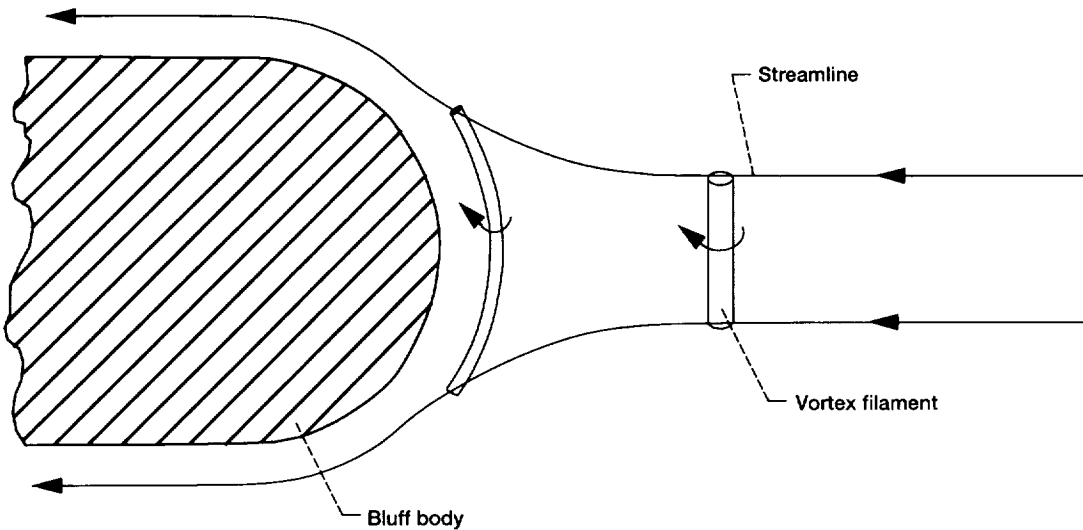


Figure 1.—Vortex filaments stretched and tilted by divergence of streamlines and acceleration around leading edge.

would cause more rapid stretching of the vertical filaments as they are convected past the leading edge thus causing higher heat transfer augmentation.

Three goals of this research were: (1) to determine if an optimum eddy size exists, (2) to study the effect of leading-edge velocity gradient on stagnation-region heat transfer augmentation, and (3) to develop a more accurate prediction tool that could be used by designers to evaluate stagnation-region heat transfer.

It has been known for many years that free-stream turbulence can augment stagnation-region heat transfer (refs. 9 and 10); however, results of experiments are inconsistent and attempts to correlate heat transfer augmentation as a function of turbulence intensity and Reynolds number, while ignoring the length scale (refs. 11 to 15), have not been entirely successful. Any resulting correlations usually predict the experimenter's data but not data from other researchers.

Although Lowery and Vachon (ref. 16) measured lateral length scale in their study of the effect of grid-generated turbulence on stagnation-region heat transfer, they did not have a sufficient variety of grids to deduce an effect of scale. Their resulting correlation, based on intensity and Reynolds number only, has been used as a standard against which subsequent data sets have been compared, sometimes with large discrepancies (see, for example, ref. 17).

There have been several attempts to isolate the effect of turbulence length scale; Yardi and Sukhatme (ref. 18) used four different grids to generate a range of length scales. The four grids were all of different geometry; specifically, two were screens and two were biplane grids, all had different rod-spacing-to-rod-diameter ratios. They showed a trend of increasing heat transfer with decreasing length scale; however, there is so much scatter in the data that their claim of

ten boundary layer thicknesses for an optimum length scale is questionable.

Dyban et al., (ref. 19) used perforated plates as well as a fully developed, turbulent pipe flow to investigate the effect of intensity and scale on stagnation-region heat transfer. Their results showed increasing augmentation with decreasing scale but they did not attempt to correlate the data based on this finding.

More recently, Ames (ref. 20) used simulated combustor segments to generate turbulence and measure its effect on heat transfer to a flat plate and to a stagnation region. Ames concentrated on relatively large scale turbulence where the ratio of the length scale to the leading-edge diameter was greater than 1.0. He used the rapid distortion theory of Hunt (ref. 21) and the measurements of Hunt and Graham (ref. 22) near a plane surface to develop a model for the spectrum of turbulence near stagnation. He integrated his model spectrum to estimate the eddy viscosity in the stagnation region. The viscosity was then used in a phenomenological model, similar to the procedure used by Smith and Kuethe (ref. 13), to develop a new correlating parameter involving Reynolds number, turbulence intensity, and what Ames calls an energy scale (the average size of the energy-containing eddies). Ames used cylinders with three different diameters to investigate stagnation-region heat transfer; his data were correlated well using his new parameter. The data of several other researchers (refs. 16 and 19) were also correlated by his parameter but with more scatter.

For the present work, four models with elliptical leading edges were fabricated with heat transfer gages in the stagnation region. The models had major-to-minor axis ratios of 1:1 (circular), 1.5:1, 2.25:1 and 3:1; all models had the same radius of curvature at the stagnation point. The models were

qualified in a low-turbulence wind tunnel by comparing measurements with a numerical solution for stagnation-region heat transfer as well as with Frössling's solution (ref. 1). Five turbulence-generating grids were fabricated. Four were square-mesh, biplane grids made from square bars with different bar widths; each of the four had identical mesh-to-bar width ratio. The fifth grid was an array of fine, parallel wires that were perpendicular to the model spanwise direction.

Turbulence intensity and integral length scale were measured as a function of distance from the grids with the model removed. Stagnation-region heat transfer was measured with each grid at various distances upstream of the model. Data were taken at Reynolds numbers based on leading-edge diameter ranging from 37 000 to 228 000. Turbulence intensities were in the range of 1.1 to 15.9 percent while the ratio of integral length scale to cylinder diameter ranged from 0.05 to 0.30. Stagnation-point velocity gradient was varied by nearly 50 percent.

Measurements of length scale and intensity are presented herein as well as the stagnation-region heat transfer results from all four models. A correlation involving the turbulence parameters and Reynolds numbers that fit the heat transfer data for the square-bar grids to within ± 4 percent is also presented. The data of other researchers is compared with the correlation. A method for determining the heat transfer distribution downstream of the stagnation point will be presented. It will also be shown that leading-edge heat transfer augmentation by free-stream turbulence is unaffected by stagnation-point velocity gradient.

Symbols

A	surface area of gauge, m^2	M	mesh spacing of bars in turbulence grid, cm
a_e	major axis of ellipse	Pr	Prandtl number
B	tunnel blockage, ratio of model thickness to tunnel height	q	heat flow, W
b	bar width of turbulence-generating grid, cm	R	leading edge radius, cm
b_e	minor axis of ellipse	Re	Reynolds number
d	diameter of model leading edge ($=2R$), cm	$R(\tau)$	autocorrelation of velocity signal
E	mean hot wire voltage, V	$r(s)$	local recovery factor
e	fluctuating output voltage from linearizer, V	s	surface distance from stagnation, cm
$Fr(s/R)$	Frössling number	T	temperature, K
G1 to G5	grid label	Tu	turbulence intensity
k	thermal conductivity of air, $\text{W}/\text{m}\cdot\text{K}$	U	mean velocity, m/sec
		U_e	effective cooling velocity, m/sec
		U_0	magnitude of velocity, m/sec
		u'	fluctuating velocity component in streamwise direction
		v'	fluctuating velocity component in spanwise direction
		W	tunnel width, cm
		x	streamwise distance, cm
		y	spanwise distance from centerline of tunnel, cm
		α	angle between U_0 and hotwire
		δ	measurement uncertainty
		κ	constant in Champagne's law, equation (1)
		λ	microscale, cm
		Λ	integral length scale of turbulence, cm
		ρ	air density, Kgm/m^3
		σ	standard deviation
		τ	time shift, sec
		Φ	heat transfer augmentation factor, equation (13)

Subscripts

<i>avg</i>	average
<i>b</i>	bar width
<i>caljet</i>	hot wire calibration jet
<i>d</i>	leading edge diameter
<i>EI</i>	electrical heating
<i>gap</i>	epoxy filled gap between gauges
<i>lam</i>	laminar
<i>r</i>	recovery
<i>rad</i>	radiation
<i>st</i>	static
<i>t</i>	total
<i>tu</i>	turbulence intensity
<i>w</i>	wall

<i>x</i>	streamwise
<i>y</i>	spanwise (parallel to model leading edge)
∞	free stream

Test Facility, Instrumentation, and Data Acquisition

Wind Tunnel

The experiments were carried out in the wind tunnel shown in figure 2, which is described in detail in an earlier report by Van Fossen and Simoneau (ref. 7). Air drawn from the test cell passed through a flow-conditioning section that consisted of identical damping screens up- and downstream of soda-straw flow straighteners. The screens were 18-mesh with 0.24-mm diameter wires and had 68.7 percent open area. The soda straws were 0.64-cm in diameter and 19.7 cm long. Air then passed through a 4.85:1 contraction before entering the 15.2-cm wide by 68.6-cm high test section. The maximum velocity attainable was about 46 m/sec. Clear tunnel turbulence levels were less than 0.5 percent for all flow rates. After leaving the test section, the flow passed through a transition section into a 10-in. pipe in which a sharp-edged, flow-measuring orifice plate with flange taps was located. Air

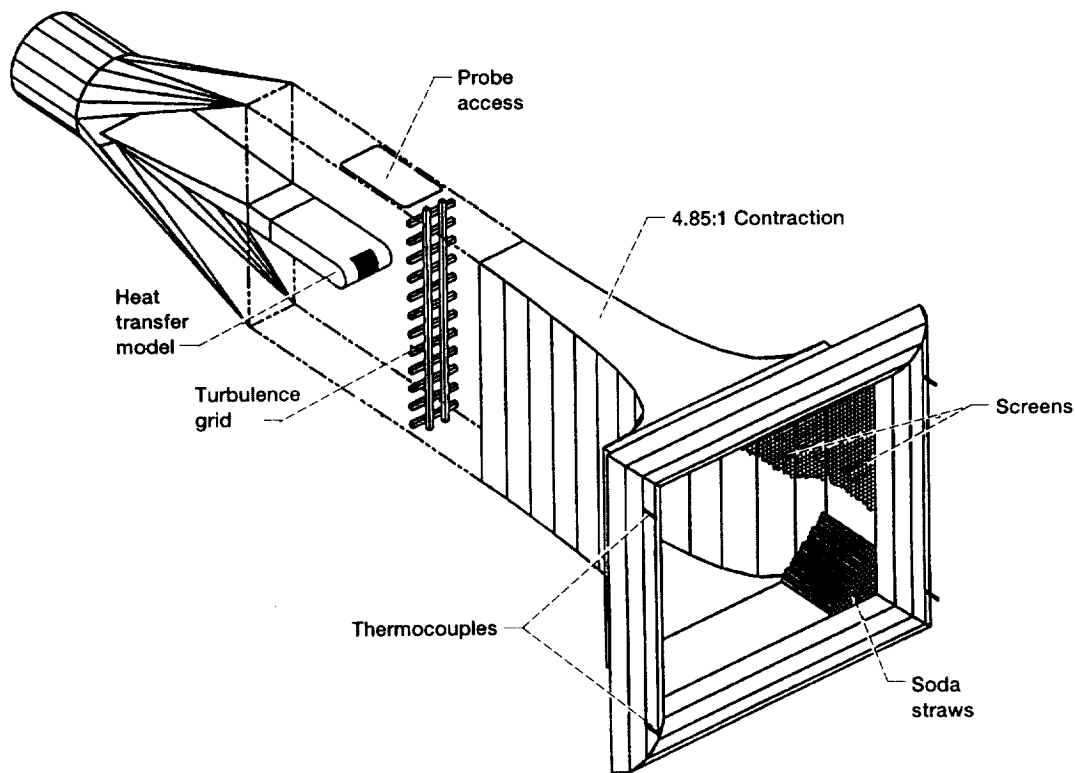


Figure 2.—Wind tunnel.

next passed through a butterfly valve which was used to control the tunnel flow rate, and then to the laboratory exhaust system. The readings from four type E thermocouples located around the perimeter of the inlet were averaged to obtain the stagnation temperature. An actuator system with four degrees of freedom was used to position a hot-wire probe at any desired x-y location within the rectangle shown in figure 2.

Turbulence Grids

Five turbulence-generating grids were used in this study. Four were square bar, square mesh, biplane grids. The fifth grid consisted of an array of parallel wires oriented perpendicular to the streamwise and spanwise directions. Grid parameters are defined in figure 3 and dimensions of the grids are given in table I. Henceforth grids will be referred to by the labels given

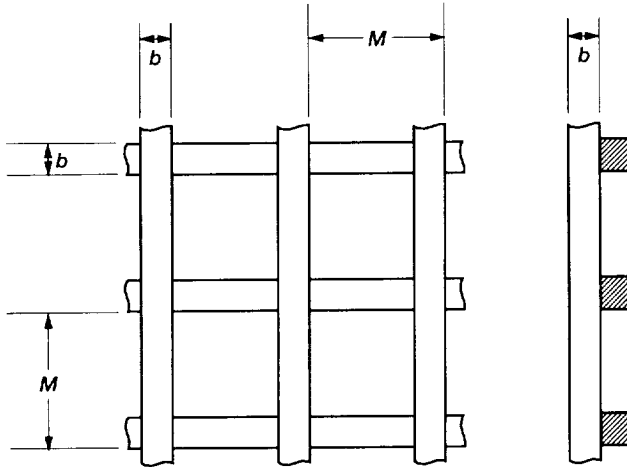


Figure 3.—Biplane grid configuration.

in this table. Grids G1 to G4 were fabricated keeping the ratio of mesh spacing to bar width constant at 4.5 yielding an open area of 60.5 percent. Grid G5 consisted of 0.51 mm wires spaced 6.35 mm apart. Turbulence-generating grids could be installed at axial locations ranging from 2.41 to 52.3 cm upstream of the model stagnation point.

Heat Transfer Models

The four heat transfer models used in this study had elliptical leading edges. The ratio of major to minor axes, a_e/b_e , were 1:1, 1.5:1, 2.25:1 and 3:1. All models had the same radius of curvature R of 3.30 cm at the stagnation point. A comparison of the model profiles and the tunnel walls is shown in figure 4(a), along with an enlarged cross-sectional view (fig. 4(b)). All models had wedge-shaped afterbodies that extended about 61 cm downstream to eliminate vortex shedding. Figure 5 is a photograph of the heat transfer models and afterbodies. The purpose of the 4 models was to provide different velocity gradients in the stagnation region to determine if this would have an effect on stagnation heat transfer augmentation. Leading-edge velocity gradients calculated with an inviscid two-dimensional panel code (ref. 23) are shown in figure 6; the calculation included the tunnel sidewalls.

The circular leading-edge model had 19 heat flux gauges and the elliptical models all had 29 heat flux gauges embedded symmetrically about the stagnation line. The dimensionless surface distance to the center of each gauge from the stagnation line is given in table II. A typical model cross section showing the heat flux gauge arrangement is shown in figure 4(b). Each heat flux gauge consisted of an aluminum strip, which was 6.60 cm long (43 percent of the model span) by 0.476 cm wide and 0.32 cm deep. A Kapton®-encapsulated, foil, electric

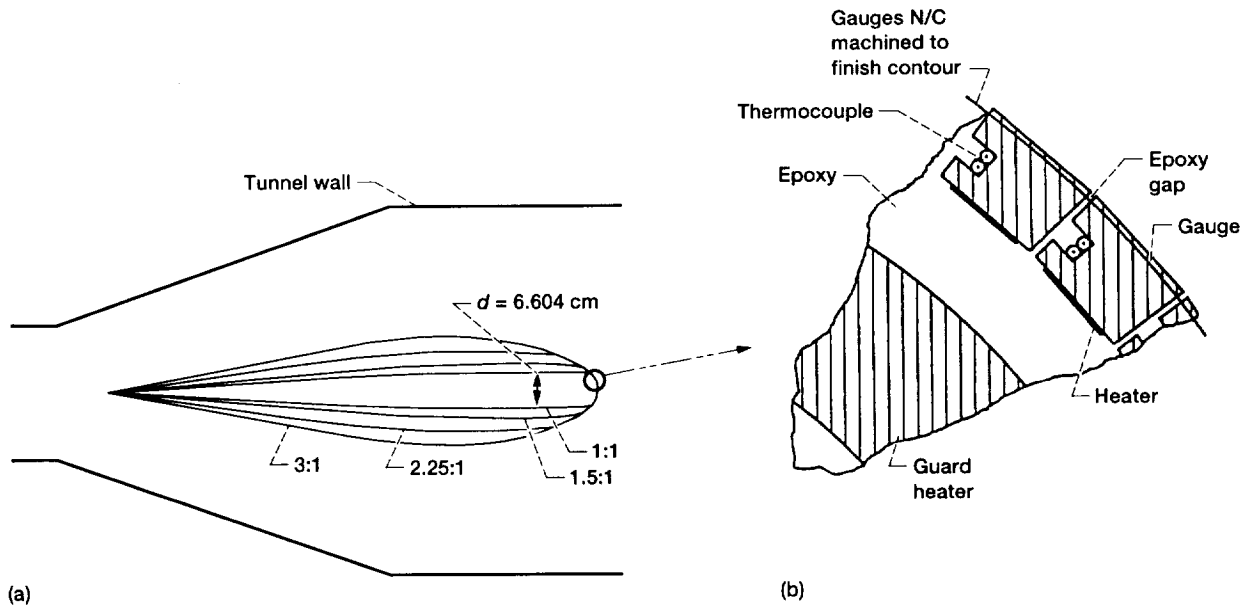


Figure 4.—Comparison of model profiles.

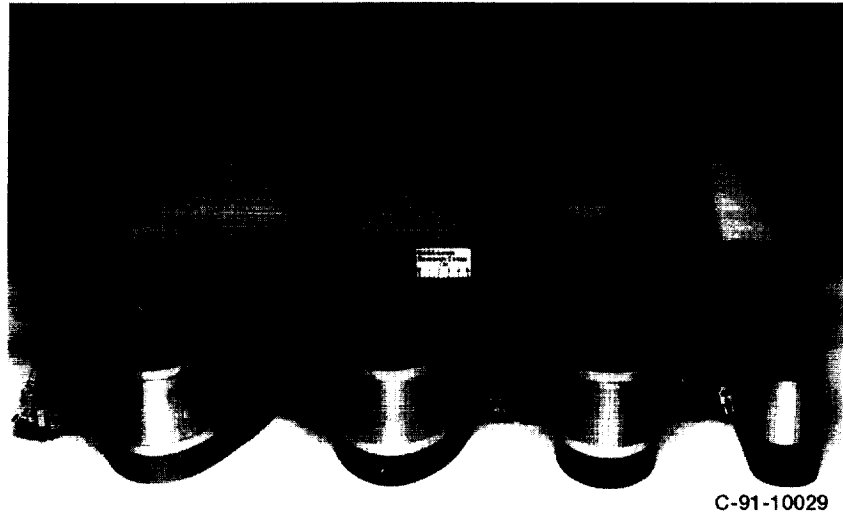


Figure 5.—Stagnation heat transfer models.

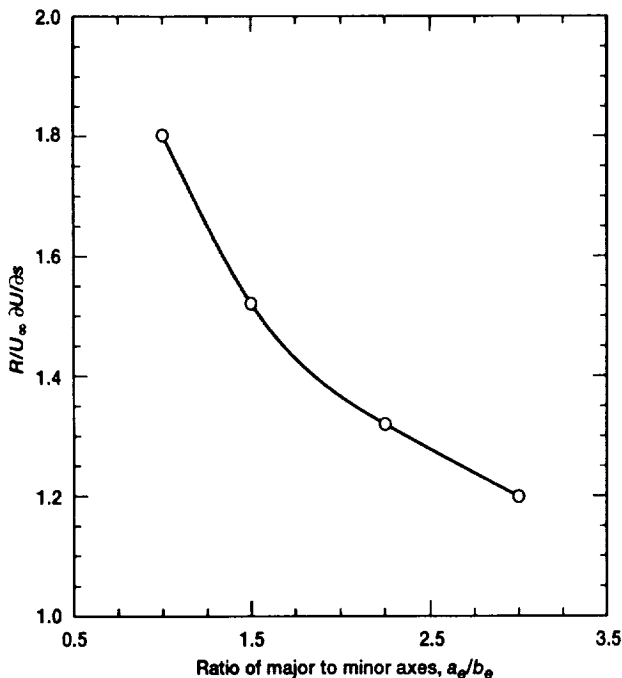


Figure 6.—Leading edge velocity gradients (calculated from panel code (ref. 23)).

heater was fastened to the back of each aluminum strip with pressure-sensitive adhesive. The temperature of each gauge was measured by a type K thermocouple embedded in a groove. The furthest downstream gauges on either side of the stagnation point were used as guard heaters to minimize heat conduction losses in the streamwise direction. A guard heater behind the heat flux gauges prevented heat conduction to the interior of the model. The average gap between the aluminum strips was 0.25 mm and was filled with epoxy. The aluminum strips were maintained at a constant temperature by a specially designed control circuit, (ref. 24). Steady state, spanwise-averaged, heat

transfer coefficients were calculated for each aluminum strip based on the electric power supplied to the strip and the wall-to-fluid temperature difference.

Hot Wire

Turbulence measurements were obtained using a two-channel, constant-temperature, linearized, hot-wire anemometer system. Turbulence intensities and autocorrelations were measured using a standard, 5 μm , single, hot wire oriented perpendicular to the flow direction. A cross-flow type X-wire probe was used for two component measurements. The hot-wire signals were linearized with analog linearizers. A signal conditioner was used for addition and subtraction of the linearized signals from the X-wire. For the single-wire data, a programmable digital multimeter was used to calculate the root mean square (rms) of the fluctuating component of the linearized bridge voltage from 100 samples. For the X-wire data, the mean square voltage was read from an integrating, analog, true rms meter with an adjustable time constant. Mean voltages were read on an integrating digital voltmeter with an adjustable time constant.

Data Acquisition

A dual-channel, Fast Fourier Transform, spectrum analyzer was used to obtain the autocorrelation data. The analyzer featured a 12-bit analog-to-digital conversion rate of 2.56 times the selected frequency and an anti-aliasing filter with a rolloff of 120 dB/octave. The selectable frequency range was from 10 Hz to 100 kHz. The analyzer could collect and digitize analog, time domain data, convert to the autocorrelation function, and average a programmable number of autocorrelations together in real time. A personal computer was interfaced to the spectrum analyzer for data storage and processing.

Steady-state operating conditions (temperatures, pressures, and gauge voltages and currents, etc.) were recorded on the laboratory data acquisition system called ESCORT (ref. 25). For every heat transfer data point, 20 readings of each data channel were recorded. These 20 readings were averaged to give a single value for each channel. To eliminate any offset between data channels caused by the solid-state multiplexers, before each day's run all the inputs to ESCORT were shorted and a zero reading was obtained. This zero reading was subtracted from each subsequent data reading.

Experimental Procedure

Hot-Wire Calibration

The hot wires used for the turbulence measurements were calibrated in an air jet at nearly the same temperature as the wind tunnel flow. Velocity calibrations were made with a two-point, iteration method in conjunction with the signal linearizers (ref. 26). The frequency response of the hot-wire anemometer system was estimated to be around 30 kHz with the standard square wave test.

A cross-flow type X-wire for the two-component turbulence measurements was calibrated, assuming that Champagne's cooling law (ref. 27) applied

$$U_e^2(\alpha) = U_0^2 \left(\cos^2 \alpha + \kappa^2 \sin^2 \alpha \right) \quad (1)$$

This relates the effective cooling velocity U_e to the actual velocity U_0 where α is the angle between U_0 and the wire, and κ is a correction factor to account for the cooling due to the tangential velocity component along the wire. The value of κ was determined experimentally by varying the angle α between 35 and 55° at jet velocities of 23 and 46 m/sec. A least-squares curve fit of equation (1) was then used to find κ . As a further check on the value of κ at the orientation used in the tests, the wire was held fixed at 45° to the flow and the effective cooling velocity recorded at velocities from 9 to 46 m/sec in steps of 4.6 m/sec. Once again, a least-squares fit was used to evaluate κ . The difference between the κ values from the two methods was around 7 percent. The actual value of κ used in the data reduction was the average from the two methods.

Prior to each use of the X-wire, the probe was installed in the calibration jet with the bisector of the angle between the wires aligned with the flow direction. Each of the wires was then linearized using the method described above for the single wire. In the wind tunnel, the X-wire was rotated until the mean voltages from both wires showed the same value, which indicated the probe was aligned with the mean flow direction.

Thermal Conductivity of Epoxy

The thermal conductivity of the epoxy used in the gaps between the aluminum heat flux gauges, which was required for data reduction, was determined experimentally. A uniform layer of epoxy 0.318 cm thick was deposited between two 6.4-cm square copper plates. An electric heater was adhesively bonded to one plate while a water cooling line was brazed to the opposite plate. Thermocouples were attached to both copper plates and the whole unit was enclosed in a vacuum chamber, which eliminated convective heat loss.

The power level to the electric heater was fixed and the unit was allowed to come to equilibrium; the voltage, current, and copper plate temperatures were then recorded. Several such runs were made at different power levels. An energy balance equated the electric power input to the sum of the heat conducted through the epoxy layer and the heat radiated from the heated plate. Gray body radiation to black surroundings was assumed. Two unknowns, the thermal conductivity of the epoxy layer and the emissivity of the copper, were simultaneously solved for by using a least-squares technique. Values obtained for emissivity and thermal conductivity were 0.83 and 0.16 W/m-K respectively.

Heat Flux Measurements

The nominal operating temperatures of the gauges were between 319 and 327 K; the average recovery temperature of the air was 300 K giving wall-to-air temperature ratios of approximately 1.06 to 1.1. All of the heat flux gauges were maintained at the same temperature within ±0.2 °C. This was accomplished by fine-tuning the gain on the thermocouple voltage amplifier in the control circuit, which in turn changed the power supplied to the gauge.

Heat flux measurements were carried out with each grid at several streamwise distances from the stagnation line of the leading edge. For each grid position, heat transfer data was acquired for at least three Reynolds numbers ranging from 37 000 to 228 000.

Data Reduction and Uncertainty Analysis

Turbulence

Intensity.—Turbulence intensities were calculated from the single hot wire and the X-wire. The local turbulence intensity for the single wire was calculated as the ratio of the rms to mean linearized voltage.

Two component turbulence intensities were calculated from the linearized signals of the X-wire. By neglecting terms to the second order in turbulence and to the third order in κ , for linearized, constant temperature operation,

Champagne (ref. 27) obtained:

$$\frac{\overline{u'^2}}{U^2} = \frac{1}{4} \left[\frac{e_1}{E_1} + \frac{e_2}{E_2} \right]^2 \quad (2)$$

$$\frac{\overline{v'^2}}{U^2} = \frac{1}{4} \left[\frac{1+\kappa^2}{1-3\kappa^2+4\kappa^4} \right] \left[\frac{e_1}{E_1} - \frac{e_2}{E_2} \right]^2 \quad (3)$$

If the bisector of the angle between the wires is aligned with the flow, the mean voltages of the two wires E_1 and E_2 are equal and the hot-wire response equations for the above quantities reduce to very simple forms requiring only the addition and subtraction of the fluctuating voltages from wires 1 and 2 (e_1 and e_2) to compute u' and v' .

Integral Length Scale.—The integral length scale describes the average eddy size associated with the turbulence. There are at least three practical ways to obtain the integral length scale:

1. Two single-wire probes are oriented parallel to each other with the wires normal to the flow direction so that one can be traversed in a direction lateral to the flow. The two signals are multiplied together and averaged over time at each lateral separation distance; the resulting cross-correlation function is integrated over separation distances from 0 to ∞ resulting in a lateral length scale Λ_y which for isotropic turbulence is half of the longitudinal scale Λ_x .

2. The power spectrum is obtained from a single-wire probe. The value of the power spectrum at zero frequency is proportional to the longitudinal length scale Λ_x .

3. The autocorrelation is obtained for a single-wire probe. Taylor's hypothesis that time and streamwise distance are related by the mean velocity is invoked; thus, the autocorrelation is equivalent to a longitudinal cross-correlation in space. The integral of the autocorrelation function then gives a time scale which, when multiplied by the mean velocity, is equivalent to the longitudinal length scale Λ_x .

Each of the above methods has its pitfalls. Method 1 is very tedious and time-consuming and also involves calibrating two hot wires and traversing across many points in space. Theoretically, the cross-correlation function should approach zero as the probe separation distance becomes large. However, low frequency noise in the flow causes the cross-correlation function to fluctuate when the two probes are separated by large distances. This makes it difficult to know where to stop integrating and thus introduces error into the lateral length scale (ref. 28).

As pointed out by Comte-Bellot and Corrsin (ref. 29), it is impossible to measure the value of the spectrum at zero frequency even if the instrument is DC-coupled. Typically, the spectrum is extrapolated back to zero frequency by using frequencies above those corresponding to scales that are physi-

cally possible in the rig. This requires judgement and can also lead to error for method 2.

In theory, methods 2 and 3 are equivalent since the autocorrelation is the transform of the power spectrum. The autocorrelation method also suffers from the low-frequency noise problem, that is low-frequency noise keeps the autocorrelation from approaching zero in a consistent manner. Many investigators have used the first zero crossing as the upper limit of integration (refs. 20, 30, and 31). Figure 7 shows a typical pair of autocorrelations taken behind our grid G1; the autocorrelations shown are the result of 400 sequential autocorrelations averaged together to form a single curve. Examination of this figure makes it clear that integrating until the first zero crossing will give very different length scales for these two cases.

The availability of a spectrum analyzer that could compute the autocorrelation and average any number of them together made method 3 the natural choice; however, low-frequency noise was still a problem. Several windowing functions that, when multiplied by the autocorrelation, caused the product to approach zero for large time delays were tried but proved unsatisfactory. It was finally decided to use a least-squares fit of the autocorrelation data by the exponential function

$$R(\tau) = e^{-C_\tau \tau} \quad (4)$$

Data between $0.33 \leq R(\tau) \leq 1.0$ were used for the curve fit; the resulting fit is seen in figure 7. The autocorrelation approaches $\tau = 0$ with a zero slope; therefore, the exponential function does not reproduce the autocorrelation for very small values of τ but the fit is satisfactory over the main

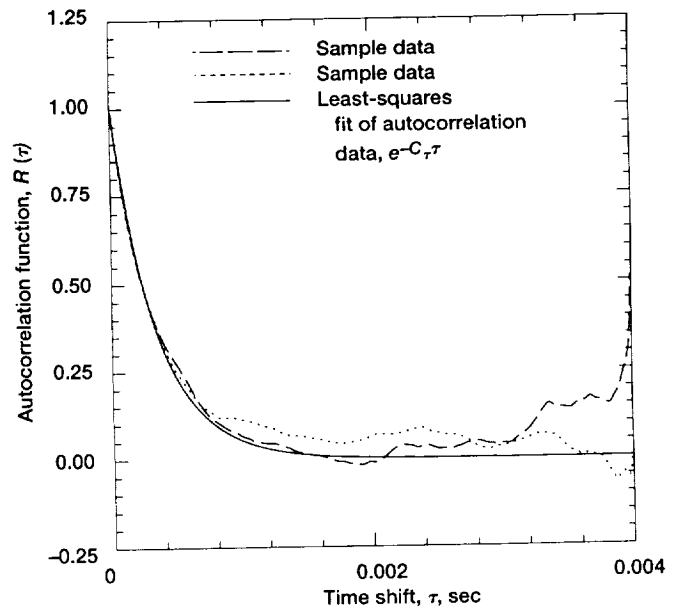


Figure 7.—Typical autocorrelation functions (grid G1, velocity, 43.9 m/sec).

range of interest and the problem of determining the upper limit of integration is solved. By integrating equation (4) between 0 and ∞ , and multiplying by the mean velocity U , the longitudinal length scale then becomes,

$$A_x = U \int_0^\infty R(\tau) d\tau = \frac{U}{C_\tau} \quad (5)$$

If the hot wire is long compared to the length scale of the flow, errors in intensity and scale, caused by averaging of flow variations over the wire length, can result. Correction for the hot-wire length was not made for the present tests; the smallest integral scale measured was 2.6 times the active length of the hot wire.

Heat Transfer

Power from the electric heaters is removed from the aluminum strips by convection to the air, radiation to the surroundings, and conduction to the epoxy gap between the gauges where it is convected to the air. An energy balance was solved for the Frössling number for each gauge as follows:

$$Fr(s/R) = \frac{(q_{EI} - q_{rad} - q_{gap})d}{A(T_w - T_r)k\sqrt{Re_d}} \quad (6)$$

where

q_{EI}	heat added by the heater (voltage \times current)
q_{rad}	heat lost by radiation
q_{gap}	heat conducted away to the epoxy gap and to the unguarded ends of the heaters
d	leading-edge diameter ($=2R$)
A	exposed gauge surface area
T_w	gauge temperature
T_r	recovery temperature at the gauge location
k	thermal conductivity of air
Re_d	Reynolds number

An estimate of the gap loss q_{gap} between the heaters can be obtained from an exact solution for two-dimensional heat conduction in a rectangle that is half of the epoxy-gap-width wide and the aluminum-gauge-depth deep. Two adjacent sides are assumed to be insulated, one side is held at the constant temperature of the aluminum strip and the final side is convecting to the air at a known temperature. The loss from the unguarded ends of the strips can be estimated from the same solution by assuming a large gap. See Van Fossen et. al. (ref. 24) for details of this analysis.

Corrections for radiation heat loss q_{rad} were also made by assuming gray body radiation to black surroundings and emissivity of 0.05 for the aluminum gage. Heat lost through

the sides and ends of the strips was on the order of 10 percent of the total heat flow, while the radiation heat loss was on the order of 0.2 percent.

The recovery temperature was calculated from

$$T_r = T_{st,\infty} + r(s) (T_t - T_{st,\infty}) \quad (7)$$

where $T_{st,\infty}$ is the static temperature upstream of the model. The local recovery factor $r(s)$ was calculated as

$$r(s) = 1 - \left(\frac{\rho U(s)}{(\rho U)_\infty} \right)^2 (1 - \sqrt{Pr}) \quad (8)$$

The local mass flow ratio $rU(s)/(rU)_\infty$ was found from a numerical solution of flow over the model (ref. 32). The analysis included the effect of the tunnel walls. Figure 8 is a comparison of recovery factors obtained by this method with those reported by Eckert and Drake (ref. 33) for a circular cylinder; agreement is quite good.

The thermal conductivity and viscosity of air were evaluated at the free-stream, total temperature from equations given by Hillsenrath et al. (ref. 34). Total temperature was used to evaluate these properties because Rigby and Van Fossen showed in a numerical study (ref. 32) that if they were based on a reference temperature that involved the wall temperature, then reversing the direction of heat flux (cooling the wall) caused an undesirable change in the Frössling number.

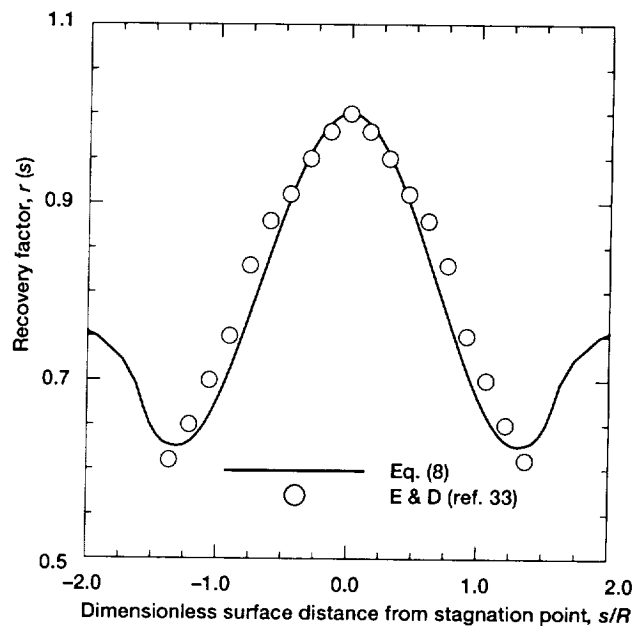


Figure 8.—Comparison of recovery factor calculated from equation (8) with data of Eckert and Drake (ref. 33).

The Reynolds number Re_d was based on the diameter of the leading edge d , and the mass-velocity was averaged between the flow area with maximum model blockage and the unblocked, upstream flow area, that is,

$$(\rho U)_{\text{avg}} = (\rho U)_{\infty} \frac{(2 - B)}{2(1 - B)} \quad (9)$$

where the blockage B is the ratio of maximum model thickness to tunnel height. Blockage ranged from 0.096 for the circular leading edge to 0.293 for the 3:1 ellipse.

Uncertainty Analysis

The method of Kline and McClintock (ref. 35) was used to combine estimates of the bias error of each measuring instrument. Estimates of the precision of each measurement were calculated from 20 samples of each steady-state measurement and combined by the same method. Results of the uncertainty analysis for the Frössling number are presented in table III.

The uncertainty in turbulence intensity and length scale was estimated with the method suggested by Yavuzkurt (ref. 36) and is presented in table IV.

Results and Discussion

Turbulence

Intensity.—Variation of turbulence intensity without the model in the test section is shown versus dimensionless distance downstream of the grid in figure 9. For all five grids, the decay of the intensity was in qualitative agreement with the correlation of Baines and Peterson (ref. 37), which is also shown in figure 9 for reference. Each grid and velocity had slightly different characteristics so intensity data for each case were fit with a power law of the form

$$Tu = a \left(\frac{x}{b} \right)^m \quad (10)$$

Coefficients for each of the fits appear in table V and the curve fit for each case is shown in figure 9. Representative plots of the variation in turbulence intensity in the spanwise direction are shown in figure 10; typically, the variation was around 5 percent.

Isotropy.—Figure 11 shows the ratio $\sqrt{u'^2}/\sqrt{v'^2}$ which is a measure of isotropy for the turbulence; a value of 1.0 would indicate isotropic flow in the x-y plane (the plane of the stagnation stream sheet). Turbulence for the square-bar, square-mesh grids (G3 and G4) seems to be nearly isotropic while that for grid G5 shows highly nonisotropic behavior with $\sqrt{u'^2}/\sqrt{v'^2}$ values ranging from a high of 1.42 down to

0.95 depending on Reynolds number and distance from the grid. In general, the turbulence from grid G5 is more anisotropic at lower flow rates and moves toward isotropy as distance from the grid increases.

The X-wire results for the streamwise turbulence component were in close agreement with those obtained using the single hot wire. For example, values of the turbulence intensity with grid G3 calculated from the single hot wire and the X-wire are within 8 percent at all Reynolds numbers.

Length Scale.—Figure 12 shows the variation of the integral length scale in the streamwise direction behind grids G1 to G5. Increase in the integral length scale with distance from the grid is apparent in all cases. This is expected, since the smaller eddies dissipate faster than the larger ones. Also shown in the figure is a correlation developed by Roach (ref. 38), who relates the growth rate of microscale with distance from the grid. His theory shows microscale variation to be dependent on Reynolds number. Roach states that it is not possible to develop a theory for the variation of integral scale with distance. He therefore assumed that the integral scale should follow the growth of microscale in the downstream direction but, based on empirical evidence, removed the Reynolds number dependence. His correlation has the form

$$\frac{\Lambda_x}{b} = I \left(\frac{x}{b} \right)^{0.5} \quad (11)$$

He determined from his data that $I = 0.2$. The present data tend to follow the square root of distance dependence of Roach's correlation but the constant is an average 35 percent larger and varies from grid to grid. Individual curve fits of the integral scale versus distance from the grid were made for each grid; the results are shown in figure 12 and in table V. These curve fits were used to determine the value of length scale when evaluating the heat transfer dependence on length scale. Note that the integral scales for grids G1 to G4 show no Reynolds number dependence but those of grid G5 are very dependent on Reynolds number.

Naudascher and Farrell (ref. 39) also developed a correlation for both the microscales and integral scales of grid turbulence. Their correlation showed a Reynolds number dependence for the integral scale. The correlation involved the ratio of microscales to integral scale at infinity which was unknown but is bracketed by values of 1.25 and 3.0; with these limiting values, their correlation bracketed the integral scale data of several other authors. The integral scale data for grids G1 to G4 are shown in figure 13 versus the Naudascher and Farrell correlation parameter. Also shown in figure 13 is their correlation with the two bracketing values discussed above. The present length scale data are correlated better by the relation of Roach.

All turbulence measurements were made without the model present. When the model is present downstream of the grid, turbulence is distorted as the stagnation point is

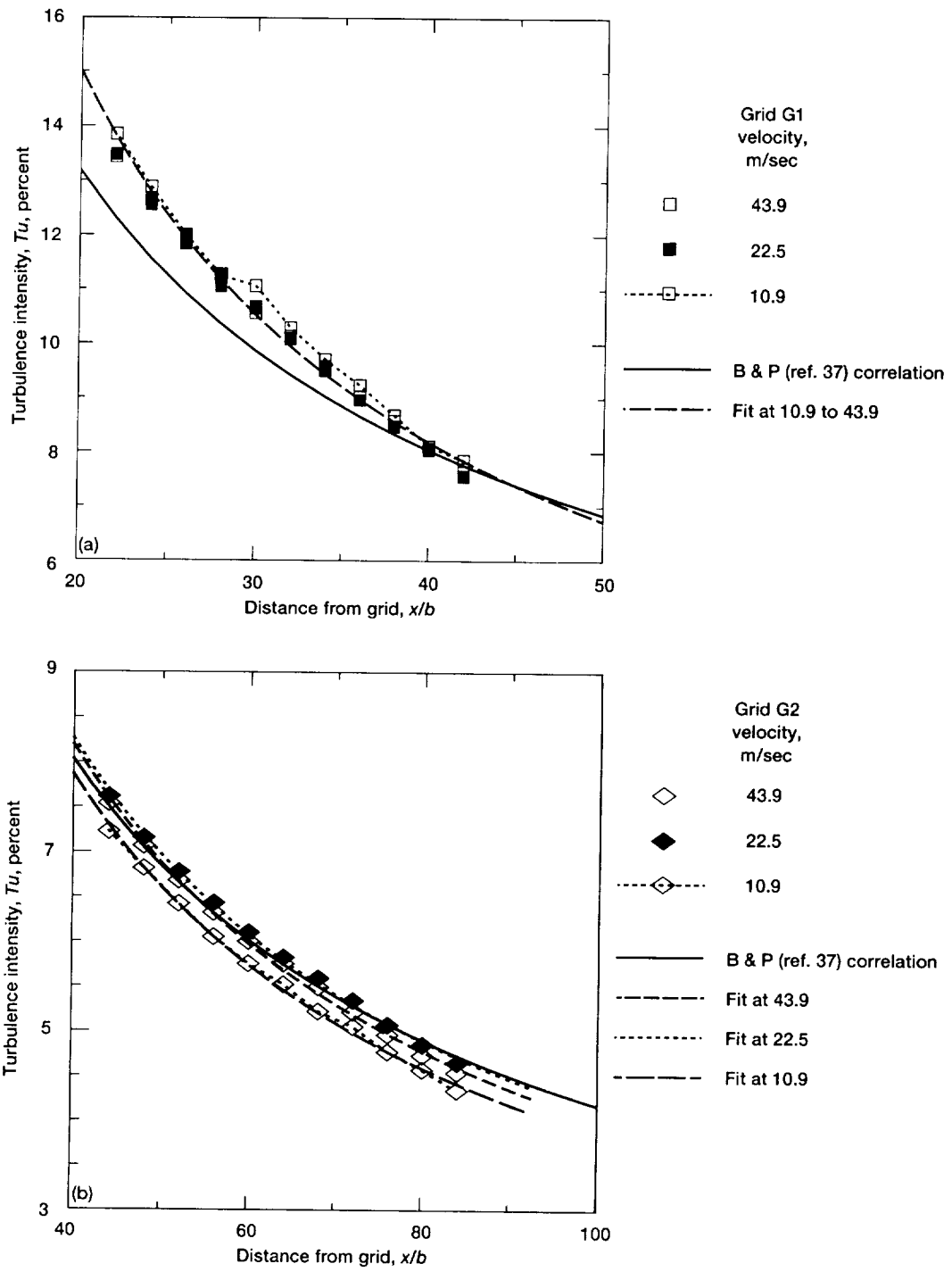


Figure 9.—Turbulence intensity versus dimensionless distance from grid for (a) Grid G1, (b) Grid G2, (c) Grid G3, (d) Grid G4, and (e) Grid G5.

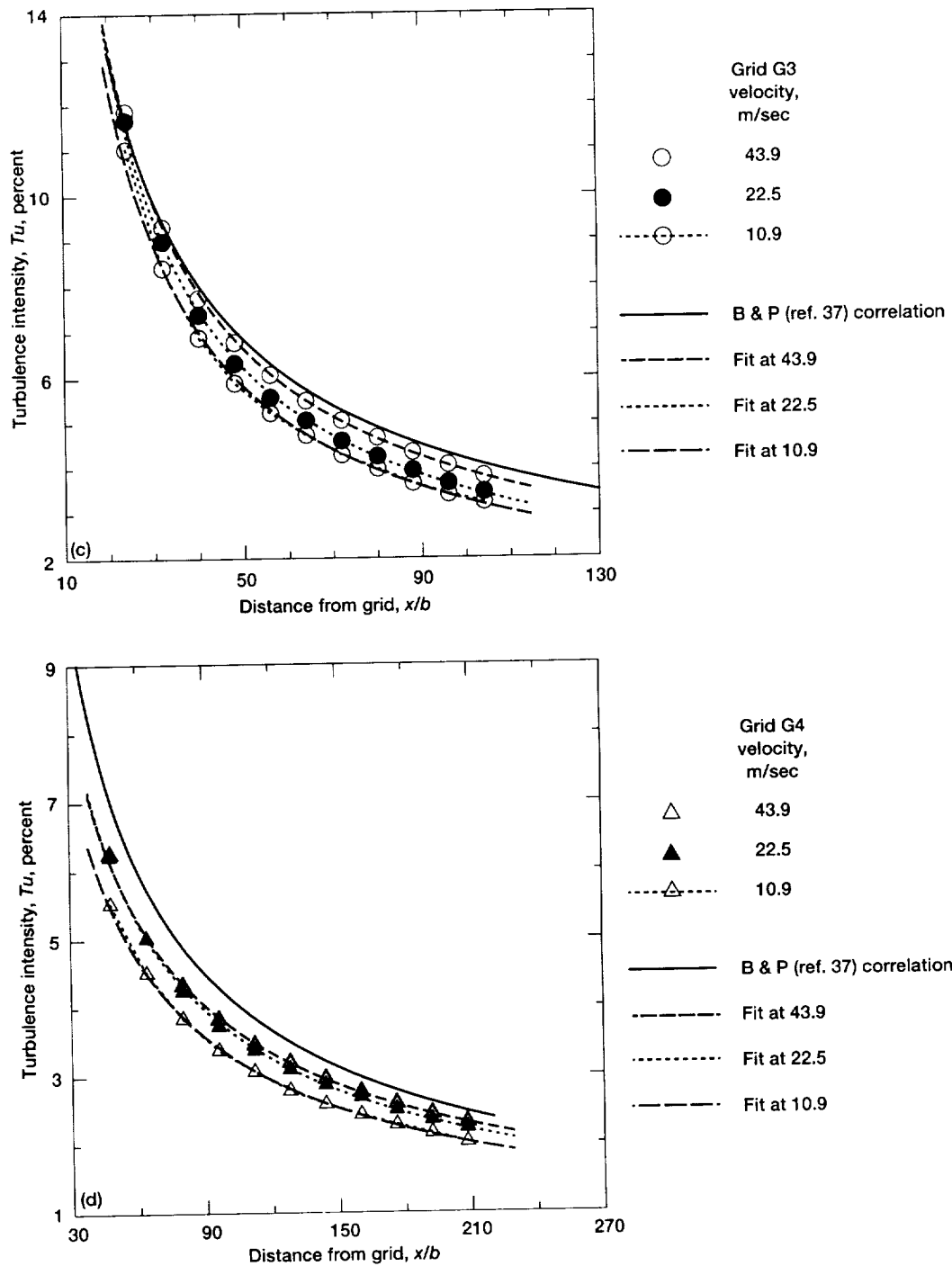


Figure 9.—Continued. (c) Grid G3. (d) Grid G4.

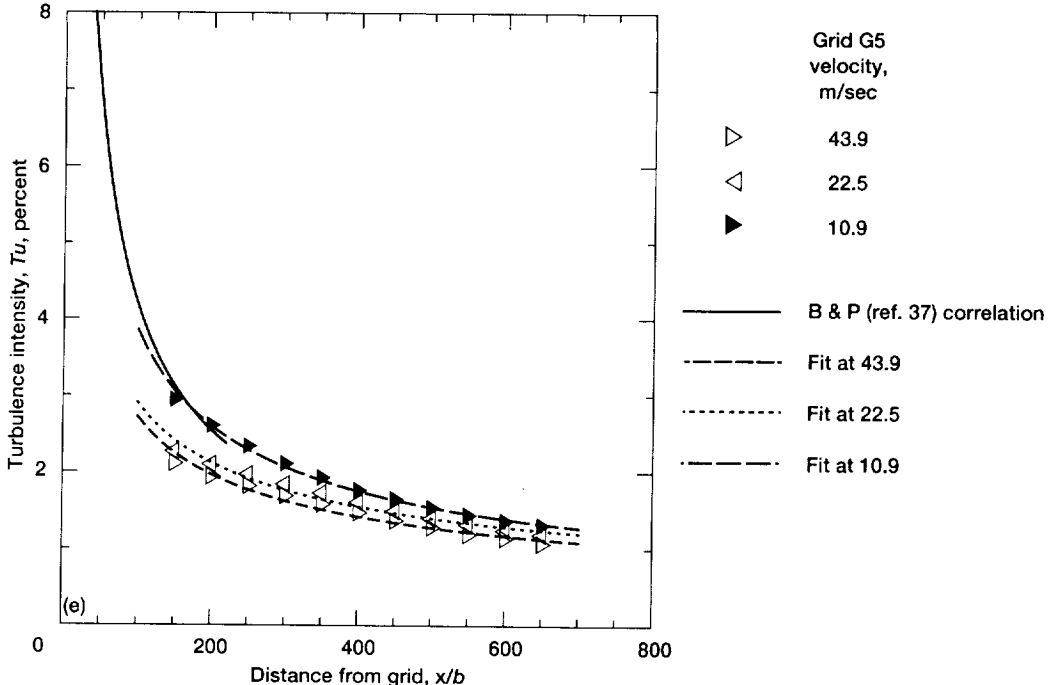


Figure 9.—Concluded. (e) Grid G5.

approached. The fluctuating component of velocity increases and the mean velocity approaches zero (ref. 40) sending intensity levels very high. This brings up the problem of where to evaluate the turbulence intensity and length scale for use in a heat transfer correlation. We felt that tests of most turbulence-producing components, (e.g., combustor) would be conducted without the model present; therefore, turbulence intensity and length scale used in the following correlations were evaluated from the curve fits in table V by using the distance from the grid to the stagnation point of the model. Turbulence intensity varied from 1.1 to 15.9 percent. The ratio of length scale to leading-edge diameter ranged from 0.05 to 0.30.

Heat Transfer

Verification of Experimental Method.—Frössling number data for each of the models is given in tables VI through IX. Data for the circular leading edge model are presented for gauges 2 to 18 and for the elliptical leading edge models for gauges 2 to 28. Gauges 1 and 19 for the circular leading edge model and 1 and 29 for the elliptical models are considered guard heaters. Gauges 10 and 15 are centered on the stagnation line for the circular and elliptical models respectively. Grid designation G0 represents the low turbulence data.

Heat transfer results in the leading-edge region with no turbulence grid in the tunnel are shown in figure 14 for the four

different models. Measured free-stream turbulence intensity in this case was less than 0.5 percent. Frössling number data are presented as a function of surface distance from stagnation that is made dimensionless by the leading edge radius R . In all cases the data agree to within the estimated experimental error with the two-dimensional numerical solution from the PARC code (ref. 32) and with the Frössling solution, which was obtained by using the velocities calculated from the panel code (ref. 23), thus confirming the accuracy of the experimental technique. The worst agreement between the experimental and numerical results is for the 2.25:1 model; experimental results are from 1.4 to 9.2 percent above the numerical results at the stagnation point. The upper limit of discrepancy is above the estimated experimental error. This model seemed to have a mind of its own; on some days the model gave results that agreed quite well with the numerical results and on other days large errors were observed. Possible causes of this error were investigated including model profile, surface irregularities, thermocouple calibration, and clear-tunnel turbulence level. The model was x-rayed to see if the internal guard heater was touching the surface heat flux gauges. No obvious cause could be found; therefore, the data for this model are presented as is.

It is interesting to note past design practice used to estimate leading-edge heat transfer to a turbine airfoil. A circle was inscribed inside the airfoil tangent to the stagnation point with the same radius as the airfoil leading edge. Heat transfer at the stagnation point for laminar flow was

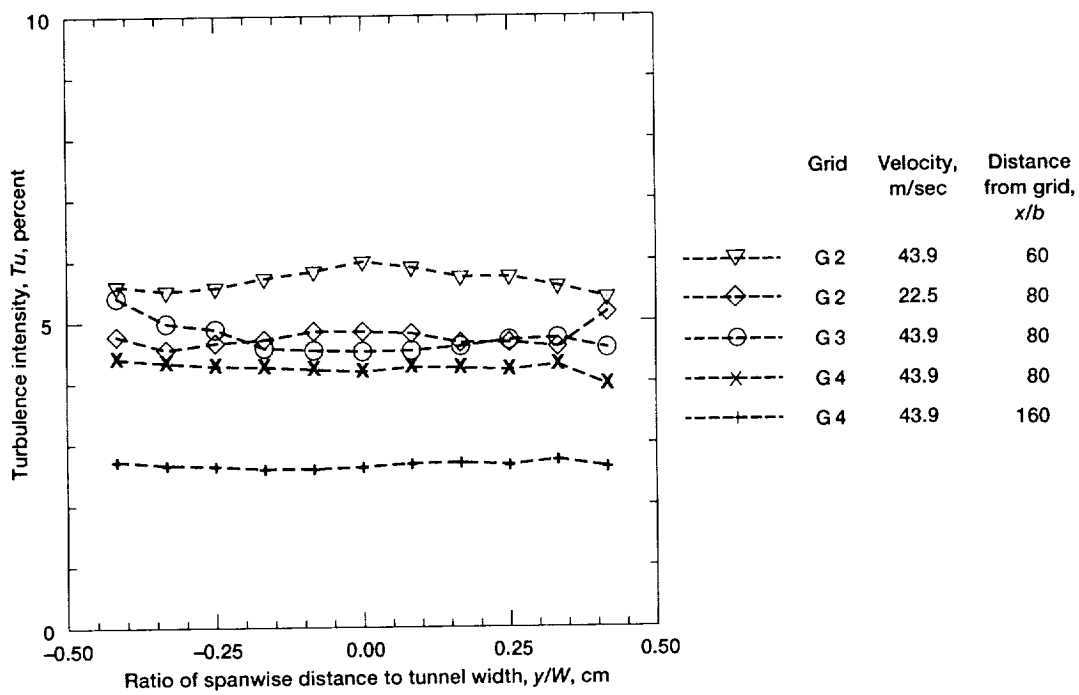


Figure 10.—Variation of turbulence intensity in the spanwise direction.

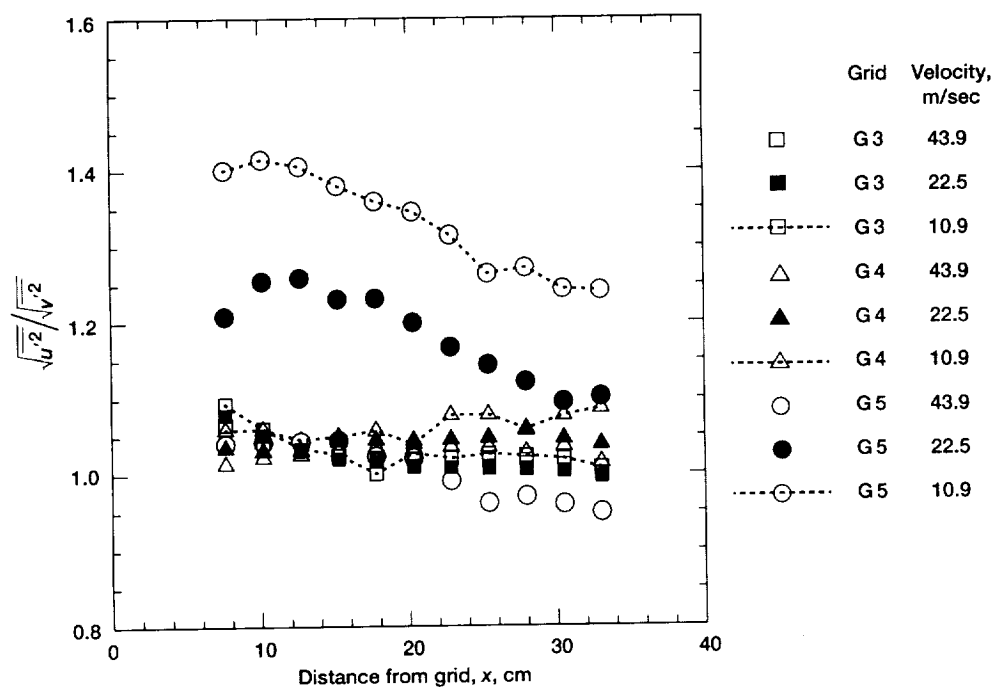


Figure 11.—Isotropy of turbulence from grids G3, G4, and G5.

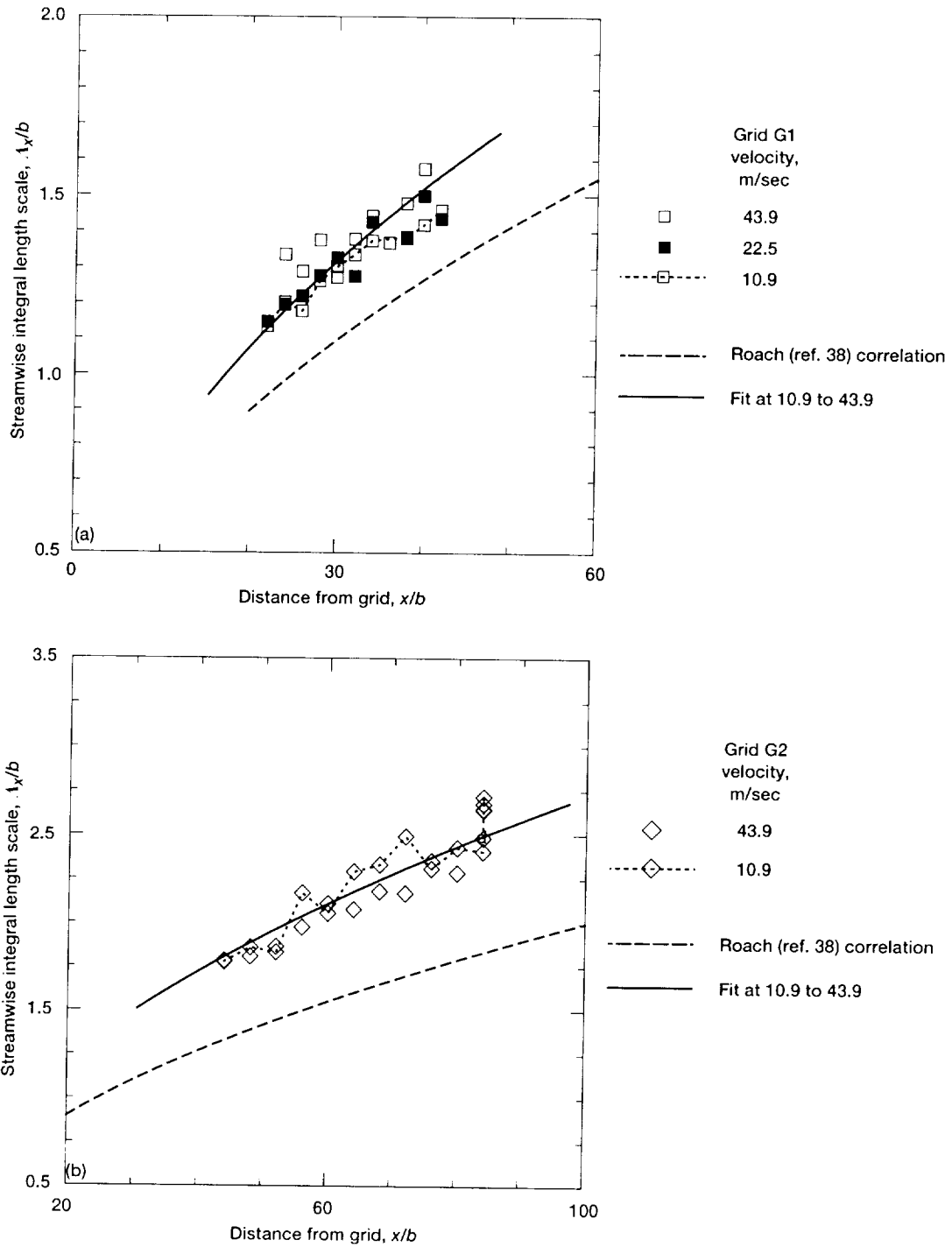


Figure 12.—Longitudinal integral scale versus dimensionless distance from the grid for (a) Grid G1, (b) Grid G2, (c) Grid G3, (d) Grid G4, and (e) Grid G5.

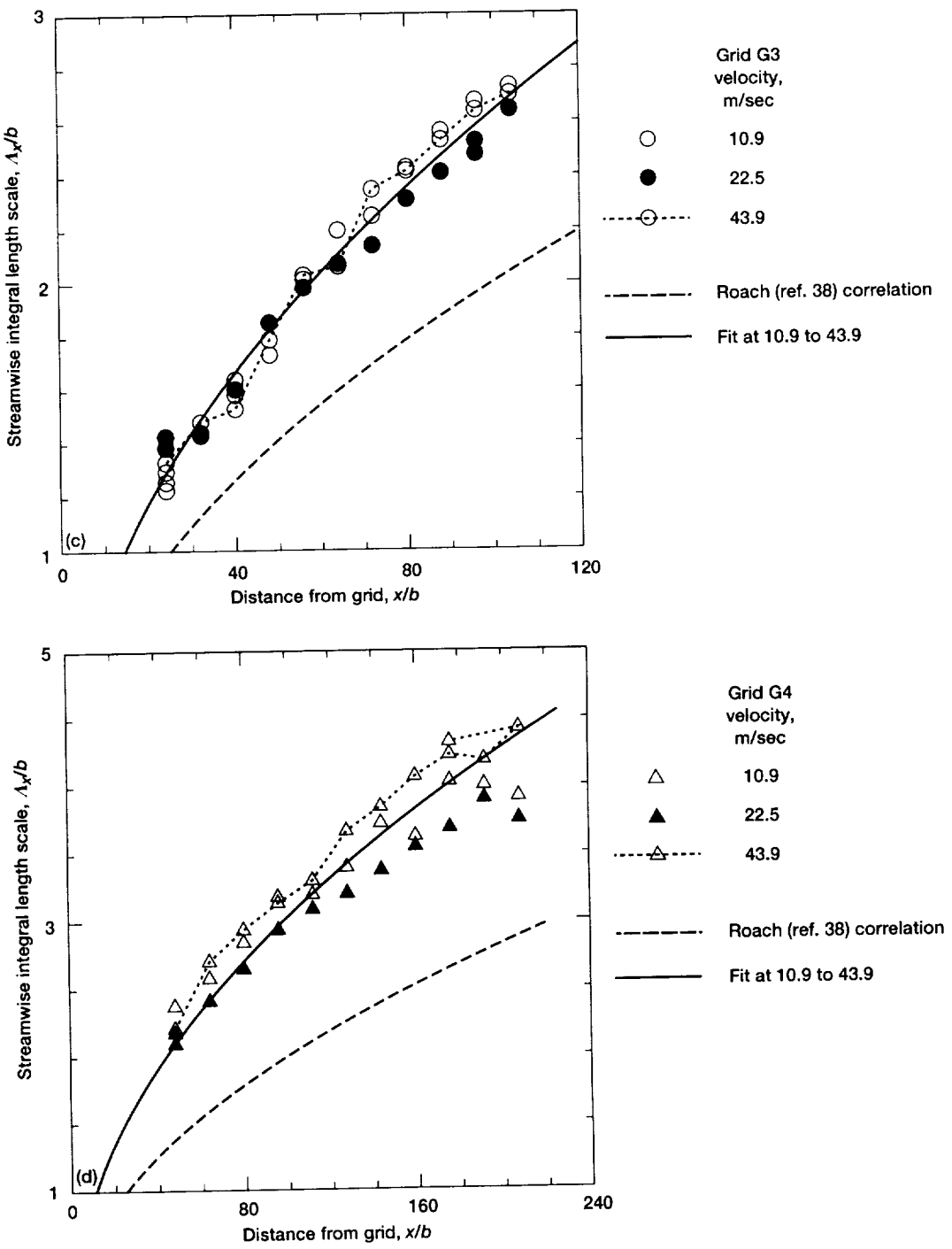


Figure 12.—Continued. (c) Grid G3. (d) Grid G4.

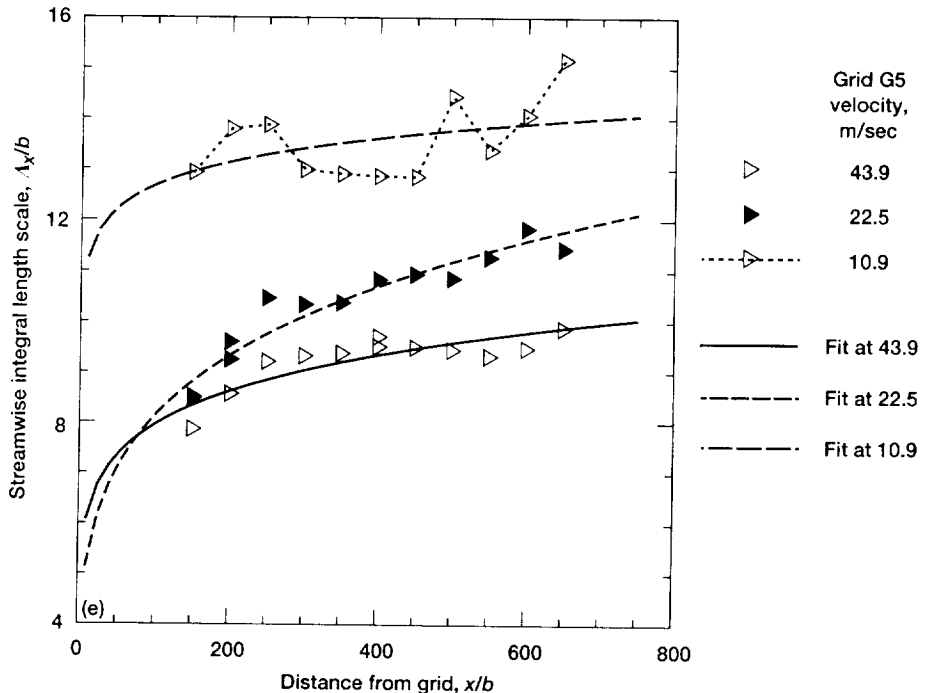


Figure 12.—Concluded. (e) Grid G5.

then calculated from a circular cylinder in cross flow correlation using the diameter of the inscribed circle. Various multipliers were then applied to this result to account for turbulence. All four models have the same radius of curvature at the leading edge but, as seen in figure 14, the stagnation-point heat transfer is different for each model. The conclusion must be that this method only works for a circular cylinder in cross flow; however, an accurate prediction of the laminar leading-edge heat transfer can be obtained from the Frössling solution given the surface velocity distribution or from a numerical solution for laminar flow over the airfoil.

Stagnation Region Augmentation—Circular Leading Edge.—Figure 15 shows the Frössling number at stagnation plotted against the correlating parameter $TuRe_d^{1/2}$ developed by Smith and Kuethe (ref. 13). The range of length scale to leading-edge diameter ratio for each grid is indicated on the legend in the figure. Immediately evident is the fact that the data from the five different grids are not correlated by the parameter $TuRe_d^{1/2}$. The heat-transfer augmentation continues to increase as scale decreases, therefore, for the present data, no optimum length scale was found. Also shown in the figure is the correlation developed by Lowery and Vachon (ref. 16). The Lowery and Vachon correlation predicts the heat transfer data only in a narrow range of scales, and as the parameter $TuRe_d^{1/2}$ increases beyond about 40, the correlation turns downward instead of continuing up as the data indicate.

The stagnation heat transfer data from the model with the circular leading edge behind the square bar grids was fit with the function

$$Fr(0) = 0.008 \sqrt{Tu Re_d^{0.8} \left(\frac{A_x}{d} \right)^{-0.574}} + C \quad (12)$$

The constant C was set to the zero turbulence Frössling number of 0.939, which was calculated from the PARC-2D code. The other constants were determined from a least-square fit of the data. The curve fit and the data are compared in figure 16; the function correlates the data to within ± 4 percent as shown by the bands drawn on either side of the correlation.

Turbulence for grids G1 to G4 was shown to be isotropic; that for grid G5 (the array of parallel wires) was not. The stagnation heat-transfer data for grid G5 are compared to the stagnation-region heat transfer correlation developed for grids G1 to G4 in figure 17. Although the data are correlated by the parameter on the abscissa, it is obvious from this figure that anisotropic turbulence with the majority of its vorticity oriented normal to the free stream, and normal to the axis of the leading edge, causes increased augmentation over isotropic turbulence. The data at high values of the abscissa in figure 17, where agreement with the correlation is the poorest, were taken closest to the wires. As distance from

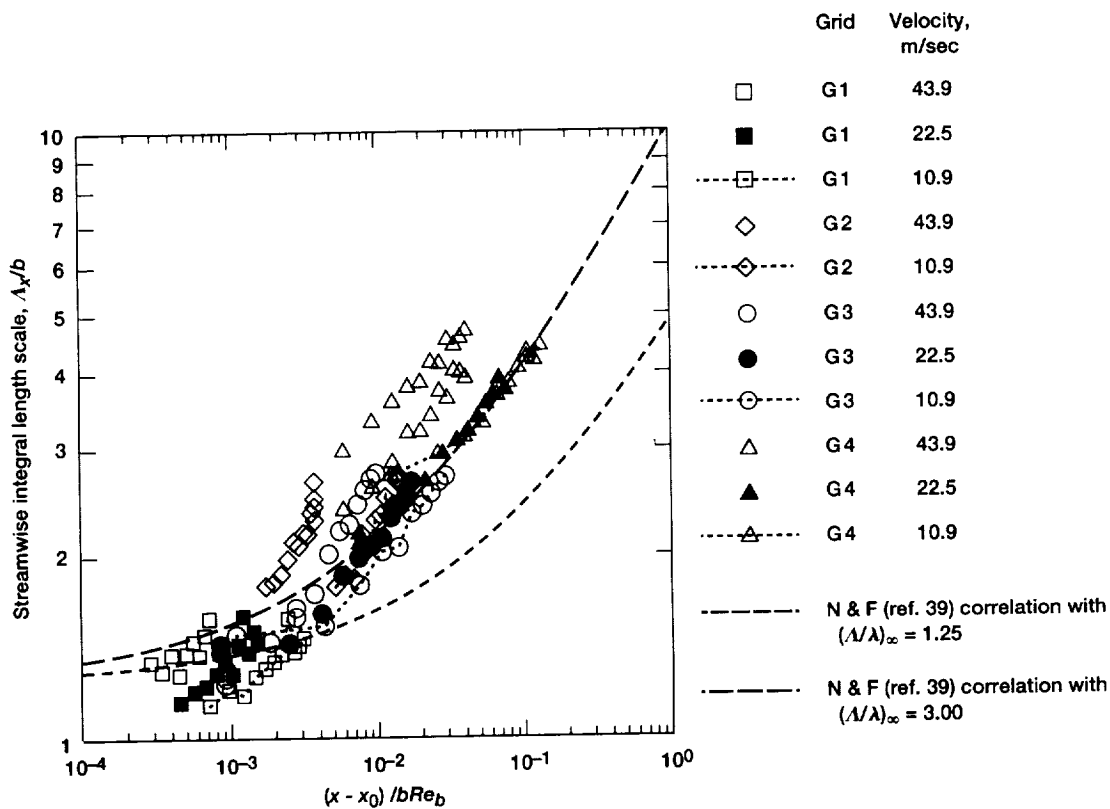


Figure 13.—Length scale data compared to the correlation of Naudascher and Farrell (ref. 39).

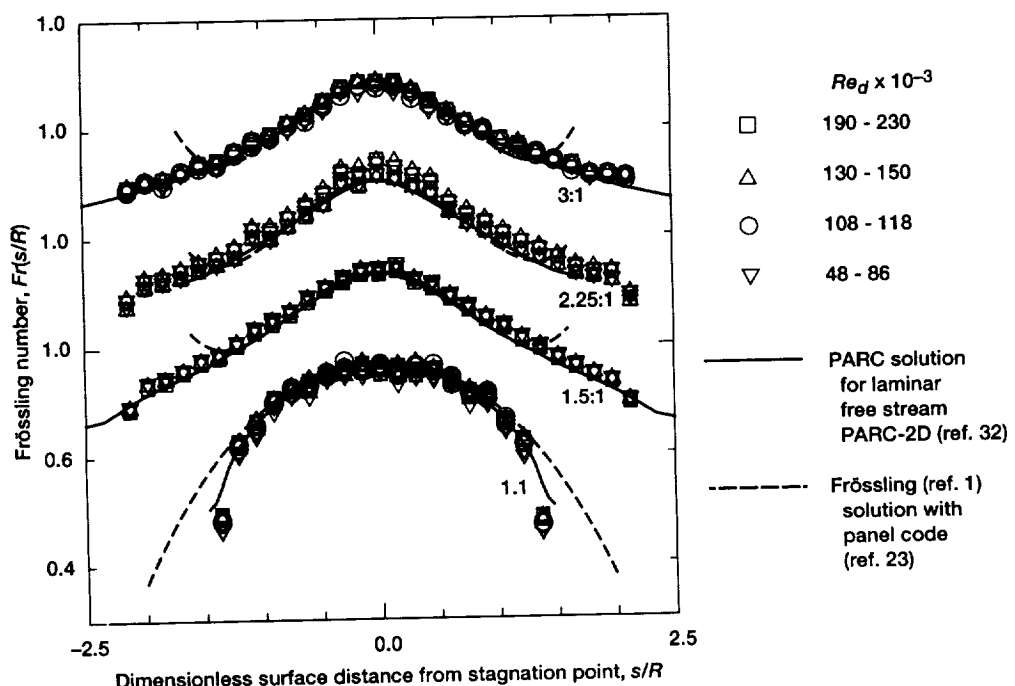


Figure 14.—Low turbulence Frössling number distribution compared to PARC-2D (ref. 32) and Frössling (ref. 1) solutions using velocity from panel code (ref. 23).

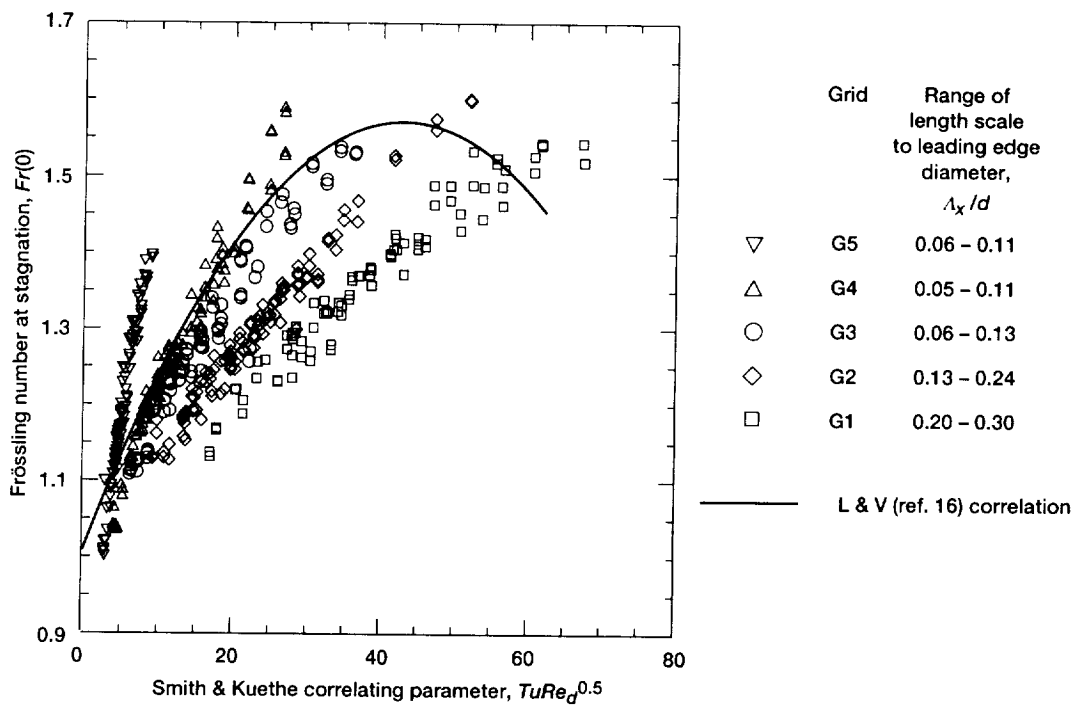


Figure 15.—Stagnation point Frössling number versus Smith & Kuethe (ref. 13) parameter showing effect of length scale.

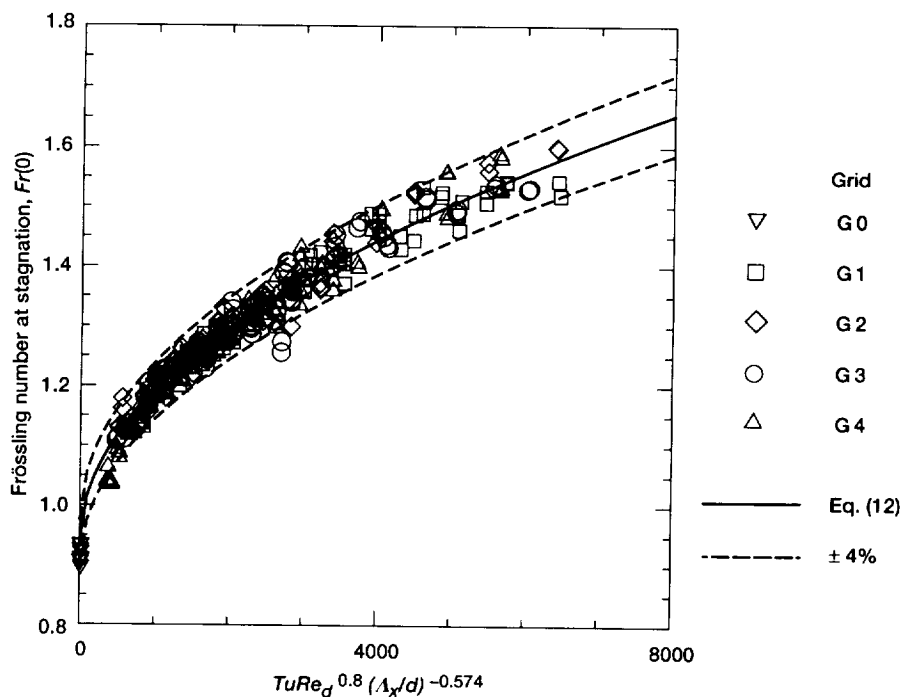


Figure 16.—Circular leading edge Frössling number data for grids G1 to G4 compared to equation (12). $Fr(0) = 0.008[TuRe_d^{0.8} (A_x/d)^{-0.574}]^{0.5} + C$; $C = 0.939$.

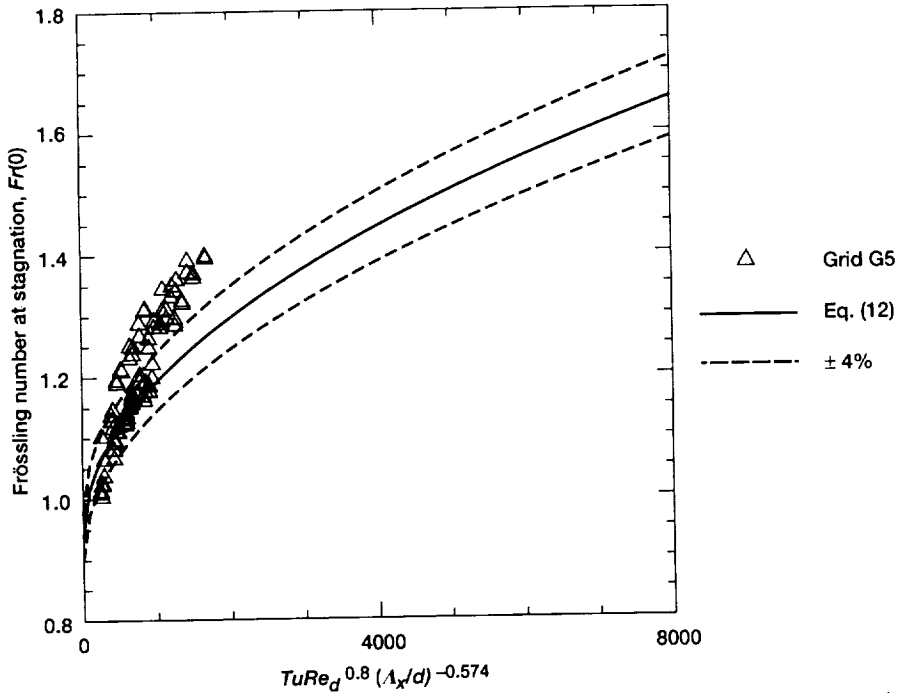


Figure 17.—Stagnation Frössling number data for grid G5 (parallel wires) compared to equation (12). $Fr(0) = 0.008[TuRe_d^{0.8}(\Lambda_x/d)^{-0.574}]^{0.5} + C; C = 0.939$.

the wires increases, the degree of anisotropy decreases as seen in figure 11 and heat transfer data agree more with the correlation.

As stated in the Introduction of this paper, Ames (ref. 20) developed a correlation for stagnation heat transfer data that involved Reynolds number, turbulence intensity, and length scale. Figure 18 shows the present circular leading edge Frössling number data for grids G1 to G5 plotted against the parameter of Ames. Also shown in this figure is a least-square fit of Ames' data based on integral length scale Λ_x instead of Ames' "energy scale." The Ames correlating parameter results in more scatter than the least-square curve fit used in equation (12). The data of Ames falls between the grids G1 to G4 (isotropic turbulence) and the grid G5 (anisotropic data). The turbulence generators used by Ames produced anisotropic turbulence with ratios of v'/u' around 1.3. Our grid G5 produced a range of v'/u' ratios from 0.95 to 1.42.

Figure 19 is a comparison of the stagnation heat transfer data of other authors (refs. 2, 13, 15, and 16) who used similar turbulence generators with equation (12). For cases where the authors did not measure length scale, it was estimated using the correlations given in table V. This was accomplished by using equation (10) with coefficients for the closest matching geometry available from table V to estimate a value of x/b from the intensity. Equation (11) was then used to calculate the length scale. Lateral length scale was measured by Lowery and Vachon (ref. 16); this was multiplied by 2 to convert it to longitudinal length scale. The data

of the other authors is in good agreement with the present correlation falling mostly within the ±10 percent bands drawn about the correlation of equation (12).

Stagnation Region Augmentation—Elliptical Leading Edges.—Rigby and Van Fossen showed by numerical calculation that the stagnation-point Frössling number with simulated turbulence (sinusoidal velocity variation upstream of the leading edge) divided by the laminar Frössling number was independent of body shape. Following this line, the correlation for the circular leading edge was modified by dividing by the laminar stagnation Frössling number. The modified correlation then gives the stagnation-point heat transfer augmentation factor Φ caused by free-stream turbulence

$$\Phi = \frac{Fr(0)_{tu}}{Fr(0)_{lam}} = 0.0085 \sqrt{Tu Re_d^{0.8} \left(\frac{\Lambda_x}{d} \right)^{-0.574} + 1} \quad (13)$$

Values of the term $Fr(0)_{lam}$ for the four models are dependent on the velocity gradient; the values are 0.939, 0.870, 0.811, 0.775 in order from the circular leading edge (1:1 ellipse) to the 3:1 ellipse. These values were also taken from the PARC-2D numerical solution with inlet mass flow defined by equation (9).

Comparison of the correlation for stagnation heat transfer augmentation by free-stream turbulence and the experimental data is shown in figure 20. The correlation was developed using only the circular leading-edge data, thus, the fit for that data is the best. In general, the fit is excellent and falls mostly

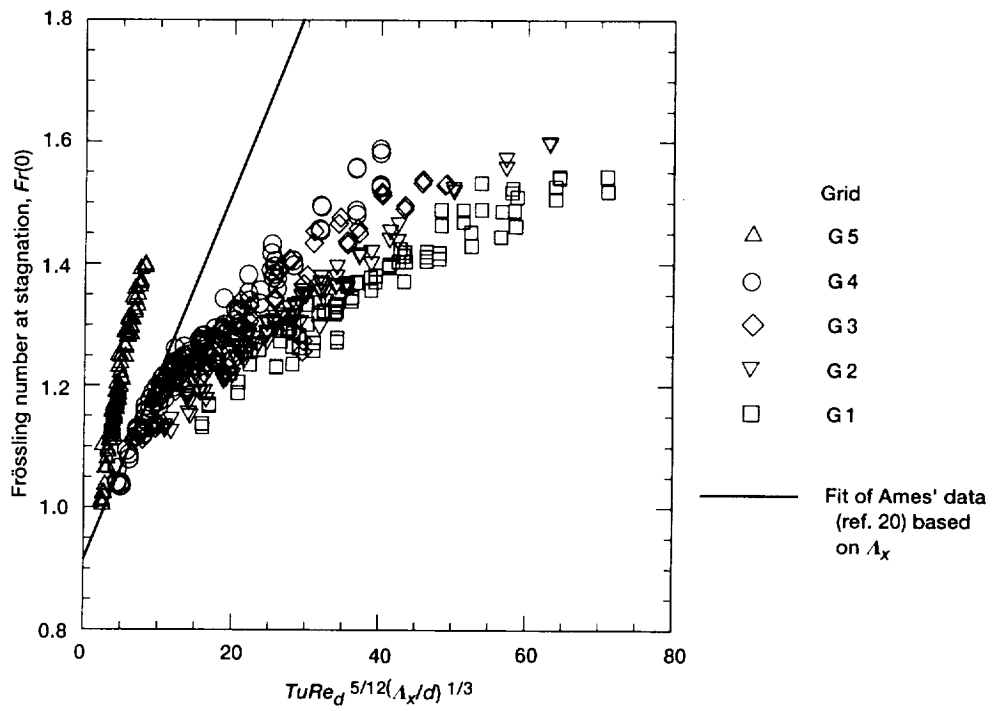


Figure 18.—Stagnation Frössling number data for circular leading edge versus Ames' correlating parameter (ref. 20).

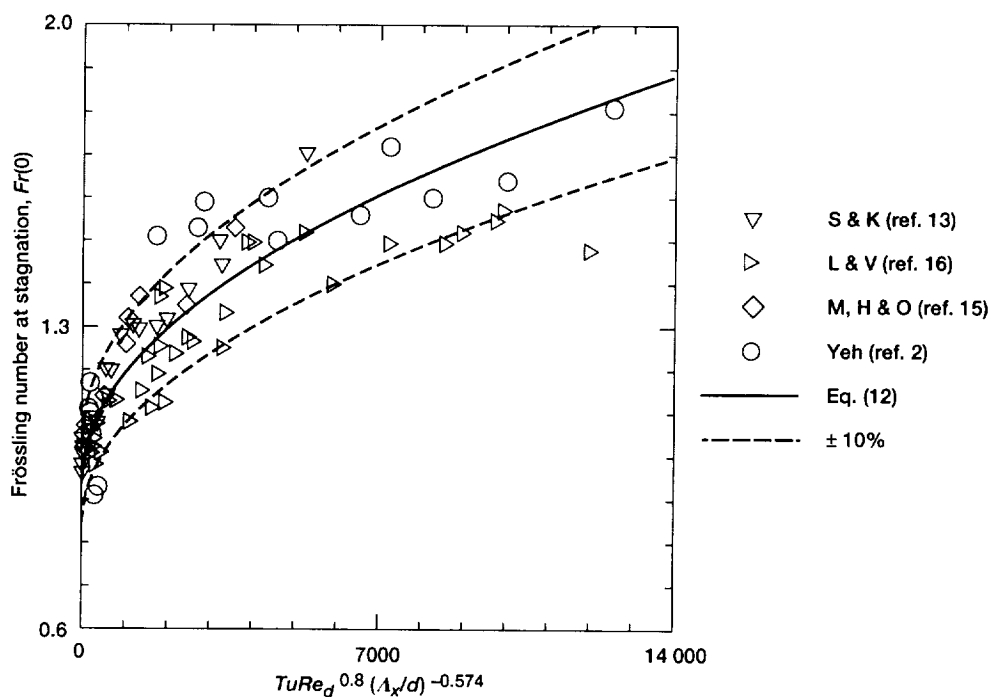


Figure 19.—Comparison of equation (12) with stagnation heat transfer data of other authors.

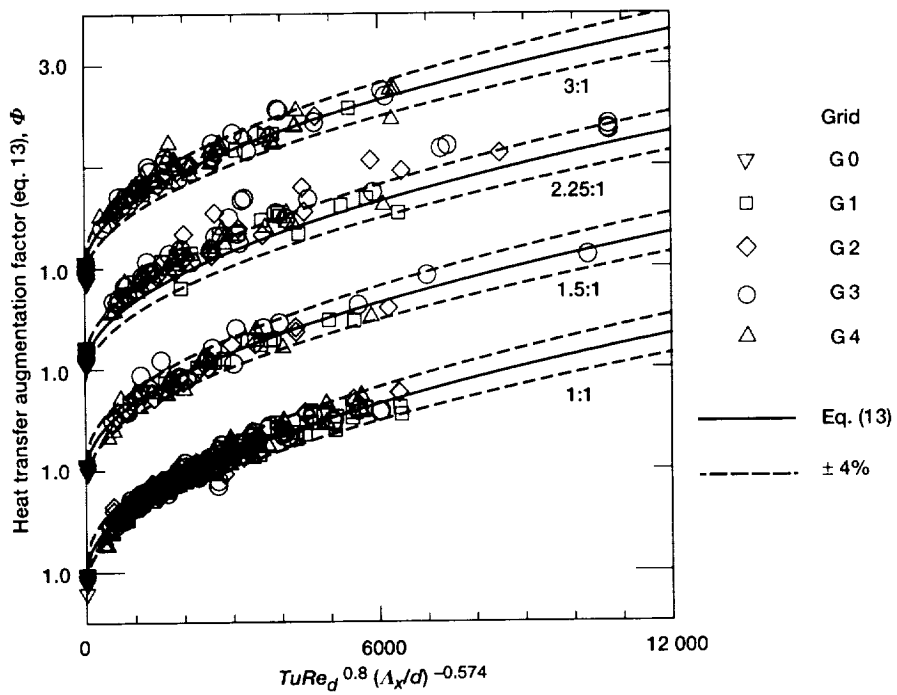


Figure 20.—Comparison of stagnation point heat transfer augmentation factor and correlation for elliptical leading edges.

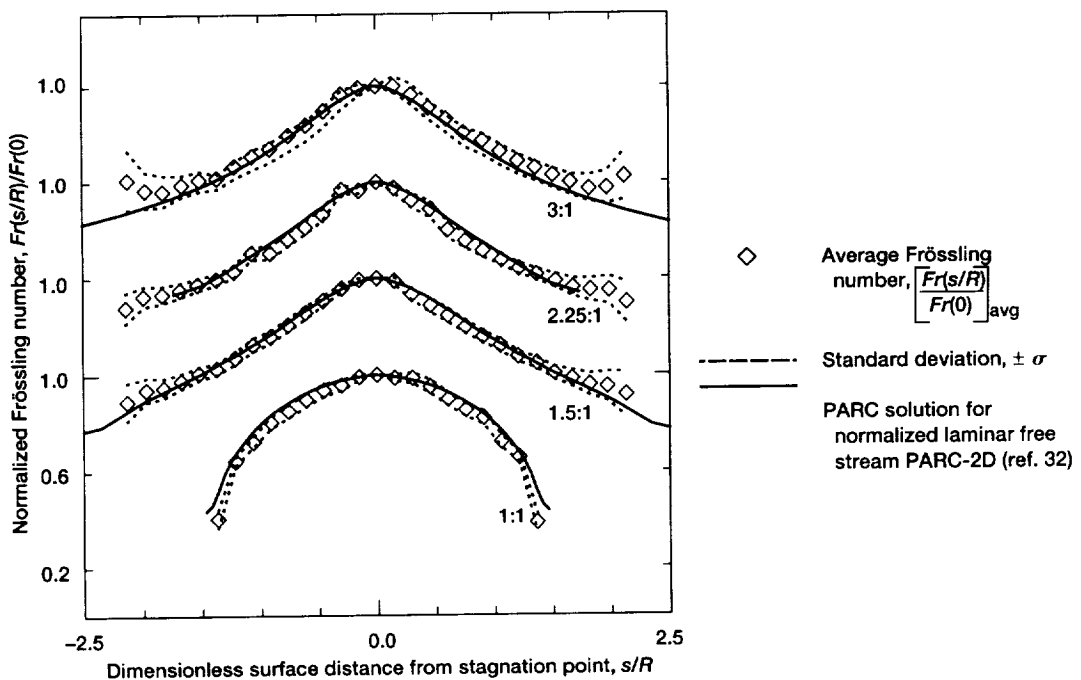


Figure 21.—Comparison of averaged, normalized, turbulent, Frössling number distribution with PARC-2D solution.

within the ± 4 percent bands drawn about the correlation. The 2.25:1 model has the most scatter; as mentioned earlier, this model had problems. If the Frössling number for the 2.25:1 model had been normalized using the average of the experimental data instead of the numerical solution, agreement with equation (13) would have been much better. The excellent agreement for the other three models confirms the validity of this correlation method.

As shown by Frössling's solution and the data in figure 14, the level of heat transfer at the stagnation point for zero turbulence flow depends on the velocity gradient. Equation (13) predicts the heat transfer augmentation above laminar levels and yet contains no term that involves the velocity gradient at the stagnation point. Thus, the hypothesis that heat transfer augmentation above laminar levels should increase in the presence of higher velocity gradients seems to be disproven by the present data.

Distribution of Heat Transfer Around Leading Edge.—Figure 21 is a plot of the Frössling number normalized by the stagnation value versus dimensionless surface distance from the stagnation point for each of the models. The square symbols represent the average of the Frössling number data for the turbulent free stream for all grids, Reynolds numbers, and grid positions. The dotted lines represent the standard deviation of the normalized data and the solid line is the PARC solution for a laminar free stream which has been similarly normalized. Agreement between the normalized turbulent heat transfer distribution and the normalized laminar distribution is good. Thus, a good prediction of the heat transfer at a given distance from the stagnation point can be obtained by using equation (13) with reference 1 to predict the stagnation heat transfer, and then multiplying by the ratio of local to stagnation heat transfer from a solution for the laminar free stream, that is,

$$Fr(s/R)_{tu} = \left(\frac{Fr(s/R)}{Fr(0)} \right)_{\text{lam}} Fr(0)_{tu} \quad (14)$$

Conclusions

Spanwise average stagnation-region heat transfer measurements were made on four models with elliptical leading edges, downstream of five turbulence generators. The ratio of major to minor axes for the elliptical leading edges ranged from 1:1 to 3:1; all the models had the same leading-edge radius of curvature. Velocity gradients at the stagnation point, made dimensionless by the leading-edge radius and free-stream velocity, ranged from 1.20 to 1.80. Four of the turbulence generators were square mesh, square bar, biplane grids with identical mesh-spacing to bar-width ratios and bar widths that ranged from 0.16 to 1.27 cm. The fifth turbulence generator was an array of parallel wires oriented normal to the model spanwise direction. Reynolds numbers based on leading-edge diameter

ranged from 37 000 to 228 000, turbulence intensities ranged from 1.1 to 15.9 percent, and the ratio of integral length scale to leading-edge diameter ranged from 0.05 to 0.30. Conclusions are summarized as follows:

1. Low turbulence heat transfer results agree with both the Frössling solution and a numerical solution to within estimated experimental accuracy, which validates the experimental method.
2. The calculation of laminar leading-edge heat transfer by cylinder in cross-flow correlations can lead to large errors for noncircular profiles.
3. Augmentation of stagnation-region heat transfer by turbulence increases as integral length scale decreases.
4. No optimum length scale was found for the turbulence-generating grids used in the present study ($A_x/d \geq 0.05$).
5. A correlation for stagnation heat transfer augmentation above laminar levels for the four square bar grids was developed, which reduced data scatter to ± 4 percent.
6. Dimensionless heat transfer augmentation is independent of body shape and, therefore, of velocity gradient at the stagnation point.
7. The heat transfer data for the array of parallel wires was correlated by the parameter that was developed, however, it was not predicted by equation (12), which indicated that augmentation must also be a function of the isotropy of the turbulent flow field.
8. The stagnation heat transfer data of other authors with similar turbulence generators was predicted to within ± 10 percent by the correlation developed in this study.
9. Frössling number downstream of stagnation, normalized by the stagnation value, can be represented by a universal curve for both laminar and turbulent flow.

National Aeronautics and Space Administration
Lewis Research Center
Cleveland, Ohio 44135, December 31, 1994

References

1. Frössling, N.: Evaporation, Heat Transfer, and Velocity Distribution in Two-Dimensional and Rotationally Symmetrical Laminar Boundary-Layer Flow. NACA TM-1432, 1958.
2. Yeh, F.C., et al.: High Reynolds Number and Turbulence Effects on Aerodynamics and Heat Transfer in a Turbine Cascade. AIAA Paper 93-2252, 1993.
3. Zimmerman, D.R.: Laser Anemometer Measurements at the Exit of a T63-C20 Combustor. (DDA-RN-79-4, Detroit Diesel Allison, NASA Contract NAS3-21267), NASA CR-159623, 1979.
4. Goebel, S.G., et al.: Measurements of Combustor Velocity and Turbulence Profiles. ASME Paper 93-GT-228, 1993.
5. Morkovin, M.V.: On the Question of Instabilities Upstream of Cylindrical Bodies. NASA CR-3231, 1979.
6. Hanarp, L.R.; and Suden, B.A.: Structure of the Boundary Layers on a Circular Cylinder in the Presence of Free Stream Turbulence. Lett Heat Mass Transfer, vol. 9, May-June 1982, pp. 169-177.

7. Van Fossen, G.J.; and Simoneau, R.J.: A Study of the Relationship Between Free-Stream Turbulence and Stagnation Region Heat Transfer. *J. Heat Transfer*, vol. 109, no. 1, 1987, pp. 10–15.
8. Rigby, D.L.; and Van Fossen, G.J.: Increased Heat Transfer to a Cylindrical Leading Edge Due to Spanwise Variations in the Free-Stream Velocity. *AIAA Paper 91-1739*, 1991.
9. Giedt, W.H.: Effect of Turbulence Level of Incident Air Stream on Local Heat Transfer From Cylinders. *J. Aeronaut. Sci.*, vol. 18, no. 11, 1951, pp. 725–730.
10. Seban, R.A.: The Influence of Free Stream Turbulence on the Local Heat Transfer From Cylinders. *J. Heat Transfer*, vol. 82c, May 1960, pp. 101–107.
11. Zapp, G.M.: The Effect of Turbulence on Local Heat Transfer Coefficient Around a Cylinder Normal to an Air Stream. M.S. Thesis, Oregon State College, Corvallis, OR, June 1950.
12. Schnautz, J.A.: Effect of Turbulence Intensity on Mass Transfer from Plates, Cylinders, and Spheres in Air Streams. PhD Thesis, Oregon State College, Corvallis, OR, June 1958.
13. Smith, M.C.; and Kuethe, A.M.: Effects of Turbulence on Laminar Skin Friction and Heat Transfer. *Phys. Fluids*, vol. 9, no. 12, Dec. 1966, pp. 2337–2344.
14. Kestin, J.; and Wood, R.T.: The Influence of Turbulence on Mass Transfer From Cylinders. *J. Heat Transfer*, vol. 93, Nov. 1971, pp. 321–327.
15. Mehendale, A.B.; Han, J.C.; and Ou, S.: Influence of High Mainstream Turbulence on Leading Edge Heat Transfer. *J. Heat Transfer*, vol. 113, Nov. 1991, pp. 843–850.
16. Lowery, G.W.; and Vachon, R.I.: Effect of Turbulence on Heat Transfer From Heated Cylinders. *Int. J. Heat Mass Transfer*, vol. 18, no. 11, 1975, pp. 1229–1242.
17. O'Brien, J.E.; and Van Fossen, G.J.: The Influence of Jet-Grid Turbulence on Heat Transfer from the Stagnation Region of a Cylinder in Crossflow. *NASA TM-87011*, 1985.
18. Yardi, N.R.; and Sukhatme, S.P.: Effects of Turbulence Intensity and Integral Length Scale of a Turbulent Free Stream on Forced Convection Heat Transfer From a Circular Cylinder in Cross Flow. International Heat Transfer Conference, 6th. Proceedings, General Papers, vol. 5: Nuclear Reactor Heat Transfer, Forced Convection, Paper FC(b)-29, Hemisphere Publ., Washington, D.C., 1978, pp. 347–352.
19. Dyban, YE.P.; Epic, E.YA.; and Kozlova L.G.: Heat Transfer in the Vicinity of the Front Stagnation Point of a Cylinder in Transverse Flow. *Heat Transfer—Soviet Research*, vol. 7, no. 2, Mar.–Apr., 1975, pp. 70–73.
20. Ames, F.E.: Heat Transfer with High Intensity, Large Scale Turbulence: The Flat Plate Turbulent Boundary Layer and the Cylindrical Stagnation Point. PhD Thesis, Stanford University, Stanford, CA, 1990.
21. Hunt, J.C.R.: A Theory of Turbulent Flow Round Two-Dimensional Bluff Bodies. *J. Fluid Mech.*, vol. 61, pt. 4, Dec. 18, 1973, pp. 625–706.
22. Hunt, J.C.R.; and Graham, J.M.R.: Free-Stream Turbulence Near Plane Boundaries. *J. Fluid Mech.*, vol. 84, Jan. 30, 1978, pp. 209–235.
23. McFarland, E.R.: A FORTRAN Computer Code for Calculating Flows in Multiple-Blade-Element Cascades. *NASA TM-87104*, 1985.
24. Van Fossen, G.J., et al.: Heat Transfer Distributions Around Nominal Ice Accretion Shapes Formed on a Cylinder in the NASA Lewis Icing Research Tunnel. *AIAA Paper 84-0017*, 1984 (also NASA TM-83557, 1984).
25. Miller, R.L.: ESCORT: A Data Acquisition and Display System to Support Research Testing. *NASA TM-78909*, 1978.
26. DISA Type 55M25 Linearizer Instruction Manual, published by DISA Information Department, p. 7, example 1.
27. Champagne, F.H.; Sleicher, C.A.; and Wehrmann, O.H.: Turbulence Measurements with Inclined Hot Wires. *J. Fluid Mech.*, vol. 28, Apr. 12, 1967, pp. 153–182.
28. Dryden H.L., et al.: Measurements of Intensity and Scale of Wind-Tunnel Turbulence and their Relation to the Critical Reynolds Number of Spheres. *NACA Report No. 581*, 1937.
29. Comte-Bellot, G.; and Corrsin, S.: Simple Eulerian Time Correlation of Full and Narrow-Band Velocity Signals in Grid-Generated, ‘Isotropic’ Turbulence. *J. Fluid Mech.*, vol. 48, pt. 2, 1971, pp. 273–337, Appendix E.
30. Wiegland, R.A.: Grid Generated Turbulence With and Without Rotation About the Streamwise Direction. PhD Thesis, Illinois Institute of Technology, Chicago, IL, 1978.
31. Tan-Atchat, J.: Effects of Axisymmetric Contractions on Turbulence of Various Scales. PhD Thesis, Illinois Institute of Technology, Chicago, IL, 1980.
32. Rigby, D.L.; and Van Fossen G.J.: Increased Heat Transfer to Elliptical Leading Edges Due to Spanwise Variations in the Freestream Momentum: Numerical and Experimental Results. *AIAA Paper 92-3070*, 1992.
33. Eckert, E.R.G.; and Drake, R.M.: *Heat and Mass Transfer*. McGraw-Hill Book Co., New York, 2nd ed., 1959, p. 266.
34. Hillsenrath, J., et al.: Tables of Thermal Properties of Gases. *NBS Circular 564*, Nov. 1955.
35. Kline, S.J.; and McClintock, F.A.: Describing Uncertainties in Single-Sample Experiments. *Mech. Eng.*, vol. 75, Jan. 1953, pp. 3–8.
36. Yavuzkurt, S.: A Guide to Uncertainty Analysis of Hot-Wire Data. *J. Fluids Eng.*, vol. 106, 1984, pp. 181–186.
37. Baines, W.D.; and Peterson, E.G.: An Investigation of Flow Through Screens. *Trans. ASME*, vol. 72, July 1951, pp. 468–480.
38. Roach, P.E.: The generation of Nearly Isotropic Turbulence By Means of Grids. *Int. J. Heat Fluid Flow*, vol. 8 no. 2, June 1987, pp 82–92.
39. Naudascher, E.; and Farrell, C.: Unified Analysis of Grid Turbulence. *Proc. ASCE, J. Eng. Mech. Div.*, vol. 96, Apr. 1970, pp. 121–141.
40. Bearman, P.W.: Some Measurements of the Distortion of Turbulence Approaching a Two-Dimensional Bluff Body. *J. Fluid Mech.*, vol. 53, pt. 3, June 13, 1972, pp. 451–467.

TABLE I.—TURBULENCE GRID DIMENSIONS

Grid	Bar width, b , cm (in.)	Mesh spacing to bar width ratio, M/b	Open area, percent
G0	No grid	-----	-----
G1	1.270 (0.500)	4.5	60.5
G2	0.635 (0.250)	4.5	60.5
G3	0.318 (0.125)	4.5	60.5
G4	0.159 (0.0630)	4.5	60.5
G5 ^a	0.051 (0.020)	12.5	92.0

^aArray of parallel wiresTABLE II.—DIMENSIONLESS SURFACE DISTANCES TO CENTER OF HEAT FLUX GAUGES MEASURED FROM STAGNATION POINT, s/R

Gauge	s/R	Gauge	s/R		
			Model ratio		
			1.5:1	2.25:1	3:1
10	0.000	15	0.000	0.000	0.000
9, 11	±0.152	14, 16	±0.151	±0.152	±0.151
8, 12	±0.303	13, 17	±0.303	±0.304	±0.301
7, 13	±0.455	12, 18	±0.456	±0.457	±0.452
6, 14	±0.607	11, 19	±0.607	±0.610	±0.604
5, 15	±0.759	10, 20	±0.759	±0.762	±0.755
4, 16	±0.910	9, 21	±0.910	±0.915	±0.907
3, 17	±0.062	8, 22	±1.062	±1.068	±1.058
2, 18	±1.214	7, 23	±1.214	±1.221	±1.210
1 ^a , 19 ^a	±1.365	6, 24	±1.366	±1.374	±1.361
		5, 25	±1.518	±1.527	±1.512
		4, 26	±1.670	±1.680	±1.664
		3, 27	±1.822	±1.833	±1.816
		2, 28	±1.975	±1.986	±1.968
		1 ^a , 29 ^a	±2.127	±2.140	±2.119

^aGuard heaters.

TABLE III.—UNCERTAINTY IN FRÖSSLING NUMBER

Error component at 20:1 odds, percent	Bias error		Precision error	
	Experimental velocity range			
	Maximum	Minimum	Maximum	Minimum
$\delta (q_{EI})/q_{EI}$	0.21	0.25	3.04	2.97
$\delta (q_{rad})/q_{rad}$	20.47	20.47	0.76	0.64
$\delta (q_{gap})/q_{gap}$	13.80	13.40	0.76	0.67
$\delta (q_{net})/q_{net}$	1.24	1.70	3.31	3.35
$\delta (d)/d$	0.12	0.12	0.00	0.00
$\delta (A)/A$	1.08	1.08	0.00	0.00
$\delta (\Delta T)/\Delta T$	4.68	4.68	0.77	0.68
$\delta (k)/k$	0.00	0.00	0.00	0.00
$\delta (Re_d)/Re_d$	5.76	11.91	0.10	2.15
$\delta (Fr)/Fr$	5.74	7.84	3.40	3.58
Combined uncertainty in $Fr(s/R)$, percent	6.67	8.62	----	----

TABLE IV.—TURBULENCE INTENSITY AND LENGTH SCALE (HOT WIRE) DATA UNCERTAINTY

Error component at 20:1 odds, percent	Bias error		Precision error	
	Experimental velocity range			
	Maximum	Minimum	Maximum	Minimum
$\delta (U_{caljet})$	3.41	15.34	0.10	0.32
δ (linearizer fit)	0.77	0.77	0.77	0.77
$\delta (Tu, \Lambda_x)$	3.50	15.36	----	----

TABLE V.—POWER LAW CURVE FITS OF TURBULENCE INTENSITY AND INTEGRAL LENGTH SCALE DATA

$$Tu = a \left(\frac{x}{b} \right)^m \quad \frac{\Lambda_x}{b} = I \left(\frac{x}{b} \right)^p$$

Grid	Velocity, m/sec	Reynolds number, Re_b	a	m	r_{Tu}	I	p	$r_{\Lambda_x/b}$
G1	43.9	38 650	206.10	-0.875	0.9950	0.240	0.500	0.6668
	22.5	18 000	206.10	-0.875	0.9950	0.240	0.500	0.6668
	10.9	7 934	206.10	-0.875	0.9950	0.240	0.500	0.6668
G2	43.9	17 190	146.3	-0.780	0.9987	0.272	0.500	0.8564
	22.5	9 514	135.3	-0.758	0.9989	0.272	0.500	0.8564
	10.9	4 452	138.9	-0.778	0.9986	0.272	0.500	0.8564
G3	43.9	8 935	132.2	-0.765	0.9997	0.264	0.500	0.9799
	22.5	4 780	156.3	-0.824	0.9995	0.264	0.500	0.9799
	10.9	2 470	149.4	-0.830	0.9992	0.264	0.500	0.9799
G4	43.9	4 571	80.15	-0.665	0.9998	0.303	0.500	0.8838
	22.5	2 297	89.46	-0.693	0.9995	0.303	0.500	0.8838
	10.9	1 174	75.05	-0.677	0.9997	0.303	0.500	0.8838
G5	43.9	1 634	23.68	-0.470	0.9852	4.658	0.116	0.8560
	22.5	792	23.38	-0.453	0.9848	3.255	0.199	0.9572
	10.9	340	52.73	-0.568	0.9975	10.011	0.051	0.4359

TABLE VI.—FRÖSSLING NUMBER FOR CIRCULAR LEADING-EDGE MODEL (1:1).

Rdg no.	Re _d	Grid	Tu, %	Λ_x/d	Gauge																	
					2	3	4	5	6	7	8	9	10	11	12	13	14	15	16	17	18	
Frössling number																						
2327	1.911	G0	0.30	2.308	0.657	0.726	0.817	0.855	0.876	0.904	0.913	0.936	0.913	0.912	0.915	0.914	0.866	0.835	0.828	0.727	0.655	
2328	1.509	G0	0.30	2.308	0.647	0.724	0.803	0.858	0.834	0.907	0.894	0.904	0.909	0.887	0.903	0.918	0.879	0.801	0.833	0.704	0.642	
2329	1.185	G0	0.30	2.308	0.643	0.716	0.798	0.853	0.863	0.893	0.948	0.918	0.936	0.899	0.927	0.932	0.887	0.824	0.830	0.733	0.641	
2332	1.899	G0	0.30	2.308	0.640	0.731	0.806	0.841	0.849	0.896	0.907	0.907	0.898	0.901	0.892	0.904	0.855	0.819	0.801	0.716	0.636	
2333	1.509	G0	0.30	2.308	0.656	0.701	0.809	0.855	0.854	0.892	0.914	0.910	0.906	0.891	0.901	0.904	0.869	0.813	0.813	0.703	0.639	
2334	1.178	G0	0.30	2.308	0.647	0.702	0.802	0.850	0.860	0.908	0.924	0.921	0.907	0.894	0.924	0.908	0.879	0.821	0.819	0.706	0.639	
2335	0.850	G0	0.30	2.308	0.606	0.674	0.763	0.829	0.819	0.880	0.892	0.893	0.908	0.861	0.885	0.876	0.859	0.781	0.789	0.686	0.591	
2338	0.856	G0	0.30	2.308	0.612	0.692	0.786	0.821	0.858	0.885	0.898	0.912	0.908	0.907	0.910	0.887	0.854	0.816	0.783	0.697	0.610	
2339	1.174	G0	0.30	2.308	0.630	0.716	0.793	0.834	0.871	0.899	0.918	0.927	0.927	0.921	0.930	0.908	0.857	0.830	0.800	0.718	0.636	
2340	1.511	G0	0.30	2.308	0.645	0.737	0.810	0.842	0.886	0.912	0.927	0.945	0.934	0.933	0.942	0.918	0.883	0.841	0.815	0.728	0.660	
2341	1.896	G0	0.30	2.308	0.645	0.729	0.802	0.842	0.878	0.903	0.920	0.939	0.923	0.929	0.930	0.917	0.871	0.831	0.810	0.728	0.651	
2170	1.873	G1	13.03	0.223	0.983	1.067	1.162	1.205	1.257	1.346	1.355	1.450	1.461	1.460	1.412	1.379	1.284	1.227	1.194	1.081	1.018	
2171	1.522	G1	13.00	0.223	0.951	1.037	1.139	1.180	1.230	1.303	1.327	1.398	1.429	1.418	1.403	1.357	1.286	1.217	1.181	1.076	1.003	
2172	1.186	G1	13.04	0.223	0.946	1.001	1.131	1.161	1.221	1.292	1.317	1.406	1.405	1.405	1.388	1.349	1.265	1.198	1.163	1.050	0.969	
2173	0.855	G1	13.13	0.223	0.908	0.985	1.119	1.143	1.202	1.278	1.373	1.381	1.362	1.353	1.328	1.241	1.167	1.143	1.014	0.937		
2174	0.442	G1	13.33	0.223	0.847	0.949	1.058	1.085	1.137	1.223	1.202	1.258	1.286	1.251	1.260	1.241	1.178	1.118	1.092	0.952	0.881	
2175	0.439	G1	13.33	0.223	0.832	0.937	1.047	1.074	1.148	1.198	1.211	1.258	1.265	1.265	1.256	1.231	1.169	1.118	1.067	0.958	0.864	
2176	0.854	G1	13.13	0.223	0.886	0.984	1.092	1.139	1.205	1.267	1.290	1.354	1.371	1.367	1.355	1.298	1.234	1.184	1.127	1.015	0.929	
2177	1.186	G1	13.04	0.223	0.912	1.013	1.120	1.166	1.232	1.289	1.326	1.399	1.420	1.415	1.397	1.339	1.263	1.214	1.157	1.045	0.968	
2178	1.515	G1	13.00	0.223	0.930	1.035	1.132	1.175	1.242	1.305	1.336	1.424	1.452	1.446	1.422	1.343	1.292	1.231	1.173	1.068	0.989	
2179	1.866	G1	13.03	0.223	0.974	1.063	1.144	1.198	1.264	1.335	1.365	1.455	1.487	1.473	1.433	1.353	1.286	1.233	1.179	1.073	1.001	
2180	1.858	G1	12.13	0.232	1.022	1.099	1.214	1.258	1.316	1.406	1.406	1.524	1.533	1.524	1.488	1.429	1.339	1.272	1.235	1.116	1.047	
2181	1.513	G1	12.10	0.232	0.982	1.053	1.176	1.222	1.284	1.360	1.395	1.470	1.488	1.475	1.433	1.405	1.302	1.252	1.215	1.088	1.010	
2182	1.186	G1	12.12	0.232	0.948	1.021	1.152	1.174	1.238	1.311	1.341	1.420	1.424	1.427	1.391	1.334	1.275	1.194	1.173	1.039	0.968	
2183	0.849	G1	12.21	0.232	0.900	0.974	1.089	1.130	1.185	1.262	1.257	1.335	1.345	1.323	1.324	1.287	1.215	1.148	1.123	0.990	0.921	
2184	0.440	G1	12.41	0.232	0.861	0.928	1.045	1.070	1.122	1.188	1.234	1.232	1.214	1.217	1.232	1.158	1.092	1.061	0.945	0.869		
2185	0.439	G1	12.41	0.232	0.828	0.931	1.030	1.073	1.131	1.171	1.180	1.224	1.230	1.222	1.229	1.208	1.135	1.088	1.052	0.938	0.857	
2186	0.848	G1	12.21	0.232	0.878	0.985	1.071	1.119	1.190	1.244	1.263	1.321	1.339	1.338	1.320	1.271	1.203	1.154	1.104	0.990	0.912	
2187	1.175	G1	12.13	0.232	0.910	1.007	1.104	1.156	1.222	1.278	1.319	1.394	1.404	1.394	1.376	1.312	1.243	1.188	1.133	1.019	0.948	
2188	1.516	G1	12.10	0.232	0.951	1.034	1.139	1.190	1.259	1.323	1.368	1.443	1.463	1.463	1.419	1.345	1.279	1.225	1.169	1.053	0.979	
2189	1.860	G1	12.13	0.232	0.965	1.048	1.149	1.201	1.272	1.340	1.375	1.469	1.489	1.489	1.434	1.364	1.290	1.230	1.177	1.063	0.996	
2212	1.884	G1	15.52	0.202	1.060	1.135	1.229	1.268	1.321	1.369	1.430	1.497	1.519	1.507	1.490	1.431	1.357	1.294	1.250	1.164	1.098	
2213	1.525	G1	15.52	0.202	1.015	1.098	1.197	1.270	1.303	1.349	1.409	1.483	1.506	1.491	1.475	1.426	1.338	1.286	1.238	1.133	1.063	
2214	1.186	G1	15.58	0.202	0.968	1.064	1.166	1.223	1.258	1.320	1.374	1.427	1.444	1.449	1.431	1.370	1.318	1.240	1.216	1.102	1.018	
2215	0.857	G1	15.69	0.202	0.940	1.029	1.127	1.197	1.243	1.296	1.336	1.371	1.409	1.389	1.396	1.369	1.269	1.194	1.191	1.048	0.966	
2216	0.435	G1	15.91	0.202	0.862	0.949	1.065	1.097	1.156	1.188	1.230	1.251	1.279	1.240	1.275	1.263	1.177	1.102	1.120	0.950	0.896	
2217	0.434	G1	15.91	0.202	0.845	0.948	1.052	1.088	1.159	1.192	1.208	1.247	1.273	1.251	1.280	1.236	1.171	1.128	1.088	0.973	0.883	
2218	0.856	G1	15.69	0.202	0.934	1.040	1.126	1.181	1.245	1.298	1.330	1.397	1.418	1.412	1.413	1.369	1.287	1.221	1.183	1.060	0.976	
2219	1.194	G1	15.58	0.202	0.981	1.064	1.169	1.221	1.285	1.333	1.379	1.453	1.486	1.478	1.461	1.413	1.326	1.273	1.218	1.098	1.023	
2220	1.525	G1	15.52	0.202	1.022	1.108	1.201	1.249	1.322	1.369	1.408	1.493	1.526	1.519	1.502	1.423	1.348	1.296	1.253	1.131	1.061	
2221	1.875	G1	15.52	0.202	1.050	1.130	1.217	1.272	1.336	1.389	1.424	1.514	1.543	1.545	1.520	1.450	1.373	1.317	1.263	1.155	1.090	
2222	1.875	G1	14.23	0.212	1.027	1.118	1.207	1.263	1.317	1.385	1.417	1.512	1.541	1.491	1.458	1.410	1.327	1.251	1.220	1.102	1.049	
2223	1.526	G1	14.22	0.212	1.003	1.097	1.204	1.258	1.314	1.369	1.423	1.503	1.524	1.495	1.467	1.394	1.288	1.247	1.217	1.096	1.029	
2224	1.192	G1	14.26	0.212	0.968	1.042	1.156	1.230	1.273	1.333	1.388	1.450	1.488	1.441	1.417	1.363	1.265	1.206	1.177	1.060	0.984	
2225	0.849	G1	14.37	0.212	0.932	1.026	1.126	1.194	1.247	1.293	1.329	1.380	1.419	1.419	1.372	1.387	1.296	1.245	1.189	1.173	1.035	0.952
2226	0.436	G1	14.58	0.212	0.840	0.939	1.039	1.086	1.133	1.159	1.226	1.227	1.271	1.235	1.258	1.210	1.156	1.101	1.089	0.946	0.863	
2227	0.435	G1	14.58	0.212	0.842	0.945	1.043	1.089	1.142	1.184	1.209	1.247	1.258	1.246	1.266	1.229	1.152	1.116	1.067	0.950	0.872	
2228	0.854	G																				

TABLE VI.—CONTINUED.

Rd'g no.	Re _d	Grid	Tu, %	Δ_x/d	Gauge Frössling number																	
					2	3	4	5	6	7	8	9	10	11	12	13	14	15	16	17	18	
2264	1.901	G1	9.44	0.269	0.902	1.005	1.086	1.148	1.210	1.265	1.294	1.366	1.399	1.361	1.342	1.297	1.222	1.163	1.125	1.013	0.936	
2265	1.557	G1	9.38	0.269	0.890	0.976	1.075	1.143	1.199	1.241	1.294	1.354	1.370	1.343	1.338	1.277	1.236	1.129	1.115	1.001	0.922	
2266	1.201	G1	9.38	0.269	0.873	0.961	1.052	1.118	1.173	1.215	1.274	1.307	1.323	1.304	1.307	1.267	1.199	1.110	1.100	0.981	0.902	
2267	0.868	G1	9.45	0.269	0.855	0.948	1.052	1.106	1.174	1.194	1.245	1.280	1.290	1.275	1.276	1.246	1.180	1.103	1.092	0.973	0.881	
2268	0.445	G1	9.62	0.269	0.829	0.921	1.039	1.088	1.127	1.171	1.188	1.222	1.220	1.203	1.217	1.201	1.153	1.072	1.073	0.935	0.858	
2269	0.450	G1	9.62	0.269	0.825	0.909	1.027	1.059	1.134	1.164	1.177	1.214	1.221	1.201	1.222	1.195	1.135	1.083	1.041	0.942	0.848	
2270	0.874	G1	9.45	0.269	0.842	0.959	1.043	1.088	1.160	1.202	1.231	1.268	1.294	1.271	1.276	1.224	1.154	1.122	1.072	0.969	0.876	
2271	1.209	G1	9.38	0.269	0.861	0.954	1.056	1.107	1.173	1.220	1.252	1.313	1.320	1.314	1.306	1.248	1.188	1.130	1.090	0.981	0.893	
2272	1.544	G1	9.38	0.269	0.875	0.978	1.068	1.127	1.193	1.234	1.276	1.348	1.370	1.351	1.328	1.274	1.200	1.158	1.108	0.999	0.909	
2273	1.905	G1	9.44	0.269	0.886	0.987	1.077	1.133	1.204	1.252	1.293	1.365	1.395	1.371	1.350	1.288	1.206	1.163	1.105	1.004	0.918	
2295	1.886	G1	8.28	0.290	0.869	0.961	1.070	1.127	1.183	1.245	1.285	1.323	1.364	1.330	1.310	1.260	1.191	1.115	1.091	0.965	0.897	
2296	1.535	G1	8.22	0.290	0.844	0.947	1.050	1.103	1.169	1.214	1.265	1.297	1.320	1.312	1.299	1.254	1.183	1.110	1.090	0.961	0.879	
2297	1.192	G1	8.21	0.290	0.829	0.942	1.034	1.102	1.156	1.206	1.247	1.286	1.294	1.283	1.279	1.249	1.160	1.108	1.076	0.947	0.867	
2298	0.864	G1	8.27	0.290	0.821	0.917	1.019	1.093	1.139	1.197	1.218	1.259	1.254	1.261	1.258	1.135	1.089	1.062	0.933	0.851		
2299	0.444	G1	8.44	0.290	0.778	0.852	0.973	1.025	1.076	1.118	1.141	1.142	1.170	1.142	1.175	1.129	1.077	1.017	1.015	0.861	0.801	
2300	0.444	G1	8.43	0.290	0.766	0.875	0.970	1.017	1.076	1.114	1.133	1.169	1.167	1.151	1.169	1.136	1.084	1.027	0.994	0.878	0.796	
2301	0.862	G1	8.27	0.290	0.816	0.909	1.024	1.074	1.139	1.181	1.207	1.246	1.258	1.246	1.246	1.214	1.138	1.088	1.037	0.930	0.843	
2302	1.195	G1	8.21	0.290	0.824	0.931	1.033	1.084	1.157	1.202	1.232	1.287	1.303	1.288	1.281	1.220	1.164	1.112	1.064	0.944	0.861	
2303	1.536	G1	8.22	0.290	0.843	0.942	1.037	1.097	1.173	1.215	1.254	1.316	1.337	1.322	1.306	1.242	1.170	1.130	1.072	0.962	0.879	
2304	1.887	G1	8.28	0.290	0.863	0.966	1.063	1.122	1.194	1.246	1.289	1.347	1.368	1.352	1.325	1.263	1.189	1.137	1.084	0.972	0.892	
2306	1.892	G1	7.94	0.297	0.855	0.960	1.050	1.117	1.169	1.229	1.254	1.312	1.318	1.308	1.293	1.241	1.183	1.122	1.080	0.956	0.885	
2307	1.534	G1	7.86	0.297	0.853	0.946	1.055	1.115	1.168	1.213	1.252	1.308	1.334	1.298	1.293	1.229	1.163	1.125	1.083	0.956	0.874	
2308	1.196	G1	7.86	0.297	0.835	0.935	1.027	1.092	1.149	1.198	1.227	1.272	1.291	1.254	1.270	1.220	1.148	1.100	1.082	0.942	0.854	
2309	0.863	G1	7.92	0.297	0.821	0.912	1.015	1.072	1.122	1.168	1.201	1.229	1.256	1.212	1.227	1.198	1.148	1.073	1.060	0.939	0.830	
2310	0.441	G1	8.08	0.297	0.759	0.870	0.962	1.009	1.065	1.088	1.110	1.136	1.132	1.129	1.137	1.142	1.063	1.007	1.006	0.871	0.789	
2311	0.437	G1	8.08	0.297	0.766	0.859	0.961	0.998	1.064	1.090	1.114	1.142	1.137	1.131	1.150	1.121	1.068	1.020	0.987	0.869	0.784	
2312	0.856	G1	7.92	0.297	0.809	0.908	1.015	1.054	1.121	1.157	1.178	1.231	1.235	1.220	1.222	1.190	1.127	1.074	1.036	0.923	0.834	
2313	1.199	G1	7.86	0.297	0.823	0.920	1.022	1.073	1.139	1.176	1.210	1.255	1.273	1.254	1.210	1.139	1.096	1.045	0.937	0.853		
2314	1.533	G1	7.86	0.297	0.837	0.941	1.032	1.092	1.154	1.205	1.235	1.287	1.301	1.292	1.272	1.215	1.154	1.106	1.057	0.951	0.863	
2315	1.895	G1	7.94	0.297	0.843	0.945	1.046	1.097	1.167	1.215	1.253	1.312	1.330	1.311	1.293	1.239	1.160	1.116	1.066	0.956	0.873	
2343	1.886	G1	13.03	0.223	0.973	1.068	1.152	1.213	1.279	1.336	1.387	1.461	1.510	1.473	1.433	1.362	1.287	1.233	1.176	1.076	1.008	
2344	1.184	G1	13.04	0.223	0.917	1.014	1.111	1.166	1.229	1.281	1.309	1.377	1.412	1.378	1.361	1.310	1.232	1.179	1.127	1.024	0.945	
2345	0.439	G1	13.33	0.223	0.837	0.911	1.034	1.070	1.129	1.179	1.180	1.218	1.236	1.227	1.217	1.202	1.130	1.082	1.042	0.925	0.849	
1948	1.905	G2	6.55	0.190	0.869	0.975	1.072	1.138	1.204	1.270	1.290	1.355	1.382	1.359	1.322	1.251	1.191	1.142	1.065	0.976	0.864	
1949	1.907	G2	6.55	0.190	0.863	0.955	1.058	1.121	1.184	1.250	1.277	1.340	1.359	1.342	1.307	1.229	1.173	1.121	1.052	0.973	0.857	
1950	1.906	G2	6.55	0.190	0.864	0.959	1.061	1.126	1.195	1.259	1.279	1.345	1.373	1.343	1.314	1.272	1.176	1.136	1.060	0.928	0.861	
1951	1.907	G2	6.55	0.190	0.863	0.966	1.063	1.129	1.193	1.258	1.283	1.356	1.370	1.347	1.316	1.250	1.190	1.143	1.059	0.942	0.866	
1952	1.908	G2	6.55	0.190	0.858	0.975	1.061	1.123	1.190	1.257	1.274	1.355	1.358	1.337	1.312	1.246	1.179	1.134	1.056	1.014	0.863	
1953	1.542	G2	6.74	0.190	0.854	0.954	1.058	1.119	1.180	1.238	1.269	1.339	1.349	1.338	1.301	1.248	1.178	1.136	1.057	0.986	0.855	
1954	1.201	G2	6.77	0.190	0.835	0.939	1.036	1.094	1.154	1.214	1.242	1.295	1.297	1.295	1.281	1.221	1.161	1.119	1.044	0.989	0.843	
1955	0.867	G2	6.67	0.190	0.807	0.901	1.006	1.061	1.122	1.180	1.189	1.256	1.250	1.241	1.247	1.212	1.137	1.054	1.032	0.918	0.833	
1956	0.457	G2	6.36	0.190	0.757	0.852	0.955	1.002	1.053	1.103	1.109	1.149	1.153	1.154	1.159	1.129	1.067	0.600	0.981	0.881	0.777	
1957	1.542	G2	6.74	0.190	0.856	0.966	1.065	1.122	1.193	1.247	1.278	1.347	1.359	1.331	1.310	1.251	1.185	1.121	1.062	0.888	0.858	
1958	1.202	G2	6.77	0.190	0.842	0.942	1.044	1.100	1.170	1.223	1.249	1.307	1.316	1.306	1.287	1.241	1.172	1.110	1.055	0.862	0.851	
1959	0.863	G2	6.67	0.190	0.816	0.907	1.017	1.059	1.130	1.187	1.197	1.255	1.264	1.251	1.255	1.213	1.146	1.092	1.035	0.915	0.835	
1960	0.450	G2	6.35	0.190	0.765	0.858	0.950	1.001	1.056	1.108	1.111	1.157	1.175	1.141	1.172	1.148	1.075	1.038	0.981	0.834	0.781	
1961	1.906	G2	6.55	0.190	0.857	0.968	1.060	1.125	1.193	1.248	1.279	1.351	1.370	1.341	1.313	1.247	1.174	1.125	1.055	1.020	0.858	
1962	1.543	G2	6.74	0.190	0.847	0.962	1.054	1.115	1.184	1.248	1.263	1.334	1.350	1.322	1.305	1.259	1.169	1.123	1.054	0.941	0.854	
1963	1.205	G2	6.77	0.190	0.831	0.934	1															

TABLE VI.—CONTINUED.

Rdg no.	Re _d	Grid	Tu, %	Λ_s/d	Gauge																
					2	3	4	5	6	7	8	9	10	11	12	13	14	15	16	17	18
Frössling number																					
2160	1.878	G2	6.57	0.190	0.837	0.926	1.039	1.088	1.156	1.236	1.231	1.305	1.299	1.301	1.282	1.234	1.162	1.092	1.067	0.937	0.865
2161	1.518	G2	6.75	0.190	0.846	0.917	1.048	1.095	1.152	1.238	1.230	1.304	1.308	1.309	1.278	1.238	1.165	1.105	1.071	0.941	0.863
2162	1.189	G2	6.77	0.190	0.838	0.916	1.054	1.086	1.158	1.231	1.244	1.294	1.305	1.286	1.279	1.255	1.151	1.105	1.084	0.938	0.864
2163	0.848	G2	6.66	0.190	0.816	0.904	1.018	1.070	1.129	1.201	1.209	1.251	1.259	1.233	1.242	1.221	1.156	1.076	1.048	0.914	0.835
2164	0.438	G2	6.34	0.190	0.797	0.839	0.994	1.026	1.080	1.131	1.169	1.173	1.185	1.166	1.181	1.155	1.113	1.018	1.032	0.885	0.806
2165	0.438	G2	6.34	0.190	0.766	0.889	0.988	1.014	1.074	1.157	1.120	1.176	1.181	1.171	1.184	1.143	1.085	1.039	0.994	0.886	0.794
2166	0.853	G2	6.66	0.190	0.807	0.909	1.014	1.075	1.137	1.200	1.214	1.262	1.266	1.257	1.249	1.206	1.144	1.086	1.035	0.922	0.828
2167	1.183	G2	6.77	0.190	0.820	0.921	1.029	1.091	1.159	1.219	1.237	1.295	1.310	1.292	1.287	1.242	1.157	1.115	1.056	0.942	0.856
2168	1.515	G2	6.75	0.190	0.830	0.941	1.038	1.098	1.171	1.223	1.253	1.319	1.339	1.326	1.298	1.254	1.173	1.124	1.065	0.952	0.861
2169	1.874	G2	6.57	0.190	0.842	0.953	1.050	1.112	1.185	1.244	1.276	1.339	1.357	1.340	1.316	1.252	1.182	1.125	1.070	0.953	0.866
2170	1.870	G2	8.47	0.161	0.931	1.016	1.124	1.184	1.238	1.302	1.342	1.399	1.468	1.437	1.419	1.355	1.275	1.205	1.167	1.040	0.965
2172	1.524	G2	8.64	0.161	0.904	0.999	1.105	1.159	1.215	1.288	1.325	1.393	1.423	1.410	1.390	1.307	1.288	1.183	1.157	1.019	0.944
2173	1.189	G2	8.65	0.161	0.875	0.948	1.084	1.119	1.177	1.237	1.277	1.324	1.369	1.345	1.329	1.314	1.229	1.137	1.127	0.981	0.909
2174	0.854	G2	8.52	0.161	0.865	0.932	1.060	1.094	1.159	1.219	1.238	1.282	1.318	1.288	1.307	1.265	1.208	1.127	1.102	0.954	0.880
2175	0.442	G2	8.16	0.161	0.809	0.891	1.005	1.039	1.109	1.144	1.177	1.176	1.211	1.182	1.228	1.191	1.139	1.047	1.044	0.906	0.809
2176	0.439	G2	8.16	0.161	0.796	0.882	0.998	1.034	1.104	1.152	1.158	1.206	1.217	1.207	1.217	1.172	1.118	1.073	1.028	0.913	0.812
2177	0.858	G2	8.52	0.161	0.827	0.934	1.028	1.091	1.157	1.209	1.239	1.292	1.308	1.303	1.306	1.257	1.189	1.138	1.086	0.967	0.876
2178	1.184	G2	8.65	0.161	0.858	0.944	1.053	1.106	1.173	1.233	1.263	1.327	1.366	1.350	1.336	1.283	1.210	1.154	1.100	0.981	0.897
2179	1.521	G2	8.64	0.161	0.873	0.977	1.074	1.127	1.201	1.257	1.299	1.371	1.403	1.402	1.377	1.313	1.240	1.180	1.120	1.001	0.918
2200	1.861	G2	8.48	0.161	0.896	1.001	1.089	1.145	1.212	1.269	1.309	1.398	1.440	1.426	1.398	1.335	1.255	1.191	1.137	1.018	0.939
2201	1.865	G2	7.56	0.174	0.913	1.006	1.120	1.170	1.238	1.320	1.339	1.408	1.418	1.405	1.369	1.313	1.246	1.162	1.131	0.996	0.923
2202	1.522	G2	7.72	0.174	0.898	0.989	1.092	1.156	1.212	1.296	1.293	1.361	1.398	1.352	1.333	1.315	1.207	1.147	1.108	0.985	0.904
2203	1.189	G2	7.74	0.174	0.887	0.943	1.077	1.125	1.182	1.261	1.279	1.322	1.351	1.320	1.324	1.255	1.210	1.121	1.088	0.960	0.877
2204	0.855	G2	7.62	0.174	0.855	0.926	1.046	1.123	1.171	1.222	1.259	1.302	1.308	1.289	1.273	1.276	1.164	1.107	1.074	0.952	0.863
2205	0.433	G2	7.27	0.174	0.826	0.888	1.008	1.017	1.118	1.151	1.182	1.181	1.216	1.170	1.202	1.193	1.112	1.048	1.023	0.889	0.820
2206	0.431	G2	7.27	0.174	0.788	0.880	0.990	1.045	1.106	1.157	1.164	1.201	1.193	1.195	1.191	1.173	1.104	1.047	1.008	0.891	0.803
2207	0.854	G2	7.62	0.174	0.831	0.940	1.040	1.090	1.169	1.223	1.249	1.296	1.305	1.286	1.287	1.232	1.173	1.109	1.059	0.942	0.854
2208	1.189	G2	7.74	0.174	0.846	0.954	1.050	1.117	1.188	1.250	1.276	1.339	1.355	1.328	1.315	1.263	1.182	1.133	1.080	0.959	0.875
2209	1.519	G2	7.72	0.174	0.857	0.966	1.063	1.123	1.206	1.262	1.304	1.361	1.382	1.363	1.342	1.280	1.201	1.146	1.094	0.977	0.883
2210	1.859	G2	7.56	0.174	0.870	0.981	1.082	1.138	1.214	1.277	1.319	1.387	1.415	1.389	1.352	1.282	1.218	1.144	1.090	0.972	0.891
2233	1.881	G2	5.65	0.209	0.851	0.945	1.036	1.095	1.151	1.203	1.252	1.289	1.320	1.300	1.282	1.238	1.162	1.107	1.088	0.929	0.871
2234	1.524	G2	5.83	0.209	0.820	0.917	1.015	1.083	1.136	1.186	1.226	1.271	1.292	1.277	1.259	1.239	1.160	1.094	1.065	0.917	0.841
2235	1.187	G2	5.86	0.209	0.807	0.900	0.995	1.059	1.127	1.169	1.180	1.250	1.246	1.231	1.224	1.185	1.126	1.062	1.030	0.899	0.828
2236	0.854	G2	5.77	0.209	0.814	0.907	1.001	1.070	1.127	1.175	1.194	1.248	1.241	1.230	1.239	1.187	1.161	1.079	1.068	0.906	0.831
2237	0.441	G2	5.47	0.209	0.757	0.867	0.946	1.013	1.060	1.104	1.125	1.141	1.147	1.142	1.135	1.113	1.073	0.997	1.001	0.842	0.772
2238	0.440	G2	5.47	0.209	0.747	0.838	0.943	0.993	1.050	1.088	1.089	1.131	1.128	1.125	1.126	1.103	1.037	0.995	0.960	0.833	0.763
2239	0.858	G2	5.77	0.209	0.790	0.894	0.991	1.047	1.122	1.159	1.187	1.222	1.233	1.225	1.225	1.190	1.109	1.074	1.030	0.906	0.817
2240	1.192	G2	5.86	0.209	0.806	0.908	1.006	1.062	1.133	1.179	1.205	1.254	1.256	1.253	1.244	1.209	1.126	1.089	1.032	0.918	0.827
2241	1.520	G2	5.83	0.209	0.798	0.912	0.997	1.062	1.132	1.177	1.206	1.266	1.274	1.262	1.259	1.208	1.134	1.092	1.035	0.920	0.837
2242	1.880	G2	5.66	0.209	0.821	0.930	1.020	1.082	1.147	1.200	1.229	1.293	1.315	1.295	1.281	1.225	1.158	1.104	1.050	0.943	0.852
2243	1.875	G2	5.27	0.218	0.825	0.924	1.018	1.075	1.143	1.183	1.214	1.270	1.287	1.260	1.245	1.207	1.142	1.076	1.043	0.917	0.841
2244	1.525	G2	5.44	0.218	0.819	0.913	1.013	1.077	1.142	1.184	1.211	1.261	1.282	1.255	1.251	1.208	1.148	1.081	1.048	0.915	0.841
2245	1.188	G2	5.47	0.218	0.794	0.897	0.989	1.055	1.113	1.154	1.182	1.211	1.220	1.213	1.215	1.168	1.117	1.059	1.020	0.889	0.817
2246	0.856	G2	5.38	0.218	0.773	0.881	0.967	1.021	1.084	1.127	1.145	1.169	1.180	1.169	1.177	1.145	1.094	1.020	1.008	0.856	0.794
2247	0.445	G2	5.10	0.218	0.757	0.865	0.958	1.012	1.061	1.105	1.130	1.159	1.130	1.154	1.147	1.146	1.060	1.011	1.004	0.843	0.776
2248	0.443	G2	5.10	0.218	0.736	0.849	0.938	0.994	1.057	1.094	1.105	1.137	1.137	1.129	1.133	1.115	1.050	1.008	0.967	0.845	0.766
2249	0.856	G2	5.38	0.218	0.787	0.891	1.002	1.053	1.122	1.166	1.190	1.223	1.231	1.222	1.224	1.182	1.113	1.067	1.021	0.896	0.813
2250	1.191	G2	5.48	0.218	0.793	0.906	1.006	1.064	1.135	1.183											

TABLE VI.—CONTINUED.

Rd'g no.	Re _d	Grid	Tu, %	Λ_x/d	Gauge																	
					2	3	4	5	6	7	8	9	10	11	12	13	14	15	16	17	18	
					Frössling number																	
2286	1.531	G2	4.68	0.241	0.800	0.875	0.994	1.054	1.117	1.170	1.185	1.217	1.214	1.212	1.221	1.164	1.120	1.047	1.026	0.883	0.820	
2287	1.195	G2	4.72	0.241	0.792	0.886	1.006	1.073	1.121	1.171	1.199	1.232	1.242	1.220	1.239	1.178	1.131	1.070	1.040	0.905	0.816	
2288	0.863	G2	4.64	0.241	0.778	0.891	0.986	1.043	1.101	1.142	1.167	1.192	1.186	1.188	1.201	1.183	1.098	1.042	1.020	0.878	0.797	
2289	0.444	G2	4.38	0.241	0.741	0.824	0.935	0.987	1.041	1.076	1.100	1.101	1.132	1.097	1.119	1.113	1.056	0.968	0.989	0.820	0.751	
2290	0.444	G2	4.38	0.241	0.728	0.830	0.928	0.973	1.043	1.076	1.084	1.112	1.130	1.105	1.120	1.094	1.019	0.990	0.947	0.832	0.751	
2291	0.866	G2	4.64	0.241	0.774	0.883	0.979	1.027	1.099	1.140	1.169	1.201	1.190	1.198	1.202	1.164	1.097	1.051	1.000	0.883	0.794	
2292	1.197	G2	4.72	0.241	0.789	0.896	0.998	1.049	1.118	1.172	1.192	1.228	1.229	1.225	1.284	1.184	1.122	1.070	1.021	0.898	0.812	
2293	1.537	G2	4.68	0.241	0.799	0.910	1.003	1.069	1.138	1.188	1.211	1.250	1.257	1.250	1.242	1.191	1.126	1.083	1.022	0.909	0.821	
2294	1.894	G2	4.51	0.241	0.800	0.905	1.006	1.073	1.136	1.190	1.218	1.258	1.269	1.262	1.248	1.202	1.135	1.079	1.022	0.912	0.820	
2316	1.887	G2	11.95	0.130	1.008	1.098	1.191	1.258	1.327	1.409	1.448	1.559	1.598	1.541	1.481	1.404	1.319	1.237	1.208	1.089	1.013	
2317	1.528	G2	12.08	0.130	0.988	1.054	1.176	1.242	1.311	1.394	1.436	1.542	1.560	1.511	1.457	1.374	1.289	1.221	1.185	1.074	0.988	
2318	1.192	G2	12.06	0.130	0.927	1.022	1.139	1.213	1.288	1.356	1.417	1.490	1.522	1.466	1.415	1.345	1.253	1.192	1.159	1.035	0.945	
2319	0.853	G2	11.89	0.130	0.895	0.972	1.101	1.170	1.237	1.296	1.358	1.419	1.442	1.393	1.370	1.326	1.229	1.147	1.135	0.992	0.897	
2320	0.435	G2	11.49	0.130	0.836	0.927	1.059	1.088	1.166	1.214	1.274	1.296	1.293	1.278	1.287	1.266	1.172	1.097	1.088	0.928	0.856	
2321	0.433	G2	11.48	0.130	0.840	0.943	1.055	1.109	1.187	1.227	1.262	1.313	1.331	1.293	1.303	1.261	1.168	1.115	1.076	0.949	0.857	
2322	0.855	G2	11.89	0.130	0.900	0.999	1.113	1.178	1.260	1.321	1.367	1.449	1.456	1.427	1.397	1.308	1.245	1.176	1.127	1.005	0.923	
2323	1.191	G2	12.06	0.130	0.937	1.037	1.151	1.210	1.293	1.363	1.428	1.511	1.527	1.488	1.439	1.340	1.269	1.206	1.154	1.038	0.951	
2324	1.526	G2	12.09	0.130	0.963	1.066	1.166	1.234	1.315	1.384	1.444	1.543	1.575	1.523	1.461	1.387	1.282	1.227	1.169	1.056	0.980	
2325	1.882	G2	11.96	0.130	0.981	1.076	1.174	1.239	1.320	1.385	1.456	1.558	1.600	1.547	1.480	1.384	1.292	1.237	1.176	1.064	0.995	
2346	0.446	G2	6.98	0.178	0.814	0.898	1.017	1.058	1.125	1.158	1.191	1.203	1.209	1.195	1.211	1.182	1.113	1.078	1.033	0.907	0.824	
2347	1.179	G2	7.42	0.178	0.842	0.938	1.036	1.094	1.163	1.208	1.245	1.298	1.334	1.301	1.300	1.237	1.174	1.122	1.072	0.949	0.865	
2348	1.875	G2	7.23	0.178	0.859	0.958	1.060	1.117	1.178	1.233	1.275	1.341	1.372	1.349	1.330	1.249	1.187	1.143	1.080	0.972	0.892	
1897	1.877	G3	4.14	0.122	0.817	0.930	1.019	1.089	1.150	1.200	1.236	1.286	1.287	1.270	1.253	1.199	1.126	1.080	1.024	0.948	0.820	
1898	1.522	G3	3.98	0.122	0.814	0.924	1.025	1.078	1.158	1.199	1.236	1.274	1.276	1.262	1.248	1.192	1.129	1.078	1.022	0.919	0.819	
1899	1.193	G3	3.83	0.122	0.801	0.912	1.011	1.069	1.137	1.188	1.208	1.249	1.244	1.234	1.236	1.185	1.117	1.065	1.011	0.893	0.799	
1900	0.872	G3	3.67	0.122	0.784	0.890	0.993	1.052	1.119	1.156	1.178	1.219	1.207	1.192	1.200	1.152	1.094	1.047	0.997	0.907	0.785	
1901	0.441	G3	3.44	0.122	0.739	0.848	0.939	1.002	1.046	1.086	1.095	1.131	1.125	1.106	1.129	1.086	1.032	0.992	0.947	0.821	0.734	
1902	1.871	G3	4.14	0.122	0.824	0.943	1.029	1.097	1.166	1.212	1.250	1.300	1.296	1.284	1.268	1.219	1.139	1.094	1.039	0.926	0.824	
1903	1.512	G3	3.98	0.122	0.826	0.939	1.031	1.107	1.162	1.217	1.238	1.290	1.277	1.269	1.262	1.223	1.137	1.086	1.040	0.886	0.822	
1904	1.185	G3	3.82	0.122	0.816	0.923	1.022	1.080	1.145	1.198	1.224	1.263	1.252	1.242	1.244	1.187	1.110	1.080	1.028	0.876	0.817	
1905	0.860	G3	3.66	0.122	0.798	0.897	1.001	1.058	1.120	1.157	1.177	1.223	1.205	1.210	1.206	1.173	1.094	1.048	1.006	0.841	0.797	
1906	0.451	G3	3.44	0.122	0.739	0.854	0.936	0.994	1.048	1.093	1.096	1.155	1.126	1.098	1.138	1.095	1.037	0.991	0.960	0.825	0.746	
1907	1.868	G3	4.14	0.122	0.854	0.946	1.043	1.109	1.175	1.222	1.265	1.318	1.300	1.286	1.276	1.218	1.169	1.109	1.049	0.867	0.850	
1908	1.522	G3	3.98	0.122	0.845	0.969	1.046	1.138	1.172	1.229	1.262	1.309	1.295	1.279	1.278	1.203	1.166	1.098	1.059	0.933	0.844	
1909	1.188	G3	3.83	0.122	0.831	0.925	1.027	1.108	1.143	1.223	1.227	1.268	1.257	1.242	1.251	1.179	1.138	1.075	1.047	0.888	0.818	
1910	0.858	G3	3.66	0.122	0.801	0.892	0.979	1.074	1.105	1.159	1.169	1.205	1.190	1.183	1.198	1.151	1.081	1.029	1.010	0.976	0.783	
1911	0.440	G3	3.44	0.122	0.769	0.838	0.940	1.004	1.032	1.085	1.092	1.132	1.128	1.097	1.134	1.120	1.007	0.977	0.947	0.770	0.726	
1912	1.867	G3	3.66	0.132	0.817	0.930	1.018	1.087	1.151	1.199	1.238	1.286	1.285	1.280	1.264	1.213	1.145	1.095	1.033	0.857	0.830	
1913	1.523	G3	3.51	0.132	0.806	0.917	1.016	1.082	1.152	1.197	1.237	1.274	1.272	1.256	1.262	1.202	1.136	1.086	1.029	0.846	0.831	
1914	1.182	G3	3.36	0.132	0.793	0.906	1.001	1.061	1.126	1.170	1.193	1.241	1.226	1.225	1.227	1.176	1.118	1.067	1.011	0.890	0.800	
1915	0.853	G3	3.21	0.132	0.771	0.884	0.975	1.041	1.107	1.137	1.165	1.198	1.191	1.177	1.192	1.145	1.081	1.041	0.990	0.867	0.781	
1916	0.438	G3	3.01	0.132	0.724	0.822	0.925	0.973	1.037	1.062	1.078	1.110	1.113	1.090	1.106	1.073	1.008	0.973	0.929	0.755	0.733	
1917	1.514	G3	3.51	0.132	0.811	0.933	1.019	1.088	1.151	1.208	1.230	1.282	1.271	1.260	1.261	1.200	1.144	1.091	1.033	0.826	0.818	
1918	1.864	G3	3.66	0.132	0.819	0.928	1.030	1.099	1.153	1.205	1.241	1.288	1.285	1.280	1.270	1.209	1.138	1.098	1.038	0.958	0.838	
1919	1.185	G3	3.36	0.132	0.791	0.897	0.988	1.049	1.114	1.157	1.189	1.229	1.218	1.204	1.222	1.160	1.104	1.052	1.007	0.898	0.796	
1920	0.850	G3	3.21	0.132	0.794	0.882	0.996	1.054	1.109	1.150	1.179	1.218	1.204	1.188	1.204	1.169	1.101	1.045	0.999	0.896	0.794	
1921	0.450	G3	3.02	0.132	0.737	0.841	0.934	0.975	1.044	1.069	1.096	1.129	1.115	1.096	1.120	1.090	1.024	0.975	0.949	0.831	0.742	
1922	1.522	G3	3.51	0.132	0.820	0.917	1.020	1.090	1													

TABLE VI.—CONTINUED.

Rd'g no.	Re _d	Grid	Tu, %	A _x /d	Gauge Frössling number																
					2	3	4	5	6	7	8	9	10	11	12	13	14	15	16	17	18
1937	0.865	G3	4.33	0.110	0.801	0.904	1.008	1.065	1.123	1.179	1.194	1.225	1.232	1.237	1.229	1.184	1.122	1.062	1.023	0.854	0.810
1938	0.442	G3	4.06	0.110	0.748	0.841	0.953	1.005	1.053	1.103	1.114	1.128	1.135	1.143	1.138	1.103	1.049	1.006	0.963	0.760	0.769
1939	1.873	G3	4.83	0.110	0.863	0.959	1.059	1.131	1.176	1.260	1.284	1.313	1.344	1.327	1.309	1.245	1.182	1.111	1.060	0.825	0.861
1940	1.528	G3	4.68	0.110	0.859	0.963	1.050	1.142	1.180	1.251	1.273	1.307	1.331	1.315	1.292	1.220	1.168	1.110	1.081	0.886	0.865
1941	1.192	G3	4.51	0.110	0.826	0.946	1.022	1.106	1.157	1.208	1.245	1.263	1.296	1.278	1.269	1.200	1.148	1.095	1.037	0.816	0.830
1942	0.858	G3	4.33	0.110	0.817	0.906	1.019	1.079	1.125	1.192	1.204	1.219	1.242	1.226	1.231	1.168	1.123	1.065	1.024	0.756	0.825
1943	0.446	G3	4.07	0.110	0.759	0.824	0.958	1.013	1.033	1.098	1.134	1.128	1.137	1.123	1.140	1.100	1.046	1.000	0.937	0.902	0.740
2032	1.889	G3	7.88	0.080	0.953	1.039	1.156	1.232	1.274	1.345	1.416	1.485	1.538	1.491	1.423	1.358	1.289	1.204	1.167	1.034	0.970
2033	1.518	G3	7.79	0.080	0.929	1.025	1.136	1.202	1.270	1.346	1.389	1.469	1.517	1.451	1.417	1.350	1.284	1.193	1.148	1.019	0.944
2034	1.198	G3	7.62	0.080	0.911	1.009	1.111	1.186	1.236	1.309	1.375	1.421	1.476	1.414	1.380	1.346	1.248	1.167	1.134	1.000	0.904
2035	0.853	G3	7.35	0.080	0.890	0.972	1.084	1.170	1.211	1.285	1.340	1.383	1.408	1.376	1.351	1.308	1.228	1.136	1.115	0.955	0.888
2036	0.432	G3	6.90	0.080	0.830	0.886	1.036	1.083	1.105	1.191	1.209	1.222	1.243	1.205	1.240	1.179	1.148	1.037	1.063	0.863	0.818
2037	0.433	G3	6.91	0.080	0.800	0.905	1.012	1.063	1.135	1.178	1.210	1.239	1.235	1.233	1.225	1.192	1.121	1.062	1.023	0.886	0.817
2038	0.860	G3	7.36	0.080	0.875	0.977	1.084	1.149	1.220	1.285	1.325	1.387	1.405	1.379	1.359	1.270	1.208	1.157	1.094	0.970	0.875
2039	1.184	G3	7.61	0.080	0.887	0.990	1.101	1.165	1.239	1.307	1.351	1.429	1.465	1.421	1.392	1.314	1.243	1.165	1.118	0.988	0.900
2040	1.522	G3	7.79	0.080	0.911	1.017	1.126	1.186	1.260	1.331	1.383	1.469	1.512	1.472	1.431	1.356	1.258	1.198	1.143	1.017	0.930
2041	1.882	G3	7.88	0.080	0.918	1.028	1.126	1.195	1.269	1.338	1.391	1.488	1.532	1.491	1.433	1.362	1.272	1.202	1.139	1.022	0.932
2042	0.440	G3	10.56	0.062	0.881	0.985	1.109	1.165	1.230	1.295	1.229	1.237	1.274	1.326	1.403	1.383	1.277	1.197	1.137	0.975	0.886
2043	0.439	G3	10.56	0.062	0.880	0.997	1.117	1.185	1.252	1.311	1.268	1.245	1.257	1.298	1.385	1.369	1.285	1.196	1.142	0.980	0.891
2044	1.879	G3	6.36	0.092	0.893	0.998	1.090	1.158	1.205	1.281	1.325	1.390	1.432	1.379	1.333	1.294	1.218	1.138	1.110	0.967	0.908
2045	1.521	G3	6.23	0.092	0.906	0.993	1.112	1.180	1.222	1.328	1.359	1.405	1.453	1.393	1.370	1.339	1.247	1.161	1.123	0.997	0.907
2046	1.180	G3	6.05	0.092	0.883	0.953	1.087	1.154	1.187	1.274	1.314	1.369	1.391	1.351	1.335	1.286	1.211	1.128	1.113	0.951	0.900
2047	0.852	G3	5.83	0.092	0.859	0.931	1.063	1.124	1.162	1.250	1.265	1.304	1.340	1.291	1.284	1.247	1.175	1.102	1.074	0.943	0.861
2048	0.441	G3	5.48	0.092	0.794	0.901	1.001	1.047	1.087	1.151	1.169	1.177	1.228	1.156	1.179	1.174	1.099	1.022	1.025	0.858	0.801
2049	0.440	G3	5.48	0.092	0.774	0.879	0.986	1.032	1.090	1.105	1.209	1.174	1.192	1.174	1.189	1.180	1.096	1.030	0.993	0.867	0.790
2050	0.861	G3	5.83	0.092	0.828	0.936	1.049	1.104	1.167	1.230	1.265	1.317	1.328	1.310	1.294	1.251	1.175	1.117	1.060	0.937	0.851
2051	1.186	G3	6.05	0.092	0.855	0.953	1.060	1.130	1.196	1.253	1.306	1.363	1.388	1.355	1.330	1.289	1.184	1.133	1.078	0.953	0.865
2052	1.514	G3	6.23	0.092	0.875	0.971	1.085	1.147	1.221	1.282	1.329	1.404	1.434	1.395	1.362	1.300	1.210	1.151	1.087	0.976	0.882
2053	1.870	G3	6.36	0.092	0.870	0.974	1.075	1.147	1.215	1.282	1.321	1.411	1.437	1.410	1.365	1.298	1.219	1.146	1.091	0.972	0.887
2054	1.875	G3	8.36	0.077	0.938	1.039	1.143	1.206	1.273	1.336	1.375	1.467	1.529	1.509	1.466	1.399	1.295	1.231	1.157	1.045	0.956
2055	1.526	G3	8.29	0.077	0.919	1.022	1.128	1.198	1.262	1.326	1.363	1.441	1.495	1.486	1.457	1.381	1.291	1.220	1.147	1.034	0.943
2056	1.193	G3	8.12	0.077	0.892	1.007	1.103	1.164	1.232	1.281	1.321	1.392	1.450	1.434	1.430	1.362	1.270	1.191	1.128	0.997	0.911
2057	0.844	G3	7.84	0.077	0.868	0.984	1.080	1.137	1.205	1.253	1.280	1.335	1.367	1.369	1.373	1.328	1.230	1.161	1.100	0.975	0.886
2058	0.440	G3	7.38	0.077	0.809	0.908	1.013	1.062	1.120	1.157	1.182	1.209	1.229	1.239	1.251	1.238	1.149	1.089	1.035	0.904	0.819
2060	0.447	G3	7.38	0.077	0.845	0.899	1.050	1.097	1.140	1.190	1.191	1.222	1.244	1.230	1.294	1.291	1.176	1.090	1.074	0.914	0.836
2061	0.864	G3	7.86	0.077	0.889	0.955	1.094	1.153	1.198	1.262	1.293	1.337	1.381	1.362	1.388	1.347	1.257	1.160	1.112	0.992	0.880
2062	1.184	G3	8.11	0.077	0.921	0.997	1.119	1.191	1.238	1.299	1.333	1.391	1.458	1.411	1.431	1.379	1.296	1.177	1.139	1.001	0.924
2063	1.523	G3	8.29	0.077	0.935	1.037	1.149	1.210	1.266	1.328	1.353	1.431	1.490	1.473	1.448	1.382	1.292	1.212	1.163	1.028	0.946
2064	1.885	G3	8.36	0.077	0.965	1.048	1.160	1.235	1.276	1.345	1.371	1.466	1.531	1.497	1.471	1.397	1.310	1.221	1.195	1.047	0.971
2349	1.874	G3	4.14	0.122	0.816	0.923	1.020	1.085	1.149	1.208	1.245	1.294	1.299	1.286	1.268	1.208	1.138	1.093	1.029	0.923	0.830
2350	1.172	G3	3.82	0.122	0.799	0.896	1.005	1.065	1.132	1.183	1.208	1.244	1.242	1.238	1.242	1.176	1.133	1.068	1.017	0.896	0.816
2351	0.437	G3	3.44	0.122	0.734	0.830	0.924	0.967	1.029	1.069	1.079	1.106	1.112	1.091	1.106	1.064	0.999	0.975	0.926	0.815	0.737
1846	1.910	G4	2.49	0.099	0.780	0.885	0.988	1.055	1.119	1.175	1.201	1.242	1.231	1.225	1.173	1.095	1.056	0.991	0.885	0.790	
1847	1.731	G4	2.51	0.099	0.786	0.889	0.996	1.062	1.124	1.176	1.206	1.247	1.242	1.231	1.229	1.174	1.109	1.063	0.999	0.894	0.796
1848	1.542	G4	2.51	0.099	0.776	0.886	0.983	1.053	1.116	1.172	1.193	1.233	1.233	1.217	1.214	1.167	1.095	1.056	0.990	0.882	0.791
1849	1.377	G4	2.50	0.099	0.767	0.873	0.975	1.040	1.102	1.146	1.175	1.212	1.209	1.206	1.202	1.159	1.087	1.048	0.989	0.879	0.784
1850	1.195	G4	2.47	0.099	0.770	0.872	0.971	1.038	1.097	1.150	1.172	1.201	1.202	1.185	1.187	1.142	1.076	1.033	0.982	0.872	0.773
1851	1.029	G4	2.42	0.099	0.756	0.866	0.959	1.021	1.088	1.133	1.157	1.197	1.189	1.171	1.179	1.128	1.066	1.026	0.965	0.859	0.769
1852	0.875	G4	2.37	0.099	0.749	0.855	0.942														

TABLE VI.—CONTINUED.

Rdg no.	Re _d	Grid	Tu %	A _{x/d}	Gauge Frössling number																	
					2	3	4	5	6	7	8	9	10	11	12	13	14	15	16	17	18	
1865	0.425	G4	2.15	0.099	0.691	0.734	0.868	0.912	0.981	0.991	1.014	1.020	1.040	0.995	1.033	1.009	0.952	0.915	0.876	0.765	0.696	
1868	1.920	G4	2.22	0.108	0.765	0.882	0.976	1.042	1.111	1.149	1.184	1.213	1.213	1.197	1.200	1.146	1.088	1.040	0.985	0.874	0.783	
1869	1.540	G4	2.24	0.108	0.770	0.873	0.969	1.031	1.097	1.136	1.161	1.186	1.186	1.169	1.190	1.138	1.082	1.036	0.986	0.867	0.782	
1870	1.200	G4	2.20	0.108	0.752	0.864	0.957	1.018	1.076	1.112	1.135	1.160	1.163	1.149	1.160	1.119	1.065	1.020	0.975	0.856	0.769	
1871	0.866	G4	2.11	0.108	0.740	0.839	0.936	1.000	1.043	1.075	1.114	1.114	1.124	1.106	1.121	1.089	1.031	0.995	0.954	0.832	0.746	
1872	0.439	G4	1.93	0.108	0.668	0.774	0.854	0.907	0.960	0.984	1.013	1.020	1.041	1.007	1.031	1.002	0.943	0.913	0.876	0.755	0.675	
1873	1.918	G4	2.22	0.108	0.780	0.883	0.982	1.049	1.106	1.139	1.174	1.204	1.209	1.196	1.208	1.153	1.103	1.057	1.004	0.881	0.800	
1874	1.532	G4	2.24	0.108	0.769	0.880	0.981	1.029	1.102	1.135	1.170	1.189	1.193	1.174	1.197	1.144	1.088	1.040	0.995	0.871	0.783	
1875	1.200	G4	2.20	0.108	0.753	0.870	0.965	1.024	1.081	1.119	1.146	1.163	1.162	1.151	1.168	1.117	1.071	1.031	0.981	0.857	0.774	
1876	0.883	G4	2.11	0.108	0.744	0.834	0.940	0.999	1.043	1.084	1.097	1.121	1.128	1.103	1.125	1.094	1.034	0.997	0.949	0.836	0.753	
1877	0.450	G4	1.93	0.108	0.676	0.760	0.862	0.903	0.980	0.968	1.021	1.018	1.039	1.033	1.029	0.993	0.945	0.937	0.874	0.750	0.684	
1878	1.914	G4	2.22	0.108	0.794	0.881	0.995	1.058	1.109	1.156	1.184	1.199	1.221	1.184	1.223	1.154	1.105	1.054	1.011	0.877	0.803	
1879	1.528	G4	2.24	0.108	0.761	0.895	0.990	1.038	1.115	1.139	1.178	1.189	1.212	1.168	1.195	1.156	1.081	1.052	1.007	0.872	0.798	
1880	1.194	G4	2.19	0.108	0.771	0.875	0.963	1.029	1.078	1.125	1.151	1.160	1.178	1.133	1.182	1.129	1.085	1.023	0.987	0.853	0.788	
1881	0.867	G4	2.11	0.108	0.754	0.838	0.934	1.010	1.050	1.082	1.114	1.118	1.130	1.101	1.132	1.086	1.052	0.988	0.963	0.832	0.758	
1882	0.455	G4	1.93	0.108	0.665	0.773	0.874	0.944	0.972	0.987	1.048	1.033	1.064	1.006	1.047	1.051	0.944	0.932	0.901	0.760	0.699	
1883	1.903	G4	2.85	0.090	0.792	0.912	0.998	1.064	1.140	1.190	1.222	1.262	1.268	1.241	1.239	1.179	1.121	1.066	1.008	0.893	0.809	
1884	1.544	G4	2.88	0.090	0.781	0.898	0.998	1.057	1.132	1.177	1.217	1.250	1.245	1.225	1.228	1.173	1.099	1.061	0.998	0.894	0.794	
1885	1.202	G4	2.84	0.090	0.778	0.885	0.984	1.059	1.119	1.170	1.195	1.228	1.227	1.204	1.203	1.159	1.100	1.051	0.991	0.880	0.792	
1886	0.863	G4	2.72	0.090	0.755	0.861	0.953	1.024	1.086	1.117	1.168	1.172	1.181	1.149	1.172	1.121	1.060	1.017	0.969	0.850	0.764	
1887	0.450	G4	2.48	0.090	0.701	0.800	0.898	0.950	1.011	1.042	1.065	1.075	1.079	1.046	1.064	1.051	0.971	0.953	0.907	0.798	0.710	
1888	1.899	G4	2.85	0.090	0.800	0.905	1.008	1.071	1.138	1.203	1.228	1.264	1.267	1.237	1.244	1.173	1.110	1.069	1.013	0.895	0.807	
1889	1.528	G4	2.88	0.090	0.796	0.908	1.001	1.067	1.142	1.192	1.224	1.251	1.251	1.227	1.234	1.182	1.107	1.068	1.012	0.893	0.802	
1890	1.191	G4	2.83	0.090	0.781	0.903	0.990	1.058	1.120	1.163	1.205	1.232	1.223	1.201	1.210	1.173	1.085	1.051	0.990	0.880	0.790	
1891	0.870	G4	2.72	0.090	0.760	0.868	0.963	1.039	1.090	1.141	1.163	1.184	1.198	1.160	1.177	1.116	1.063	1.031	0.973	0.862	0.770	
1892	0.452	G4	2.48	0.090	0.715	0.799	0.908	0.964	1.013	1.052	1.071	1.076	1.087	1.044	1.087	1.019	0.999	0.955	0.922	0.804	0.719	
1893	1.899	G4	2.85	0.090	0.808	0.931	1.016	1.095	1.149	1.205	1.237	1.264	1.282	1.233	1.256	1.186	1.126	1.073	1.021	0.901	0.820	
1894	1.533	G4	2.88	0.090	0.806	0.896	1.012	1.078	1.144	1.191	1.234	1.263	1.256	1.219	1.242	1.195	1.122	1.066	1.025	0.897	0.815	
1895	1.206	G4	2.84	0.090	0.811	0.905	1.010	1.081	1.145	1.200	1.215	1.248	1.261	1.211	1.232	1.197	1.110	1.068	1.032	0.897	0.808	
1896	0.445	G4	3.11	0.076	0.724	0.826	0.930	0.981	1.036	1.075	1.083	1.112	1.120	1.100	1.125	1.084	1.031	0.985	0.947	0.821	0.736	
1898	0.864	G4	3.45	0.076	0.780	0.887	0.981	1.042	1.100	1.140	1.164	1.199	1.207	1.202	1.222	1.179	1.127	1.069	1.018	0.897	0.802	
1899	1.200	G4	3.59	0.076	0.795	0.912	1.003	1.060	1.122	1.176	1.202	1.242	1.255	1.252	1.260	1.212	1.150	1.091	1.035	0.920	0.793	
1900	1.530	G4	3.64	0.076	0.810	0.911	1.011	1.073	1.140	1.194	1.222	1.275	1.293	1.285	1.288	1.233	1.165	1.107	1.049	0.926	0.837	
1901	1.894	G4	3.57	0.076	0.814	0.925	1.025	1.080	1.147	1.190	1.223	1.279	1.296	1.294	1.287	1.243	1.169	1.114	1.051	0.938	0.841	
1902	1.890	G4	3.57	0.076	0.822	0.938	1.028	1.088	1.149	1.197	1.232	1.286	1.302	1.297	1.293	1.238	1.180	1.114	1.059	0.942	0.850	
1903	1.527	G4	3.64	0.076	0.817	0.923	1.027	1.080	1.148	1.192	1.237	1.286	1.300	1.294	1.301	1.245	1.173	1.115	1.055	0.937	0.835	
1904	1.191	G4	3.59	0.076	0.802	0.913	1.000	1.067	1.134	1.173	1.209	1.251	1.259	1.254	1.271	1.214	1.155	1.100	1.040	0.917	0.825	
1905	0.864	G4	3.45	0.076	0.790	0.880	0.994	1.046	1.106	1.143	1.177	1.208	1.208	1.207	1.233	1.196	1.135	1.078	1.031	0.905	0.811	
1906	0.447	G4	3.12	0.076	0.724	0.835	0.928	0.982	1.046	1.070	1.096	1.109	1.130	1.100	1.137	1.075	1.048	0.982	0.956	0.829	0.740	
1907	0.449	G4	3.12	0.076	0.748	0.860	0.923	0.999	1.047	1.060	1.095	1.106	1.144	1.076	1.143	1.079	1.053	0.973	0.964	0.816	0.749	
1908	0.865	G4	3.45	0.076	0.813	0.909	0.997	1.069	1.112	1.150	1.193	1.215	1.235	1.218	1.245	1.190	1.162	1.076	1.047	0.910	0.822	
1909	1.190	G4	3.59	0.076	0.830	0.931	1.012	1.081	1.177	1.183	1.222	1.260	1.283	1.272	1.293	1.215	1.190	1.101	1.070	0.932	0.840	
1910	1.523	G4	3.64	0.076	0.843	0.952	1.081	1.118	1.182	1.231	1.301	1.326	1.343	1.324	1.363	1.295	1.224	1.170	1.104	0.960	0.876	
1911	1.881	G4	3.58	0.076	0.871	0.965	1.056	1.127	1.185	1.226	1.267	1.300	1.319	1.316	1.319	1.267	1.208	1.141	1.091	0.964	0.872	
1912	0.441	G4	3.11	0.076	0.701	0.818	0.930	0.958	1.034	1.045	1.107	1.058	1.120	1.092	1.124	1.081	1.034	0.943	0.953	0.803	0.717	
1913	1.186	G4	3.59	0.076	0.830	0.920	1.015	1.094	1.143	1.188	1.229	1.270	1.270	1.263	1.282	1.225	1.187	1.109	1.064	0.929	0.831	
1914	1.873	G4	3.58	0.076	0.850	0.970	1.044	1.125	1.169	1.218	1.259	1.311	1.324	1.285	1.305	1.258	1.212	1.125	1.088	0.955	0.858	
1915	1.876	G4	4.60	0.063	0.838	0.944	1.050	1.116	1.195	1.248	1.303	1.373	1.397	1.361	1.324	1.243	1.170	1.111	1.058	0.943	0.853	
1916	1.517	G4	4.72	0.063	0.842																	

TABLE VI.—CONTINUED.

Rd'g no.	Re _d	Grid	Tu. %	Δ_x/d	Gauge Frössling number																	
					2	3	4	5	6	7	8	9	10	11	12	13	14	15	16	17	18	
1999	0.432	G4	4.00	0.063	0.785	0.884	0.971	1.046	1.083	1.144	1.194	1.179	1.216	1.146	1.192	1.119	1.107	0.981	1.011	0.848	0.768	
2000	1.882	G4	6.14	0.050	0.903	1.012	1.113	1.187	1.246	1.317	1.365	1.451	1.529	1.460	1.405	1.350	1.255	1.154	1.116	0.996	0.906	
2001	1.519	G4	6.34	0.050	0.897	1.006	1.101	1.187	1.249	1.319	1.370	1.452	1.487	1.468	1.409	1.341	1.266	1.162	1.128	0.993	0.902	
2002	1.184	G4	6.29	0.050	0.866	0.987	1.078	1.158	1.213	1.276	1.349	1.411	1.457	1.431	1.376	1.315	1.227	1.143	1.099	0.958	0.869	
2003	0.847	G4	6.01	0.050	0.851	0.946	1.060	1.133	1.183	1.262	1.300	1.337	1.390	1.345	1.356	1.267	1.197	1.098	1.085	0.939	0.852	
2004	0.442	G4	5.37	0.050	0.812	0.903	1.010	1.071	1.149	1.181	1.229	1.267	1.275	1.248	1.256	1.210	1.116	1.046	1.034	0.863	0.811	
2005	0.441	G4	5.37	0.050	0.793	0.903	1.002	1.066	1.141	1.188	1.221	1.258	1.269	1.250	1.247	1.187	1.112	1.049	1.016	0.880	0.804	
2006	0.862	G4	6.03	0.050	0.839	0.955	1.058	1.121	1.195	1.253	1.281	1.346	1.378	1.367	1.349	1.282	1.191	1.116	1.066	0.943	0.848	
2007	1.194	G4	6.30	0.050	0.853	0.964	1.081	1.138	1.216	1.289	1.331	1.410	1.454	1.439	1.396	1.309	1.208	1.145	1.082	0.962	0.873	
2008	1.524	G4	6.34	0.050	0.875	0.988	1.094	1.157	1.245	1.304	1.343	1.440	1.480	1.460	1.408	1.321	1.228	1.165	1.099	0.980	0.887	
2009	1.876	G4	6.14	0.050	0.883	0.991	1.098	1.168	1.241	1.317	1.359	1.460	1.525	1.484	1.422	1.333	1.231	1.166	1.107	0.987	0.898	
2010	1.880	G4	4.30	0.066	0.872	0.971	1.080	1.140	1.185	1.262	1.283	1.341	1.375	1.344	1.343	1.290	1.220	1.141	1.113	0.955	0.917	
2011	1.535	G4	4.39	0.066	0.867	0.951	1.059	1.136	1.182	1.251	1.287	1.343	1.357	1.331	1.346	1.280	1.229	1.142	1.107	0.970	0.886	
2012	1.193	G4	4.35	0.066	0.845	0.939	1.047	1.106	1.164	1.218	1.244	1.292	1.326	1.277	1.309	1.256	1.194	1.116	1.080	0.951	0.859	
2013	0.863	G4	4.17	0.066	0.814	0.911	1.027	1.082	1.126	1.188	1.206	1.259	1.275	1.229	1.252	1.239	1.171	1.085	1.053	0.922	0.838	
2014	0.443	G4	3.75	0.066	0.772	0.874	0.961	1.035	1.071	1.139	1.130	1.154	1.173	1.151	1.158	1.138	1.050	1.023	0.982	0.859	0.785	
2015	0.444	G4	3.75	0.066	0.755	0.872	0.970	1.022	1.081	1.106	1.131	1.160	1.165	1.137	1.170	1.120	1.072	1.014	0.979	0.853	0.765	
2016	0.864	G4	4.17	0.066	0.797	0.914	1.012	1.066	1.132	1.176	1.196	1.246	1.249	1.240	1.265	1.199	1.156	1.097	1.044	0.929	0.828	
2017	1.192	G4	4.35	0.066	0.822	0.929	1.034	1.093	1.162	1.205	1.236	1.295	1.308	1.296	1.299	1.244	1.174	1.116	1.058	0.948	0.847	
2018	1.526	G4	4.39	0.066	0.829	0.944	1.035	1.103	1.170	1.218	1.255	1.319	1.335	1.319	1.314	1.257	1.196	1.132	1.069	0.958	0.858	
2019	1.878	G4	4.30	0.066	0.840	0.954	1.045	1.108	1.173	1.233	1.268	1.331	1.359	1.341	1.324	1.274	1.192	1.134	1.073	0.961	0.868	
2021	1.880	G4	6.14	0.050	1.136	1.213	1.321	1.413	1.459	1.532	1.545	1.563	1.582	1.639	1.666	1.600	1.494	1.392	1.334	1.188	1.149	
2022	1.519	G4	6.34	0.050	1.073	1.175	1.277	1.359	1.423	1.482	1.493	1.521	1.558	1.594	1.620	1.535	1.481	1.347	1.291	1.152	1.076	
2023	1.195	G4	6.30	0.050	1.032	1.131	1.241	1.327	1.390	1.464	1.463	1.476	1.495	1.545	1.572	1.556	1.424	1.317	1.263	1.109	1.021	
2024	0.854	G4	6.02	0.050	0.984	1.043	1.193	1.284	1.348	1.441	1.416	1.392	1.432	1.442	1.511	1.502	1.376	1.262	1.220	1.054	0.972	
2025	0.440	G4	5.37	0.050	0.924	1.004	1.116	1.200	1.263	1.305	1.276	1.256	1.276	1.302	1.399	1.355	1.303	1.196	1.154	0.990	0.866	
2026	0.437	G4	5.36	0.050	0.893	1.000	1.121	1.190	1.267	1.309	1.273	1.250	1.247	1.307	1.398	1.364	1.284	1.212	1.136	0.986	0.890	
2027	0.852	G4	6.02	0.050	0.947	1.085	1.189	1.270	1.353	1.412	1.403	1.411	1.417	1.463	1.510	1.456	1.361	1.271	1.201	1.057	0.961	
2028	1.196	G4	6.30	0.050	1.001	1.120	1.221	1.300	1.385	1.440	1.436	1.464	1.494	1.546	1.591	1.508	1.414	1.314	1.238	1.100	1.005	
2029	1.515	G4	6.34	0.050	1.051	1.155	1.264	1.342	1.424	1.485	1.488	1.512	1.556	1.614	1.640	1.554	1.455	1.355	1.277	1.143	1.051	
2030	1.871	G4	6.15	0.050	1.083	1.181	1.289	1.367	1.446	1.507	1.517	1.552	1.588	1.642	1.656	1.574	1.466	1.375	1.300	1.168	1.085	
2065	1.902	G5	1.71	0.066	0.867	0.972	1.080	1.154	1.195	1.288	1.263	1.317	1.320	1.313	1.310	1.264	1.211	1.135	1.103	0.958	0.882	
2066	1.520	G5	1.71	0.066	0.850	0.961	1.079	1.130	1.180	1.261	1.261	1.300	1.297	1.296	1.292	1.243	1.203	1.117	1.080	0.952	0.860	
2067	1.184	G5	1.86	0.071	0.845	0.930	1.044	1.126	1.170	1.220	1.233	1.274	1.280	1.263	1.261	1.234	1.186	1.102	1.066	0.931	0.843	
2068	0.851	G5	1.86	0.081	0.817	0.911	1.009	1.093	1.119	1.210	1.196	1.241	1.248	1.219	1.219	1.183	1.155	1.068	1.046	0.894	0.818	
2069	0.430	G5	2.20	0.102	0.758	0.813	0.931	1.016	1.067	1.070	1.130	1.147	1.116	1.131	1.137	1.096	1.047	0.995	0.982	0.823	0.750	
2070	0.426	G5	2.20	0.103	0.732	0.830	0.948	0.990	1.064	1.100	1.118	1.158	1.145	1.129	1.138	1.113	1.045	1.005	0.961	0.837	0.745	
2071	0.845	G5	1.86	0.081	0.805	0.917	1.023	1.082	1.152	1.194	1.218	1.253	1.236	1.232	1.244	1.203	1.150	1.090	1.041	0.913	0.826	
2072	1.189	G5	1.86	0.071	0.827	0.942	1.049	1.110	1.182	1.227	1.235	1.288	1.292	1.277	1.279	1.232	1.177	1.115	1.062	0.939	0.850	
2073	1.519	G5	1.71	0.066	0.837	0.964	1.060	1.126	1.191	1.239	1.269	1.311	1.311	1.304	1.298	1.261	1.197	1.131	1.077	0.953	0.860	
2074	1.893	G5	1.71	0.066	0.847	0.961	1.068	1.132	1.202	1.249	1.278	1.318	1.325	1.318	1.313	1.269	1.198	1.134	1.079	0.960	0.870	
2075	1.895	G5	1.61	0.068	0.845	0.945	1.065	1.136	1.168	1.260	1.243	1.292	1.284	1.280	1.285	1.237	1.173	1.112	1.076	0.947	0.861	
2076	1.515	G5	1.61	0.068	0.852	0.958	1.062	1.130	1.174	1.252	1.245	1.299	1.281	1.293	1.282	1.240	1.206	1.115	1.081	0.950	0.858	
2077	1.185	G5	1.75	0.073	0.824	0.927	1.038	1.098	1.149	1.217	1.222	1.252	1.248	1.233	1.253	1.214	1.145	1.086	1.055	0.914	0.836	
2078	0.857	G5	1.75	0.083	0.803	0.920	1.030	1.077	1.140	1.186	1.207	1.231	1.250	1.219	1.226	1.208	1.121	1.075	1.047	0.896	0.830	
2079	0.437	G5	2.04	0.103	0.730	0.826	0.948	0.996	1.053	1.087	1.101	1.141	1.128	1.107	1.140	1.099	1.053	0.982	0.969	0.814	0.746	
2080	0.435	G5	2.04	0.103	0.730	0.827	0.947	0.987	1.043	1.106	1.089	1.150	1.137	1.124	1.131	1.109	1.031	0.991	0.950	0.826	0.752	
2081	0.851	G5	1.75	0.083	0.793	0.906	1.006	1.070	1.131	1.174	1.196	1.232	1.231	1.218	1.224	1.184	1.130	1.064	1.025	0.905	0.813	
2082	1.182	G5	1.75	0.073	0.81																	

TABLE VI.—CONCLUDED.

Rd'g no.	Re _d	Grid	Tu, %	Λ_x/d	Gauge																	
					2	3	4	5	6	7	8	9	10	11	12	13	14	15	16	17	18	
Frössling number																						
2097	1.924	G5	1.86	0.065	0.904	0.996	1.114	1.183	1.243	1.298	1.323	1.374	1.368	1.368	1.349	1.313	1.240	1.180	1.134	1.000	0.909	
2098	1.532	G5	1.86	0.063	0.884	0.992	1.107	1.172	1.228	1.312	1.318	1.355	1.359	1.345	1.335	1.293	1.221	1.170	1.123	0.994	0.900	
2099	1.199	G5	2.01	0.067	0.872	0.971	1.095	1.150	1.211	1.281	1.289	1.332	1.344	1.328	1.316	1.282	1.221	1.147	1.105	0.977	0.880	
2100	0.860	G5	2.01	0.078	0.831	0.946	1.058	1.114	1.165	1.245	1.263	1.279	1.288	1.258	1.274	1.241	1.180	1.112	1.072	0.939	0.845	
2101	0.439	G5	2.43	0.101	0.780	0.861	0.990	1.032	1.086	1.149	1.161	1.172	1.189	1.150	1.179	1.156	1.092	1.022	0.994	0.861	0.789	
2102	0.434	G5	2.43	0.101	0.763	0.859	0.982	1.026	1.098	1.124	1.162	1.180	1.194	1.169	1.181	1.158	1.087	1.041	0.999	0.866	0.781	
2103	0.868	G5	2.01	0.078	0.827	0.929	1.041	1.101	1.173	1.219	1.241	1.279	1.266	1.269	1.270	1.235	1.152	1.121	1.056	0.939	0.847	
2104	1.193	G5	2.01	0.068	0.844	0.951	1.065	1.131	1.200	1.251	1.271	1.318	1.308	1.303	1.301	1.262	1.192	1.138	1.078	0.964	0.866	
2105	1.522	G5	1.86	0.063	0.855	0.983	1.085	1.146	1.220	1.268	1.291	1.347	1.341	1.340	1.329	1.265	1.206	1.157	1.099	0.977	0.882	
2106	1.915	G5	1.86	0.065	0.861	0.975	1.083	1.145	1.221	1.278	1.304	1.357	1.363	1.348	1.330	1.287	1.209	1.160	1.094	0.981	0.891	
2107	1.916	G5	1.26	0.074	0.808	0.900	1.011	1.057	1.130	1.175	1.194	1.216	1.221	1.210	1.213	1.168	1.112	1.057	1.018	0.891	0.814	
2108	1.527	G5	1.26	0.076	0.805	0.870	0.991	1.051	1.100	1.149	1.176	1.194	1.203	1.183	1.193	1.155	1.107	1.040	1.008	0.877	0.800	
2109	1.191	G5	1.39	0.082	0.770	0.876	0.968	1.029	1.073	1.125	1.149	1.175	1.171	1.156	1.173	1.135	1.075	1.017	0.986	0.860	0.775	
2110	0.859	G5	1.39	0.090	0.738	0.831	0.918	0.982	1.024	1.068	1.088	1.117	1.109	1.100	1.103	1.082	1.034	0.957	0.944	0.821	0.725	
2111	0.443	G5	1.52	0.105	0.688	0.753	0.858	0.911	0.955	0.995	1.020	1.023	1.064	1.005	1.046	0.999	0.957	0.902	0.886	0.765	0.689	
2113	0.445	G5	1.52	0.105	0.665	0.767	0.868	0.899	0.965	0.993	1.003	1.034	1.036	1.026	1.041	1.010	0.951	0.915	0.874	0.761	0.682	
2114	0.860	G5	1.39	0.090	0.728	0.828	0.923	0.982	1.039	1.080	1.092	1.129	1.120	1.112	1.135	1.094	1.033	0.988	0.947	0.822	0.741	
2115	1.187	G5	1.39	0.082	0.752	0.858	0.964	1.009	1.072	1.123	1.133	1.167	1.165	1.157	1.169	1.129	1.062	1.017	0.970	0.854	0.766	
2116	1.526	G5	1.26	0.076	0.774	0.875	0.986	1.033	1.101	1.145	1.160	1.200	1.192	1.195	1.195	1.159	1.094	1.044	0.999	0.879	0.789	
2117	1.907	G5	1.26	0.074	0.768	0.881	0.978	1.037	1.100	1.151	1.166	1.206	1.198	1.198	1.196	1.143	1.088	1.043	0.991	0.876	0.789	
2118	1.905	G5	1.22	0.075	0.781	0.858	0.967	1.042	1.076	1.140	1.152	1.178	1.176	1.183	1.174	1.136	1.068	1.026	0.982	0.860	0.790	
2119	1.519	G5	1.22	0.078	0.772	0.873	0.990	1.040	1.083	1.165	1.160	1.195	1.174	1.195	1.182	1.155	1.110	1.027	0.999	0.860	0.802	
2120	1.194	G5	1.34	0.083	0.766	0.824	0.961	1.010	1.052	1.116	1.121	1.145	1.154	1.134	1.155	1.107	1.063	0.991	0.970	0.830	0.763	
2121	0.851	G5	1.34	0.092	0.720	0.813	0.919	0.973	1.009	1.055	1.077	1.095	1.111	1.080	1.111	1.064	1.040	0.949	0.936	0.801	0.735	
2122	0.434	G5	1.46	0.106	0.674	0.756	0.876	0.915	0.947	0.976	1.016	1.022	1.023	1.013	1.039	0.988	0.929	0.892	0.891	0.747	0.674	
2123	0.433	G5	1.46	0.106	0.676	0.757	0.861	0.897	0.957	0.991	0.997	1.029	1.023	1.015	1.026	1.001	0.930	0.909	0.858	0.758	0.674	
2124	0.855	G5	1.34	0.091	0.721	0.820	0.922	0.971	1.027	1.079	1.087	1.113	1.110	1.102	1.114	1.076	1.016	0.975	0.927	0.816	0.732	
2125	1.190	G5	1.34	0.083	0.740	0.854	0.943	1.001	1.063	1.110	1.124	1.162	1.149	1.153	1.154	1.111	1.055	1.011	0.958	0.847	0.763	
2126	1.520	G5	1.22	0.078	0.759	0.859	0.967	1.014	1.083	1.134	1.149	1.182	1.169	1.174	1.173	1.140	1.075	1.024	0.968	0.864	0.774	
2127	1.903	G5	1.22	0.075	0.763	0.867	0.971	1.027	1.089	1.139	1.149	1.194	1.185	1.184	1.183	1.140	1.080	1.029	0.984	0.867	0.777	
2129	1.929	G5	1.16	0.076	0.757	0.869	0.966	1.025	1.081	1.134	1.152	1.180	1.191	1.164	1.176	1.143	1.080	1.016	0.977	0.865	0.777	
2130	1.538	G5	1.16	0.080	0.761	0.839	0.963	1.015	1.072	1.114	1.138	1.178	1.162	1.150	1.161	1.117	1.071	1.010	0.964	0.856	0.775	
2131	1.199	G5	1.27	0.085	0.752	0.838	0.951	0.985	1.048	1.095	1.107	1.142	1.133	1.141	1.138	1.105	1.053	0.990	0.953	0.836	0.747	
2132	0.863	G5	1.27	0.093	0.708	0.803	0.918	0.955	1.016	1.059	1.068	1.102	1.091	1.087	1.106	1.080	1.019	0.956	0.932	0.814	0.728	
2133	0.440	G5	1.37	0.107	0.660	0.756	0.862	0.894	0.949	0.983	0.998	1.011	1.022	0.986	1.024	1.005	0.938	0.881	0.886	0.751	0.683	
2134	0.438	G5	1.37	0.107	0.654	0.743	0.842	0.888	0.939	0.971	0.981	1.015	1.003	1.002	1.014	0.973	0.930	0.887	0.859	0.744	0.663	
2135	0.856	G5	1.27	0.093	0.701	0.812	0.901	0.957	1.013	1.059	1.062	1.101	1.096	1.093	1.092	1.066	1.008	0.956	0.921	0.804	0.722	
2136	1.185	G5	1.27	0.085	0.716	0.835	0.933	0.984	1.042	1.087	1.102	1.135	1.124	1.130	1.130	1.108	1.036	0.993	0.937	0.831	0.734	
2137	1.529	G5	1.16	0.080	0.744	0.843	0.948	1.001	1.067	1.114	1.128	1.165	1.166	1.157	1.164	1.115	1.060	1.009	0.962	0.843	0.756	
2138	1.918	G5	1.16	0.076	0.750	0.858	0.952	1.014	1.074	1.127	1.143	1.179	1.175	1.173	1.176	1.136	1.068	1.018	0.967	0.853	0.766	
2139	1.914	G5	1.13	0.077	0.774	0.886	0.998	1.047	1.103	1.155	1.171	1.204	1.189	1.205	1.190	1.170	1.110	1.038	1.008	0.871	0.796	
2140	1.522	G5	1.13	0.081	0.780	0.847	0.972	1.030	1.082	1.133	1.141	1.181	1.158	1.165	1.171	1.125	1.080	1.023	1.002	0.852	0.782	
2141	1.187	G5	1.24	0.087	0.753	0.827	0.942	0.984	1.033	1.092	1.107	1.134	1.121	1.118	1.126	1.100	1.039	0.987	0.952	0.821	0.752	
2142	0.858	G5	1.24	0.094	0.710	0.790	0.909	0.958	0.995	1.049	1.066	1.112	1.066	1.078	1.098	1.048	1.012	0.937	0.947	0.796	0.723	
2143	0.437	G5	1.32	0.107	0.671	0.741	0.866	0.889	0.932	0.985	0.978	1.000	1.008	0.983	1.005	0.982	0.936	0.864	0.894	0.722	0.681	
2144	0.435	G5	1.32	0.107	0.651	0.752	0.842	0.877	0.941	0.963	0.976	1.001	1.012	0.985	1.002	0.963	0.928	0.889	0.845	0.736	0.666	
2145	0.852	G5	1.24	0.094	0.703	0.809	0.902	0.950	1.002	1.046	1.050	1.089	1.080	1.075	1.086	1.052	0.993	0.951	0.915	0.799	0.707	
2146	1.188	G5	1.24	0.086	0.723</td																	

TABLE VII.—FRÖSSLING NUMBER FOR 1.5:1 MODEL.

Rdg no.	Re _d	Grid	Tu. %	Λ_{η}/d	Gauge																												
					2	3	4	5	6	7	8	9	10	11	12	13	14	15	16	17	18	19	20	21	22	23	24	25	26	27	28		
287	2.046	G0	0.30	2.308	0.459	0.488	0.509	0.550	0.569	0.615	0.661	0.694	0.730	0.775	0.815	0.844	0.873	0.874	0.884	0.884	0.884	0.884	0.884	0.884	0.884	0.884	0.884	0.884	0.884	0.884	0.884	0.884	
288	1.305	G0	0.30	2.308	0.469	0.485	0.516	0.551	0.566	0.618	0.663	0.690	0.731	0.773	0.815	0.848	0.876	0.877	0.886	0.886	0.886	0.886	0.886	0.886	0.886	0.886	0.886	0.886	0.886	0.886	0.886	0.886	0.886
289	0.480	G0	0.30	2.308	0.476	0.484	0.524	0.562	0.571	0.624	0.672	0.696	0.737	0.789	0.822	0.850	0.878	0.884	0.891	0.884	0.884	0.884	0.884	0.884	0.884	0.884	0.884	0.884	0.884	0.884	0.884	0.884	
290	0.479	G0	0.30	2.308	0.478	0.498	0.521	0.561	0.579	0.624	0.677	0.708	0.735	0.789	0.825	0.861	0.888	0.891	0.904	0.851	0.837	0.792	0.754	0.709	0.684	0.637	0.603	0.564	0.533	0.501	0.475		
291	1.276	G0	0.30	2.308	0.467	0.484	0.518	0.550	0.574	0.617	0.666	0.699	0.732	0.778	0.816	0.848	0.882	0.880	0.887	0.845	0.818	0.784	0.743	0.706	0.665	0.628	0.596	0.556	0.526	0.494	0.469		
292	2.046	G0	0.30	2.308	0.458	0.472	0.512	0.544	0.563	0.606	0.653	0.683	0.718	0.764	0.805	0.835	0.863	0.864	0.875	0.831	0.808	0.770	0.729	0.693	0.661	0.616	0.585	0.546	0.516	0.484	0.461		
294	1.995	G1	13.20	0.222	1.050	1.014	1.015	1.022	1.030	1.063	1.109	1.161	1.223	1.294	1.364	1.442	1.507	1.501	1.463	1.360	1.289	1.179	1.130	1.095	1.059	1.042	1.016	1.033	1.046	1.077			
295	1.231	G1	13.20	0.222	0.987	0.879	0.907	0.939	0.960	1.012	1.081	1.125	1.183	1.256	1.329	1.403	1.453	1.446	1.419	1.317	1.253	1.191	1.139	1.085	1.041	0.994	0.96	0.922	0.903	0.887	0.895		
296	0.464	G1	13.20	0.222	0.720	0.733	0.780	0.830	0.849	0.921	0.995	1.034	1.095	1.160	1.218	1.275	1.307	1.298	1.290	1.202	1.157	1.099	1.047	1.000	0.948	0.902	0.866	0.811	0.765	0.732	0.713		
297	0.471	G1	8.34	0.289	0.644	0.655	0.703	0.753	0.778	0.839	0.912	0.952	1.001	1.063	1.114	1.173	1.207	1.218	1.223	1.152	1.115	1.086	1.013	0.958	0.905	0.846	0.807	0.758	0.710	0.675	0.647		
298	1.237	G1	8.34	0.289	0.707	0.727	0.757	0.801	0.833	0.889	0.955	1.003	1.061	1.142	1.197	1.268	1.329	1.334	1.336	1.296	1.243	1.186	1.132	1.076	1.016	0.962	0.904	0.861	0.807	0.771	0.736	0.725	
299	1.701	G1	8.34	0.289	0.762	0.764	0.789	0.828	0.851	0.910	0.971	1.022	1.078	1.149	1.222	1.296	1.365	1.373	1.362	1.267	1.201	1.143	1.082	1.030	0.976	0.918	0.886	0.832	0.809	0.785	0.790		
300	1.757	G1	10.04	0.260	0.638	0.627	0.644	0.670	0.689	0.940	1.002	1.043	1.105	1.174	1.246	1.326	1.388	1.403	1.377	1.282	1.209	1.153	1.093	1.041	0.998	0.942	0.911	0.872	0.859	0.848	0.868		
301	1.270	G1	10.04	0.260	0.745	0.758	0.787	0.823	0.850	0.904	0.968	1.014	1.075	1.147	1.211	1.285	1.340	1.340	1.334	1.245	1.176	1.125	1.064	1.011	0.963	0.909	0.872	0.820	0.791	0.769	0.758		
302	0.464	G1	10.04	0.260	0.657	0.631	0.716	0.746	0.779	0.845	0.907	0.955	1.006	1.076	1.118	1.178	1.201	1.210	1.215	1.143	1.106	1.053	0.990	0.951	0.891	0.841	0.808	0.737	0.716	0.670	0.639		
472	0.500	G1	12.20	0.232	0.658	0.672	0.718	0.760	0.774	0.844	0.908	0.942	1.008	1.032	1.055	1.104	1.152	1.174	1.170	1.156	1.085	1.038	0.991	0.935	0.890	0.859	0.820	0.800	0.906	0.853	0.853		
473	1.278	G1	12.20	0.232	0.797	0.791	0.823	0.851	0.872	0.921	0.968	1.031	1.085	1.144	1.206	1.272	1.311	1.318	1.287	1.205	1.144	1.089	1.036	0.987	0.951	0.902	0.884	0.829	0.800	0.906			
474	2.029	G1	12.20	0.232	0.931	0.905	0.941	0.918	0.926	0.963	1.019	1.056	1.109	1.179	1.240	1.318	1.381	1.383	1.347	1.257	1.190	1.139	1.091	1.040	1.010	0.962	0.959	0.927	0.937	0.956	0.988		
476	2.024	G1	7.99	0.297	0.736	0.726	0.745	0.777	0.795	0.843	0.903	0.944	1.001	1.056	1.125	1.188	1.244	1.251	1.226	1.148	1.092	1.035	0.984	0.934	0.894	0.840	0.812	0.771	0.755	0.767	0.767		
477	1.286	G1	7.99	0.297	0.653	0.665	0.705	0.759	0.783	0.816	0.863	0.915	0.976	1.033	1.095	1.148	1.192	1.247	1.298	1.228	1.176	1.112	1.066	1.026	0.986	0.945	0.905	0.863	0.820	0.788	0.753	0.753	
478	0.482	G1	7.99	0.297	0.590	0.614	0.651	0.697	0.715	0.780	0.842	0.871	0.933	0.972	1.027	1.070	1.098	1.104	1.104	1.091	1.039	1.001	0.957	0.938	0.890	0.820	0.744	0.726	0.679	0.645	0.602	0.582	
479	0.483	G1	9.50	0.248	0.626	0.677	0.715	0.729	0.792	0.864	0.924	0.958	1.005	1.050	1.103	1.131	1.136	1.124	1.062	1.032	0.977	0.915	0.881	0.834	0.779	0.740	0.695	0.661	0.616	0.598			
480	1.280	G1	9.50	0.248	0.691	0.700	0.735	0.772	0.797	0.846	0.916	0.958	1.011	1.070	1.136	1.197	1.245	1.290	1.232	1.155	1.106	1.042	0.988	0.938	0.893	0.853	0.805	0.774	0.728	0.695	0.663	0.633	
481	2.037	G1	9.50	0.248	0.790	0.773	0.791	0.816	0.828	0.873	0.933	0.972	1.031	1.085	1.158	1.229	1.288	1.299	1.245	1.162	1.117	1.065	1.008	0.948	0.905	0.863	0.822	0.780	0.758	0.729	0.695	0.663	
483	2.033	G1	8.99	0.277	0.786	0.773	0.784	0.811	0.824	0.879	0.934	0.975	1.041	1.096	1.174	1.247	1.301	1.315	1.263	1.208	1.128	1.083	1.019	0.971	0.929	0.884	0.852	0.812	0.770	0.733	0.700		
484	1.275	G1	8.99	0.277	0.667	0.684	0.715	0.752	0.776	0.831	0.896	0.932	0.994	1.049	1.115	1.177	1.217	1.223	1.202	1.131	1.068	1.021	0.963	0.914	0.873	0.834	0.779	0.740	0.695	0.661	0.638		
485	0.506	G1	8.99	0.277	0.602	0.621	0.661	0.702	0.724	0.787	0.850	0.884	0.941	0.999	1.043	1.090	1.134	1.190	1.255	1.342	1.381	1.341	1.263	1.182	1.137	1.087	1.046	1.013	0.973	0.945	0.908	0.871	0.844
486	0.513	G1	10.01	0.260	0.605	0.624	0.664	0.701	0.728	0.786	0.852	0.883	0.944	1.002	1.049	1.106	1.142	1.192	1.260	1.307	1.378	1.322	1.262	1.196	1.122	1.063	1.015	0.950	0.900	0.877	0.835	0.804	0.815
487	1.277	G1	10.01	0.260	0.688	0.697	0.723	0.758	0.778	0.831	0.896	0.933	0.994	1.057	1.118	1.186	1.224	1.242	1.216	1.145	1.082	1.031	0.977	0.929	0.886	0.840	0.803	0.749	0.733	0.701	0.700		
488	2.046	G1	10.01	0.260	0.825	0.798	0.802	0.822	0.835	0.875	0.935	0.977	1.034	1.092	1.164	1.247	1.300	1.319	1.286	1.200	1.127	1.078	1.021	0.974	0.932	0.884	0.849	0.813	0.837	0.845	0.815		
499	2.040	G1	13.11	0.222	0.971	0.939	0.944	0.950	0.985	1.035	1.074	1.134	1.190	1.255	1.342	1.382	1.381	1.341	1.233	1.160	1.097	1.039	0.985	0.939	0.890	0.859	0.811	0.795	0.779	0.789			
500	1.277	G1	13.11	0.222	0.803	0.800	0.823	0.847	0.872	0.921	0.979	1.022	1.081	1.150	1.205	1.281	1.316	1.315	1.284	1.192	1.123	1.064	1.015	0.951	0.908	0.858	0.801	0.767	0.731	0.637	0.611		
501	0.502	G1	13.11	0.222	0.666	0.667	0.707</td																										

TABLE VII.—CONCLUDED.

Rd ^g no.	Re _d	Grid	Tu. %	Λ_x/d	Gauge Frössling number																											
					2	3	4	5	6	7	8	9	10	11	12	13	14	15	16	17	18	19	20	21	22	23	24	25	26	27	28	
469	2.049	G2	4.85	0.232	0.613	0.625	0.658	0.695	0.721	0.772	0.837	0.882	0.943	0.997	1.065	1.121	1.156	1.173	1.152	1.095	1.034	0.984	0.928	0.878	0.833	0.773	0.743	0.690	0.663	0.632	0.631	
490	1.273	G2	4.97	0.232	0.563	0.587	0.628	0.671	0.701	0.748	0.810	0.858	0.914	0.972	1.028	1.081	1.107	1.117	1.119	1.108	1.014	0.972	0.913	0.865	0.818	0.760	0.722	0.672	0.637	0.593	0.573	
491	0.498	G2	4.66	0.232	0.550	0.565	0.609	0.648	0.672	0.730	0.791	0.825	0.884	0.936	0.972	1.017	1.038	1.051	1.061	1.004	0.965	0.926	0.867	0.828	0.787	0.736	0.693	0.647	0.608	0.565	0.546	
493	2.047	G2	5.43	0.215	0.654	0.656	0.690	0.717	0.753	0.801	0.861	0.910	0.970	1.040	1.093	1.165	1.208	1.217	1.200	1.130	1.068	1.024	0.962	0.906	0.863	0.807	0.773	0.719	0.694	0.665	0.677	
494	1.286	G2	5.54	0.215	0.577	0.603	0.642	0.681	0.711	0.764	0.827	0.866	0.931	0.986	1.045	1.105	1.132	1.145	1.145	1.086	1.029	0.989	0.934	0.881	0.832	0.776	0.739	0.685	0.649	0.605	0.592	
495	0.498	G2	5.22	0.215	0.556	0.573	0.615	0.661	0.680	0.740	0.799	0.826	0.899	0.941	0.983	1.031	1.054	1.063	1.068	1.014	0.977	0.933	0.882	0.839	0.795	0.745	0.709	0.652	0.618	0.572	0.553	
496	0.507	G2	5.50	0.208	0.567	0.578	0.625	0.667	0.692	0.742	0.815	0.839	0.899	0.952	0.994	1.040	1.068	1.073	1.080	1.027	0.990	0.948	0.894	0.846	0.811	0.750	0.713	0.662	0.624	0.580	0.560	
497	1.278	G2	5.83	0.208	0.591	0.609	0.648	0.689	0.711	0.771	0.834	0.875	0.935	1.001	1.049	1.109	1.135	1.155	1.159	1.092	1.041	0.993	0.937	0.886	0.843	0.784	0.747	0.689	0.657	0.621	0.597	
498	2.043	G2	5.73	0.208	0.662	0.663	0.693	0.730	0.754	0.807	0.863	0.916	0.968	1.033	1.095	1.165	1.205	1.219	1.206	1.130	1.065	1.019	0.969	0.906	0.866	0.808	0.783	0.723	0.703	0.679	0.684	
315	0.493	G3	5.17	0.096	0.597	0.620	0.661	0.722	0.741	0.801	0.878	0.915	0.968	1.049	1.093	1.148	1.185	1.196	1.188	1.141	1.091	1.031	0.977	0.927	0.863	0.817	0.769	0.720	0.671	0.628	0.598	
316	1.282	G3	5.53	0.096	0.643	0.657	0.700	0.754	0.778	0.830	0.906	0.947	1.011	1.085	1.148	1.213	1.279	1.289	1.272	1.219	1.199	1.132	1.072	1.009	0.958	0.901	0.839	0.806	0.744	0.709	0.675	0.653
317	1.986	G3	5.96	0.096	0.739	0.734	0.755	0.795	0.824	0.869	0.941	0.991	1.115	1.198	1.274	1.353	1.374	1.337	1.247	1.173	1.112	1.050	0.995	0.937	0.880	0.848	0.795	0.774	0.760	0.766		
318	1.988	G3	7.65	0.082	0.823	0.805	0.812	0.842	0.867	0.913	0.985	1.036	1.100	1.180	1.270	1.361	1.446	1.436	1.369	1.262	1.187	1.138	1.078	1.023	0.982	0.924	0.866	0.856	0.859	0.893		
319	1.247	G3	7.24	0.082	0.679	0.692	0.729	0.769	0.804	0.862	0.936	0.986	1.047	1.132	1.217	1.303	1.368	1.358	1.313	1.210	1.145	1.091	1.029	0.977	0.928	0.876	0.835	0.782	0.749	0.717	0.712	
320	0.464	G3	6.78	0.082	0.619	0.650	0.689	0.743	0.761	0.830	0.904	0.939	1.010	1.080	1.161	1.217	1.260	1.247	1.229	1.149	1.109	1.053	0.994	0.944	0.889	0.841	0.793	0.744	0.700	0.652	0.635	
460	0.512	G3	4.13	0.110	0.557	0.578	0.618	0.658	0.678	0.735	0.811	0.832	0.885	0.939	0.988	1.034	1.064	1.072	1.073	1.030	0.990	0.939	0.894	0.841	0.805	0.747	0.711	0.666	0.622	0.585	0.557	
461	1.282	G3	4.42	0.110	0.595	0.614	0.660	0.710	0.729	0.786	0.854	0.897	0.961	1.016	1.081	1.136	1.180	1.190	1.119	1.073	1.014	0.956	0.904	0.854	0.791	0.756	0.702	0.666	0.625	0.603		
462	2.024	G3	4.84	0.110	0.641	0.649	0.684	0.724	0.747	0.800	0.866	0.915	0.968	1.031	1.100	1.162	1.227	1.235	1.215	1.141	1.081	1.025	0.969	0.913	0.869	0.807	0.777	0.720	0.694	0.662	0.644	
469	2.025	G3	3.67	0.132	0.593	0.612	0.650	0.693	0.719	0.775	0.841	0.882	0.944	1.007	1.061	1.125	1.172	1.183	1.172	1.113	1.055	1.000	0.947	0.890	0.843	0.782	0.747	0.687	0.655	0.620	0.603	
470	1.291	G3	3.28	0.132	0.570	0.594	0.635	0.683	0.709	0.762	0.835	0.875	0.934	0.992	1.051	1.101	1.138	1.152	1.149	1.093	1.043	0.995	0.931	0.881	0.832	0.773	0.735	0.677	0.640	0.599	0.572	
471	0.485	G3	3.06	0.132	0.534	0.559	0.598	0.639	0.668	0.715	0.781	0.816	0.866	0.916	0.965	1.007	1.028	1.040	1.043	0.996	0.958	0.920	0.866	0.820	0.780	0.742	0.687	0.632	0.598	0.534		
502	0.497	G3	10.85	0.062	0.666	0.682	0.729	0.773	0.804	0.861	0.942	0.989	1.067	1.159	1.227	1.325	1.366	1.356	1.331	1.242	1.172	1.126	1.059	0.999	0.947	0.895	0.852	0.781	0.754	0.699	0.681	
503	1.285	G3	11.55	0.062	0.855	0.845	0.844	0.885	0.910	0.966	1.026	1.079	1.152	1.235	1.321	1.438	1.519	1.538	1.481	1.365	1.276	1.217	1.153	1.097	1.042	0.994	0.966	0.913	0.892	0.813	0.791	
504	2.031	G3	11.79	0.062	1.084	1.038	1.027	1.015	1.011	1.048	1.142	1.213	1.299	1.379	1.501	1.589	1.606	1.540	1.420	1.326	1.274	1.216	1.161	1.124	1.080	1.087	1.062	1.095	1.120	1.174		
321	0.482	G4	2.99	0.079	0.559	0.582	0.625	0.680	0.703	0.757	0.829	0.859	0.923	0.974	1.032	1.076	1.114	1.144	1.166	1.126	1.065	1.009	0.988	0.966	0.919	0.866	0.819	0.765	0.724	0.688	0.651	
322	1.270	G4	3.30	0.079	0.582	0.611	0.648	0.734	0.786	0.855	0.900	0.963	1.024	1.083	1.134	1.173	1.185	1.174	1.113	1.065	1.009	0.960	0.902	0.849	0.792	0.752	0.696	0.655	0.611	0.588		
323	1.989	G4	3.37	0.079	0.612	0.634	0.674	0.712	0.746	0.802	0.872	0.918	0.979	1.046	1.117	1.184	1.243	1.253	1.237	1.163	1.097	1.040	0.978	0.924	0.870	0.809	0.774	0.711	0.680	0.635	0.620	
324	1.986	G4	4.24	0.066	0.646	0.663	0.699	0.744	0.774	0.828	0.896	0.949	1.012	1.087	1.165	1.245	1.324	1.351	1.326	1.239	1.164	1.093	1.024	0.961	0.908	0.843	0.804	0.743	0.710	0.677	0.665	
325	1.249	G4	4.18	0.066	0.587	0.610	0.654	0.697	0.729	0.784	0.850	0.900	0.962	1.024	1.101	1.172	1.230	1.248	1.249	1.175	1.114	1.061	1.007	0.943	0.892	0.845	0.787	0.740	0.683	0.650	0.628	
326	0.491	G4	3.77	0.066	0.569	0.595	0.641	0.682	0.712	0.770	0.840	0.867	0.931	0.991	1.038	1.088	1.115	1.136	1.152	1.100	1.059	1.004	0.947	0.893	0.834	0.786	0.738	0.686	0.646	0.597	0.577	
449	2.033	G4	6.01	0.051	0.711	0.700	0.728	0.751	0.782	0.834	0.898	0.938	1.011	1.071	1.156	1.253	1.360	1.395	1.330	1.218	1.130	1.065	1.001	0.952	0.905	0.840	0.814	0.762	0.744	0.729	0.750	
454	2.044	G4	2.49	0.099	0.581	0.621	0.660	0.692	0.745	0.810	0.852	0.910	0.967	1.028	1.081	1.121	1.196	1.269	1.289	1.271	1.185	1.120	1.057	0.992	0.936	0.887	0.826	0.786	0.732	0.698	0.650	0.632
455	1.276	G4	6.01	0.051	0.625	0.640	0.689	0.726	0.757	0.816	0.865	0.927	0.996	1.055	1.121	1.196	1.269	1.321	1.271	1.181</												

TABLE VIII.—FRÖSSLING NUMBER FOR 2:25:1 MODEL.

Rdg no.	Re _d	Grid	Tu, %	Λ_x/d	Gauge Frössling number																											
					2	3	4	5	6	7	8	9	10	11	12	13	14	15	16	17	18	19	20	21	22	23	24	25	26	27	28	
250	2.152	G0	0.25	2.308	0.443	0.453	0.478	0.502	0.528	0.557	0.624	0.625	0.679	0.714	0.757	0.838	0.833	0.860	0.857	0.823	0.796	0.729	0.587	0.645	0.605	0.575	0.548	0.515	0.485	0.454	0.450	
251	1.298	G0	0.25	2.308	0.436	0.444	0.473	0.497	0.523	0.552	0.616	0.618	0.664	0.710	0.749	0.829	0.824	0.850	0.846	0.815	0.784	0.723	0.674	0.638	0.596	0.565	0.539	0.508	0.475	0.461	0.445	
252	0.469	G0	0.25	2.308	0.438	0.451	0.475	0.499	0.518	0.550	0.620	0.608	0.674	0.701	0.749	0.817	0.821	0.842	0.838	0.812	0.776	0.714	0.669	0.632	0.590	0.557	0.520	0.482	0.459	0.451		
274	2.125	G0	0.25	2.308	0.444	0.458	0.484	0.506	0.529	0.563	0.627	0.631	0.681	0.716	0.765	0.844	0.841	0.848	0.846	0.828	0.807	0.735	0.687	0.652	0.613	0.575	0.550	0.522	0.488	0.468	0.456	
275	2.124	G0	0.25	2.308	0.447	0.458	0.487	0.507	0.530	0.560	0.630	0.639	0.689	0.725	0.771	0.848	0.847	0.871	0.872	0.831	0.808	0.746	0.691	0.651	0.613	0.580	0.555	0.520	0.491	0.469	0.459	
276	1.396	G0	0.25	2.308	0.450	0.465	0.484	0.512	0.531	0.566	0.636	0.632	0.692	0.726	0.770	0.850	0.848	0.876	0.875	0.833	0.809	0.737	0.690	0.656	0.614	0.578	0.558	0.520	0.492	0.471	0.450	
277	0.574	G0	0.25	2.308	0.449	0.461	0.484	0.507	0.527	0.560	0.634	0.626	0.684	0.716	0.761	0.838	0.833	0.863	0.867	0.820	0.791	0.732	0.682	0.650	0.600	0.575	0.546	0.519	0.488	0.458	0.451	
279	0.528	G0	0.25	2.308	0.456	0.460	0.490	0.516	0.533	0.565	0.641	0.628	0.679	0.720	0.765	0.842	0.836	0.876	0.853	0.833	0.805	0.721	0.682	0.654	0.613	0.583	0.553	0.527	0.495	0.468	0.472	
280	0.529	G0	0.25	2.308	0.452	0.465	0.491	0.512	0.537	0.564	0.644	0.632	0.680	0.725	0.770	0.844	0.851	0.878	0.862	0.833	0.805	0.728	0.686	0.660	0.613	0.583	0.554	0.529	0.498	0.473	0.476	
281	1.342	G0	0.25	2.308	0.457	0.466	0.489	0.514	0.540	0.570	0.643	0.644	0.686	0.733	0.781	0.855	0.860	0.883	0.875	0.833	0.809	0.737	0.690	0.656	0.614	0.578	0.558	0.528	0.494	0.460	0.458	
282	2.137	G0	0.25	2.308	0.441	0.455	0.479	0.504	0.530	0.559	0.631	0.676	0.721	0.767	0.843	0.842	0.867	0.861	0.827	0.807	0.726	0.688	0.654	0.614	0.577	0.551	0.517	0.487	0.465	0.460		
283	2.136	G0	0.25	2.308	0.444	0.459	0.481	0.505	0.529	0.560	0.632	0.633	0.675	0.724	0.767	0.844	0.835	0.865	0.828	0.804	0.726	0.684	0.653	0.612	0.576	0.551	0.518	0.487	0.466	0.459		
284	2.135	G0	0.25	2.308	0.446	0.464	0.485	0.509	0.531	0.564	0.633	0.638	0.680	0.724	0.770	0.848	0.848	0.855	0.874	0.833	0.814	0.730	0.690	0.655	0.617	0.581	0.554	0.521	0.489	0.471	0.461	
578	2.180	G0	0.25	2.308	0.420	0.439	0.456	0.486	0.504	0.535	0.600	0.603	0.646	0.691	0.725	0.807	0.789	0.833	0.818	0.788	0.768	0.766	0.696	0.649	0.622	0.581	0.550	0.524	0.496	0.462	0.447	0.431
579	1.341	G0	0.25	2.308	0.426	0.444	0.468	0.496	0.510	0.539	0.609	0.605	0.650	0.696	0.730	0.813	0.796	0.836	0.823	0.793	0.771	0.698	0.657	0.624	0.581	0.551	0.534	0.492	0.467	0.449	0.437	
580	0.522	G0	0.25	2.308	0.430	0.444	0.466	0.490	0.505	0.532	0.613	0.648	0.689	0.726	0.760	0.806	0.798	0.832	0.819	0.787	0.761	0.695	0.647	0.620	0.576	0.551	0.522	0.490	0.464	0.450	0.436	
581	0.522	G0	0.25	2.308	0.429	0.442	0.460	0.487	0.500	0.532	0.609	0.595	0.640	0.683	0.722	0.801	0.794	0.825	0.814	0.784	0.758	0.688	0.645	0.618	0.570	0.546	0.527	0.491	0.462	0.444	0.433	
582	1.358	G0	0.25	2.308	0.425	0.437	0.455	0.485	0.501	0.526	0.603	0.598	0.642	0.684	0.720	0.799	0.788	0.821	0.812	0.781	0.752	0.691	0.646	0.619	0.577	0.543	0.521	0.487	0.458	0.430		
583	2.176	G0	0.25	2.308	0.424	0.437	0.458	0.483	0.505	0.527	0.602	0.596	0.644	0.680	0.723	0.804	0.787	0.829	0.817	0.789	0.759	0.692	0.651	0.617	0.581	0.551	0.522	0.493	0.463	0.432		
585	2.160	G0	0.25	2.308	0.423	0.441	0.462	0.489	0.508	0.538	0.602	0.605	0.651	0.696	0.734	0.812	0.793	0.834	0.827	0.796	0.769	0.698	0.661	0.623	0.584	0.553	0.526	0.496	0.463	0.437		
586	1.370	G0	0.25	2.308	0.431	0.459	0.485	0.510	0.541	0.565	0.610	0.651	0.696	0.733	0.812	0.802	0.837	0.831	0.798	0.774	0.699	0.659	0.623	0.587	0.553	0.526	0.498	0.468	0.446	0.435		
587	0.524	G0	0.25	2.308	0.438	0.455	0.485	0.513	0.541	0.568	0.608	0.609	0.653	0.692	0.731	0.815	0.801	0.830	0.792	0.771	0.749	0.698	0.657	0.628	0.596	0.560	0.530	0.502	0.467	0.452	0.442	
269	2.137	G1	1.431	0.211	0.938	0.922	0.917	0.915	0.927	0.948	1.027	1.016	1.081	1.140	1.211	1.349	1.351	1.391	1.328	1.254	1.202	1.096	1.046	1.008	0.980	0.957	0.924	0.898	0.864	0.834	0.793	0.769
270	1.320	G1	1.431	0.211	0.814	0.811	0.821	0.843	0.853	0.886	0.975	0.968	1.036	1.097	1.169	1.294	1.285	1.320	1.267	1.196	1.145	1.043	0.987	0.948	0.904	0.875	0.838	0.802	0.815	0.834	0.803	
271	0.484	G1	1.431	0.211	0.655	0.679	0.695	0.721	0.750	0.789	0.866	0.876	0.939	0.981	1.039	1.133	1.105	1.137	1.107	1.060	1.019	0.935	0.880	0.834	0.791	0.754	0.734	0.707	0.671	0.653	0.634	
658	2.148	G1	1.319	0.222	0.897	0.876	0.878	0.883	0.904	0.900	0.980	1.053	1.120	1.188	1.332	1.355	1.323	1.323	1.298	1.241	1.161	1.117	1.003	0.959	0.917	0.908	0.909	0.911	0.933	0.959	0.959	
659	1.334	G1	1.319	0.222	0.780	0.792	0.811	0.831	0.872	0.968	0.988	1.029	1.130	1.289	1.309	1.259	1.166	1.119	1.009	0.962	0.915	0.887	0.820	0.834	0.809	0.790	0.793	0.797	0.797			
660	0.523	G1	1.319	0.222	0.640	0.654	0.682	0.714	0.736	0.785	0.886	0.875	0.946	1.011	1.068	1.177	1.143	1.173	1.147	1.071	1.036	0.931	0.880	0.839	0.788	0.756	0.727	0.692	0.658	0.641	0.635	
661	0.472	G1	1.226	0.232	0.6423	0.640	0.686	0.701	0.719	0.769	0.866	0.854	0.925	0.987	1.041	1.149	1.114	1.154	1.131	1.057	1.021	0.911	0.864	0.821	0.769	0.737	0.709	0.671	0.636	0.624	0.611	
662	1.346	G1	1.226	0.232	0.744	0.748	0.765	0.780	0.802	0.837	0.936	0.920	0.997	1.058	1.122	1.260	1.250	1.285	1.241	1.161	1.117	1.003	0.959	0.910	0.871	0.805	0.818	0.790	0.769	0.774		
663	2.150	G1	1.226	0.232	0.849	0.836	0.839	0.852	0.880	0.968	0.953	1.019	1.080	1.056	1.299	1.297	1.323	1.273	1.192	1.144	1.033	0.989	0.952	0.921	0.888	0.881	0.879	0.881	0.905	0.929		
665	2.130	G1	1.03	0.260	0.790	0.774	0.780	0.800	0.825	0.917	0.908	0.975	1.035	1.114	1.250	1.255	1.299	1.245	1.162	1.124	1.043	0.943	0.883	0.843	0.824	0.817	0.811	0.830	0.859	0.859		
666	1.336	G1	1.03	0.260	0.691	0.686	0.701	0.728	0.752	0.785	0.862	0.877	0.948	1.009	1.076	1.204	1.203	1.242	1.201	1.123	1.086	0.972	0.923	0.874	0.832	0						

TABLE VIII.—CONTINUED.

Rdg no.	Re _d	Grid	Tu, %	Λ_x/d	Gauge																											
					2	3	4	5	6	7	8	9	10	11	12	13	14	15	16	17	18	19	20	21	22	23	24	25	26	27	28	
654	0.521	G2	10.74	0.135	0.625	0.635	0.670	0.698	0.728	0.768	0.871	0.862	0.943	1.014	1.081	1.209	1.196	1.241	1.217	1.143	1.093	0.987	0.934	0.878	0.821	0.782	0.748	0.709	0.668	0.663	0.637	
655	0.527	G2	7.02	0.178	0.565	0.579	0.608	0.646	0.663	0.708	0.804	0.786	0.859	0.913	0.965	1.068	1.053	1.090	1.075	1.017	0.980	0.846	0.851	0.794	0.748	0.700	0.680	0.634	0.603	0.585	0.565	
656	1.353	G2	7.39	0.178	0.607	0.622	0.642	0.669	0.694	0.734	0.822	0.819	0.890	0.958	1.016	1.145	1.141	1.181	1.149	1.077	1.042	0.933	0.889	0.830	0.785	0.746	0.713	0.680	0.649	0.638	0.626	
657	2.144	G2	7.31	0.178	0.688	0.695	0.710	0.736	0.765	0.860	0.850	0.918	0.988	1.055	1.190	1.190	1.239	1.194	1.115	1.067	0.962	0.913	0.863	0.823	0.781	0.756	0.737	0.719	0.730	0.744		
658	0.528	G2	5.50	0.208	0.544	0.560	0.581	0.620	0.639	0.681	0.764	0.766	0.823	0.879	0.920	1.025	1.004	1.042	1.033	0.978	0.952	0.862	0.815	0.772	0.721	0.680	0.650	0.616	0.578	0.561	0.546	
659	1.367	G2	5.83	0.208	0.575	0.585	0.604	0.639	0.669	0.706	0.792	0.860	0.920	0.974	1.090	1.075	1.124	1.101	1.045	1.007	0.906	0.852	0.811	0.760	0.716	0.683	0.644	0.618	0.597	0.583		
670	2.130	G2	5.73	0.208	0.634	0.650	0.660	0.675	0.699	0.733	0.820	0.824	0.886	0.942	1.006	1.137	1.132	1.173	1.132	1.066	1.026	0.923	0.868	0.823	0.782	0.742	0.712	0.687	0.664	0.658	0.673	
671	2.124	G2	4.95	0.232	0.608	0.616	0.632	0.659	0.685	0.722	0.809	0.815	0.879	0.937	0.998	1.126	1.116	1.167	1.128	1.071	1.027	0.927	0.870	0.820	0.777	0.729	0.701	0.673	0.646	0.631	0.638	
672	1.338	G2	4.97	0.232	0.567	0.575	0.602	0.636	0.659	0.699	0.787	0.791	0.852	0.905	0.961	1.076	1.061	1.108	1.118	1.035	1.000	0.905	0.847	0.800	0.758	0.710	0.678	0.638	0.604	0.585	0.569	
673	0.523	G2	4.46	0.232	0.534	0.546	0.572	0.605	0.629	0.668	0.755	0.753	0.810	0.866	0.905	1.004	0.979	1.025	1.015	0.961	0.937	0.847	0.796	0.758	0.705	0.670	0.640	0.601	0.568	0.549	0.537	
681	0.523	G2	13.08	0.119	0.664	0.688	0.713	0.748	0.778	0.823	0.933	0.944	1.038	1.115	1.204	1.343	1.303	1.309	1.230	1.134	1.073	0.963	0.915	0.880	0.828	0.798	0.771	0.739	0.698	0.683	0.681	
682	1.351	G2	13.56	0.119	0.841	0.844	0.855	0.873	0.896	0.934	1.047	1.050	1.146	1.243	1.346	1.521	1.482	1.476	1.355	1.239	1.176	1.063	1.017	0.982	0.950	0.921	0.900	0.868	0.873	0.873	0.892	
683	2.142	G2	13.64	0.119	0.979	0.970	0.963	0.963	0.980	1.002	1.106	1.102	1.190	1.282	1.384	1.563	1.518	1.497	1.383	1.268	1.212	1.108	1.064	1.043	1.023	1.002	1.003	1.014	1.016	1.042	1.084	
262	2.101	G3	6.39	0.092	0.709	0.708	0.712	0.734	0.758	0.797	0.863	0.891	0.959	1.028	1.106	1.258	1.281	1.340	1.277	1.199	1.131	1.027	0.964	0.905	0.862	0.819	0.786	0.764	0.746	0.748	0.773	
263	1.322	G3	5.96	0.092	0.631	0.643	0.667	0.704	0.726	0.770	0.858	0.870	0.941	1.007	1.083	1.217	1.234	1.281	1.241	1.170	1.141	1.006	0.943	0.881	0.832	0.785	0.753	0.714	0.682	0.662	0.655	
264	0.498	G3	5.58	0.092	0.571	0.587	0.616	0.649	0.678	0.720	0.812	0.811	0.886	0.944	1.002	1.104	1.106	1.142	1.133	1.083	1.042	0.944	0.881	0.830	0.774	0.732	0.698	0.656	0.617	0.593	0.584	
265	0.479	G3	4.13	0.110	0.551	0.570	0.595	0.630	0.651	0.687	0.776	0.768	0.836	0.893	0.941	1.035	1.026	1.061	1.061	1.019	0.977	0.902	0.844	0.798	0.750	0.704	0.676	0.635	0.600	0.571	0.564	
266	1.316	G3	4.42	0.110	0.584	0.606	0.633	0.662	0.692	0.734	0.819	0.823	0.900	0.958	1.016	1.137	1.133	1.182	1.182	1.156	1.097	1.055	0.959	0.895	0.845	0.797	0.745	0.714	0.674	0.635	0.616	0.593
267	2.095	G3	4.84	0.110	0.636	0.641	0.662	0.685	0.719	0.756	0.842	0.852	0.923	0.980	1.050	1.177	1.186	1.231	1.196	1.129	1.077	0.976	0.916	0.863	0.817	0.770	0.737	0.704	0.675	0.663	0.666	
591	2.132	G3	4.84	0.110	0.630	0.637	0.655	0.681	0.708	0.740	0.832	0.835	0.903	0.974	1.030	1.165	1.159	1.213	1.167	1.100	1.055	0.947	0.898	0.843	0.802	0.754	0.724	0.692	0.667	0.661	0.651	
592	1.356	G3	4.42	0.110	0.586	0.604	0.626	0.652	0.691	0.729	0.817	0.821	0.887	0.945	1.008	1.134	1.134	1.171	1.171	1.135	1.081	0.939	0.933	0.883	0.825	0.782	0.736	0.699	0.663	0.623	0.592	
593	0.518	G3	4.13	0.110	0.548	0.559	0.584	0.617	0.643	0.681	0.761	0.825	0.877	0.917	0.975	1.046	1.131	1.326	1.374	1.295	1.198	1.136	1.096	0.960	0.910	0.871	0.838	0.787	0.752	0.711	0.682	0.652
594	0.521	G3	3.52	0.121	0.535	0.550	0.574	0.601	0.634	0.670	0.760	0.761	0.820	0.870	0.914	1.017	1.002	1.038	1.030	0.938	0.902	0.858	0.857	0.817	0.767	0.715	0.676	0.645	0.607	0.572	0.546	
595	1.350	G3	3.78	0.121	0.569	0.582	0.609	0.647	0.674	0.712	0.799	0.805	0.873	0.932	0.987	1.109	1.109	1.146	1.146	1.120	1.065	1.023	0.920	0.867	0.815	0.763	0.721	0.680	0.643	0.610	0.575	
596	2.130	G3	4.18	0.121	0.606	0.615	0.635	0.664	0.694	0.729	0.822	0.826	0.897	0.958	1.015	1.143	1.143	1.193	1.156	1.095	1.047	0.945	0.886	0.835	0.782	0.739	0.713	0.672	0.643	0.637		
642	2.129	G3	7.65	0.082	0.755	0.751	0.742	0.761	0.782	0.810	0.840	0.882	0.925	0.975	1.046	1.131	1.303	1.326	1.374	1.295	1.198	1.136	1.096	0.960	0.910	0.871	0.838	0.793	0.752	0.711	0.680	0.650
643	1.362	G3	7.24	0.082	0.639	0.654	0.666	0.694	0.722	0.757	0.851	0.855	0.926	0.992	1.076	1.242	1.242	1.256	1.308	1.244	1.148	1.092	0.972	0.910	0.862	0.814	0.756	0.742	0.713	0.679	0.670	
644	0.530	G3	6.78	0.082	0.576	0.586	0.608	0.644	0.672	0.706	0.810	0.804	0.872	0.932	1.000	1.135	1.136	1.179	1.145	1.081	1.031	0.920	0.866	0.815	0.767	0.704	0.688	0.655	0.608	0.582		
645	5.10	G3	5.97	0.097	0.556	0.593	0.632	0.660	0.698	0.798	0.793	0.856	0.914	0.966	1.078	1.069	1.107	1.092	1.047	1.004	0.906	0.851	0.800	0.751	0.709	0.675	0.635	0.596	0.556			
646	1.354	G3	5.46	0.097	0.620	0.628	0.652	0.684	0.709	0.748	0.844	0.847	0.918	0.973	1.049	1.181	1.233	1.193	1.129	1.080	0.969	0.911	0.864	0.823	0.779	0.745	0.695	0.642	0.631			
647	2.126	G3	5.88	0.097	0.689	0.698	0.718	0.740	0.779	0.868	0.871	0.937	1.010	1.079	1.227	1.241	1.236	1.159	1.099	0.996	0.937	0.886	0.836	0.797	0.766	0.722	0.733	0.751				
684	2.137	G3	11.79	0.062	0.963	0.947	0.936	0.926	0.932	0.956	1.050	1.039	1.113	1.187	1.283	1.472	1.518	1.576	1.480	1.361	1.293	1.169	1.09	1.071	1.043	1.010	0.999	1.054	1.099	1.099	1.099	
695	1.354	G3	11.55	0.062	0.798	0.804	0.826	0.848	0.881	0.960	1.024	1.040	1.114	1.181	1.248	1.318	1.433	1.513	1.458	1.321	1.291	1.177	1.119	1.077	1.046	1.013	1.015	1.029	1.03			

TABLE VIII.—CONCLUDED.

Rdg no.	Re _d	Grid	Tu. %	Λ_x/d	Gauge Frössling number																											
					2	3	4	5	6	7	8	9	10	11	12	13	14	15	16	17	18	19	20	21	22	23	24	25	26	27	28	
255	2.105	G4	3.58	0.075	0.619	0.634	0.655	0.688	0.719	0.760	0.851	0.863	0.936	1.009	1.063	1.208	1.204	1.224	1.169	1.103	1.050	0.960	0.898	0.847	0.801	0.752	0.723	0.687	0.653	0.637	0.635	
256	2.107	G4	4.61	0.062	0.650	0.655	0.675	0.702	0.723	0.768	0.850	0.858	0.923	0.981	1.046	1.181	1.201	1.265	1.238	1.178	1.121	1.023	0.950	0.892	0.836	0.790	0.755	0.721	0.690	0.679	0.684	
257	1.341	G4	4.57	0.062	0.601	0.615	0.643	0.670	0.708	0.746	0.834	0.840	0.907	0.962	1.022	1.138	1.144	1.199	1.196	1.147	1.096	1.002	0.932	0.870	0.818	0.767	0.728	0.684	0.649	0.622	0.607	
258	0.499	G4	4.11	0.062	0.564	0.582	0.604	0.637	0.673	0.710	0.804	0.802	0.867	0.905	0.950	1.041	1.035	1.096	1.109	1.078	1.041	0.954	0.890	0.834	0.774	0.731	0.694	0.651	0.609	0.581	0.572	
259	0.504	G4	4.11	0.062	0.554	0.578	0.610	0.639	0.666	0.712	0.797	0.866	0.917	0.970	1.066	1.065	1.106	1.111	1.078	1.033	0.946	0.882	0.830	0.769	0.724	0.690	0.650	0.605	0.579	0.570		
260	1.313	G4	4.57	0.062	0.584	0.599	0.626	0.659	0.689	0.730	0.821	0.820	0.898	0.965	1.038	1.166	1.188	1.245	1.228	1.165	1.104	0.993	0.919	0.858	0.805	0.751	0.715	0.675	0.639	0.612	0.599	
261	2.102	G4	4.61	0.062	0.627	0.634	0.653	0.680	0.708	0.747	0.831	0.839	0.911	0.975	1.067	1.205	1.233	1.295	1.256	1.178	1.114	1.002	0.930	0.867	0.819	0.770	0.736	0.701	0.673	0.659	0.666	
597	2.128	G4	2.85	0.089	0.562	0.575	0.597	0.631	0.660	0.693	0.785	0.784	0.849	0.909	0.968	1.091	1.084	1.141	1.121	1.069	1.034	0.926	0.871	0.810	0.767	0.715	0.681	0.642	0.607	0.586	0.579	
598	1.347	G4	2.76	0.089	0.543	0.558	0.586	0.618	0.648	0.686	0.773	0.779	0.840	0.892	0.948	1.066	1.056	1.106	1.108	1.098	1.054	1.015	0.909	0.859	0.802	0.754	0.708	0.669	0.629	0.591	0.563	0.550
599	0.519	G4	2.51	0.089	0.506	0.519	0.549	0.578	0.607	0.637	0.730	0.719	0.783	0.835	0.866	0.981	0.955	0.983	0.942	0.903	0.823	0.777	0.726	0.685	0.648	0.617	0.576	0.540	0.523	0.506		
633	0.540	G4	2.19	0.099	0.507	0.518	0.543	0.577	0.596	0.636	0.721	0.716	0.783	0.823	0.869	0.973	0.959	0.989	0.975	0.934	0.899	0.819	0.763	0.724	0.673	0.644	0.604	0.572	0.534	0.510	0.508	
634	1.354	G4	2.40	0.099	0.537	0.554	0.581	0.612	0.641	0.683	0.771	0.772	0.836	0.889	0.942	1.048	1.031	1.077	1.057	1.012	0.972	0.879	0.824	0.775	0.728	0.683	0.646	0.608	0.571	0.544	0.536	
635	2.126	G4	2.49	0.099	0.566	0.577	0.598	0.636	0.659	0.699	0.784	0.791	0.859	0.916	0.976	1.092	1.085	1.130	1.103	1.046	1.006	0.907	0.851	0.798	0.761	0.707	0.667	0.636	0.600	0.578	0.576	
636	2.125	G4	4.24	0.086	0.624	0.629	0.647	0.676	0.698	0.737	0.829	0.829	0.899	0.968	1.036	1.181	1.199	1.262	1.222	1.154	1.102	0.983	0.917	0.864	0.813	0.748	0.730	0.698	0.667	0.651	0.666	
637	1.365	G4	4.18	0.086	0.571	0.582	0.607	0.640	0.670	0.711	0.803	0.806	0.873	0.933	1.004	1.130	1.143	1.198	1.177	1.119	1.070	0.959	0.891	0.837	0.783	0.721	0.696	0.658	0.620	0.592	0.584	
638	0.516	G4	3.77	0.086	0.541	0.553	0.590	0.614	0.645	0.685	0.779	0.772	0.840	0.895	0.937	1.039	1.023	1.057	1.047	1.014	0.985	0.890	0.842	0.783	0.735	0.706	0.656	0.623	0.582	0.557	0.544	
639	0.532	G4	2.99	0.079	0.519	0.534	0.560	0.593	0.626	0.656	0.748	0.751	0.807	0.869	0.906	1.013	1.090	1.030	1.074	1.047	1.017	0.942	0.848	0.801	0.747	0.704	0.668	0.627	0.593	0.554	0.538	0.516
640	1.355	G4	3.30	0.079	0.563	0.582	0.612	0.639	0.677	0.711	0.811	0.810	0.877	0.931	1.001	1.113	1.101	1.144	1.112	1.064	1.024	0.917	0.864	0.814	0.762	0.718	0.681	0.646	0.601	0.582	0.564	
641	2.126	G4	3.37	0.079	0.588	0.595	0.620	0.648	0.679	0.715	0.805	0.810	0.872	0.935	1.095	1.132	1.133	1.184	1.156	1.094	1.049	0.940	0.881	0.827	0.779	0.723	0.695	0.660	0.626	0.613	0.603	
678	2.145	G4	6.01	0.051	0.695	0.695	0.70	0.725	0.751	0.78	0.883	0.885	0.960	1.02	1.089	1.242	1.265	1.331	1.266	1.182	1.125	1.006	0.944	0.898	0.850	0.805	0.775	0.748	0.727	0.731	0.758	
679	1.365	G4	6.01	0.051	0.617	0.639	0.664	0.696	0.732	0.770	0.872	0.876	0.954	1.013	1.081	1.217	1.217	1.235	1.158	1.109	0.994	0.934	0.882	0.829	0.779	0.739	0.707	0.663	0.650	0.638		
680	0.520	G4	5.37	0.051	0.555	0.581	0.607	0.642	0.674	0.718	0.816	0.815	0.892	0.943	1.006	1.123	1.12	1.157	1.148	1.086	1.043	0.937	0.881	0.828	0.771	0.727	0.688	0.652	0.605	0.578	0.569	

TABLE IX.—FRÖSSLING NUMBER FOR 3:1 MODEL.

Rd ^g no.	Re _d	Grid	Tu.	Λ_x/d	Gauge Frössling number																										
					2	3	4	5	6	7	8	9	10	11	12	13	14	15	16	17	18	19	20	21	22	23	24	25	26	27	28
16	0.777	G0	0.30	2.308	0.412	0.409	0.444	0.468	0.463	0.513	0.546	0.571	0.597	0.643	0.672	0.740	0.746	0.749	0.756	0.711	0.680	0.646	0.606	0.587	0.538	0.528	0.494	0.469	0.453	0.412	0.425
17	1.083	G0	0.30	2.308	0.408	0.412	0.436	0.467	0.512	0.547	0.568	0.602	0.640	0.676	0.738	0.747	0.749	0.752	0.713	0.685	0.645	0.604	0.585	0.541	0.526	0.496	0.468	0.452	0.414	0.422	
18	1.516	G0	0.30	2.308	0.409	0.418	0.442	0.473	0.516	0.547	0.569	0.614	0.644	0.691	0.743	0.764	0.770	0.756	0.728	0.689	0.655	0.622	0.591	0.550	0.532	0.500	0.475	0.456	0.421	0.422	
19	1.513	G0	0.30	2.308	0.408	0.422	0.445	0.475	0.523	0.561	0.570	0.618	0.649	0.691	0.743	0.767	0.769	0.758	0.731	0.692	0.654	0.620	0.588	0.550	0.533	0.502	0.477	0.459	0.421	0.424	
20	1.888	G0	0.30	2.308	0.409	0.417	0.449	0.476	0.525	0.567	0.571	0.620	0.653	0.698	0.746	0.771	0.772	0.759	0.731	0.698	0.660	0.624	0.592	0.553	0.535	0.504	0.479	0.460	0.423	0.425	
21	1.888	G0	0.30	2.308	0.412	0.422	0.449	0.475	0.523	0.567	0.569	0.622	0.654	0.698	0.748	0.774	0.777	0.757	0.739	0.700	0.661	0.625	0.594	0.555	0.537	0.505	0.480	0.461	0.425	0.427	
22	2.327	G0	0.30	2.308	0.408	0.413	0.440	0.471	0.513	0.558	0.569	0.612	0.647	0.691	0.738	0.761	0.764	0.752	0.726	0.685	0.651	0.615	0.584	0.550	0.525	0.499	0.475	0.449	0.421	0.418	
23	2.332	G0	0.30	2.308	0.409	0.414	0.440	0.470	0.478	0.512	0.561	0.567	0.614	0.643	0.688	0.737	0.763	0.759	0.756	0.724	0.687	0.648	0.614	0.586	0.548	0.525	0.499	0.474	0.451	0.420	0.418
24	2.501	G0	0.30	2.308	0.413	0.399	0.442	0.471	0.465	0.512	0.543	0.564	0.598	0.632	0.668	0.738	0.732	0.758	0.733	0.720	0.665	0.646	0.601	0.591	0.534	0.521	0.495	0.474	0.451	0.417	
25	2.502	G0	0.30	2.308	0.414	0.402	0.444	0.468	0.465	0.513	0.546	0.566	0.601	0.635	0.674	0.745	0.738	0.757	0.734	0.724	0.668	0.648	0.605	0.591	0.537	0.511	0.499	0.477	0.452	0.419	
26	1.055	G0	0.30	2.308	0.423	0.417	0.452	0.480	0.480	0.524	0.562	0.580	0.620	0.648	0.704	0.749	0.768	0.780	0.764	0.739	0.695	0.663	0.623	0.602	0.555	0.532	0.512	0.484	0.460	0.430	
27	1.059	G0	0.30	2.308	0.415	0.417	0.448	0.474	0.475	0.520	0.559	0.573	0.613	0.641	0.694	0.745	0.759	0.767	0.765	0.732	0.686	0.658	0.617	0.594	0.550	0.531	0.508	0.475	0.455	0.425	0.424
28	1.521	G0	0.30	2.308	0.418	0.423	0.451	0.479	0.481	0.524	0.562	0.580	0.620	0.653	0.702	0.753	0.769	0.774	0.772	0.739	0.696	0.662	0.623	0.600	0.556	0.538	0.509	0.479	0.460	0.429	0.424
29	1.522	G0	0.30	2.308	0.418	0.414	0.402	0.444	0.468	0.465	0.513	0.546	0.566	0.601	0.635	0.674	0.745	0.769	0.776	0.762	0.745	0.694	0.663	0.622	0.599	0.561	0.544	0.506	0.478	0.458	0.423
30	1.866	G0	0.30	2.308	0.421	0.417	0.454	0.475	0.485	0.524	0.564	0.586	0.619	0.658	0.704	0.750	0.773	0.778	0.766	0.743	0.701	0.664	0.628	0.599	0.558	0.539	0.507	0.485	0.459	0.428	0.426
31	1.865	G0	0.30	2.308	0.423	0.422	0.457	0.479	0.491	0.528	0.572	0.587	0.625	0.663	0.709	0.755	0.780	0.784	0.771	0.747	0.703	0.670	0.630	0.604	0.563	0.542	0.511	0.489	0.465	0.435	0.430
32	2.317	G0	0.30	2.308	0.415	0.421	0.449	0.474	0.483	0.522	0.561	0.585	0.619	0.654	0.703	0.747	0.772	0.774	0.765	0.737	0.697	0.662	0.623	0.600	0.556	0.538	0.509	0.479	0.459	0.424	0.426
33	2.319	G0	0.30	2.308	0.415	0.419	0.449	0.475	0.488	0.524	0.560	0.580	0.612	0.657	0.705	0.750	0.772	0.773	0.766	0.740	0.700	0.663	0.625	0.598	0.557	0.538	0.503	0.480	0.460	0.426	0.427
34	2.319	G0	0.30	2.308	0.414	0.419	0.450	0.481	0.488	0.525	0.563	0.585	0.625	0.655	0.706	0.756	0.773	0.773	0.755	0.736	0.704	0.664	0.626	0.599	0.560	0.539	0.508	0.480	0.460	0.424	0.426
114	1.687	G0	0.30	2.308	0.426	0.400	0.467	0.461	0.479	0.517	0.543	0.581	0.616	0.629	0.703	0.723	0.760	0.768	0.751	0.727	0.684	0.658	0.603	0.566	0.522	0.501	0.478	0.453	0.423	0.430	
115	1.690	G0	0.30	2.308	0.419	0.385	0.457	0.450	0.471	0.504	0.533	0.574	0.607	0.641	0.683	0.721	0.754	0.764	0.746	0.747	0.714	0.679	0.645	0.599	0.551	0.545	0.512	0.480	0.459	0.424	0.426
116	1.094	G0	0.30	2.308	0.410	0.394	0.450	0.439	0.460	0.488	0.509	0.540	0.567	0.612	0.628	0.683	0.721	0.751	0.749	0.755	0.726	0.684	0.641	0.607	0.585	0.545	0.514	0.476	0.435	0.422	0.417
117	1.473	G0	0.30	2.308	0.408	0.397	0.447	0.457	0.467	0.511	0.533	0.564	0.609	0.584	0.678	0.723	0.751	0.740	0.755	0.723	0.681	0.644	0.603	0.585	0.546	0.513	0.495	0.467	0.445	0.411	
118	1.866	G0	0.30	2.308	0.407	0.400	0.444	0.448	0.486	0.508	0.532	0.563	0.606	0.638	0.677	0.718	0.748	0.743	0.751	0.725	0.675	0.641	0.601	0.580	0.545	0.513	0.493	0.467	0.442	0.411	
119	2.291	G0	0.30	2.308	0.403	0.398	0.439	0.439	0.464	0.500	0.533	0.562	0.599	0.630	0.666	0.723	0.734	0.730	0.723	0.688	0.658	0.623	0.596	0.557	0.530	0.506	0.489	0.463	0.440	0.411	0.407
122	2.258	G0	0.30	2.308	0.395	0.396	0.436	0.454	0.466	0.502	0.530	0.559	0.605	0.633	0.665	0.719	0.741	0.742	0.737	0.735	0.707	0.669	0.636	0.596	0.573	0.539	0.509	0.487	0.462	0.441	0.411
123	1.391	G0	0.30	2.308	0.407	0.414	0.447	0.469	0.479	0.511	0.546	0.574	0.618	0.641	0.685	0.737	0.754	0.757	0.755	0.728	0.688	0.654	0.606	0.594	0.569	0.539	0.503	0.475	0.446	0.421	0.422
124	1.507	G0	0.30	2.308	0.423	0.418	0.448	0.477	0.510	0.551	0.571	0.616	0.643	0.680	0.739	0.764	0.779	0.759	0.728	0.683	0.656	0.613	0.590	0.558	0.525	0.501	0.478	0.452	0.420	0.428	
229	0.530	G0	0.30	2.308	0.428	0.424	0.466	0.483	0.494	0.526	0.570	0.590	0.637	0.667	0.712	0.760	0.774	0.794	0.777	0.752	0.710	0.685	0.631	0.617	0.573	0.541	0.519	0.496	0.465	0.439	0.438
230	0.985	G0	0.30	2.308	0.426	0.424	0.467	0.488	0.499	0.536	0.574	0.595	0.639	0.674	0.719	0.760	0.785	0.789	0.778	0.757	0.717	0.689	0.651	0.628	0.597	0.562	0.546	0.520	0.585	0.441	0.434
231	1.577	G0	0.30	2.308	0.424	0.427	0.466	0.486	0.501	0.535	0.571	0.589	0.639	0.675	0.721	0.762	0.784	0.784	0.757	0.713	0.685	0.657	0.621	0.597	0.567	0.536	0.503	0.475	0.443	0.435	
232	2.251	G0	0.30	2.308	0.413	0.415	0.452	0.468	0.488	0.524	0.554	0.581	0.623	0.658	0.701	0.747	0.775	0.773	0.764	0.734	0.703	0.667	0.633	0.601	0.577	0.549	0.529	0.506	0.479	0.451	0.423
125	2.223	G1	8.02	0.296	0.716	0.643	0.690	0.883	0.733	0.755	0.764	0.747	0.749	0.752	0.713	0.749	0.751	0.752	0.750	0.728	0.688	0.651	0.621	0.597	0.573	0.541	0.519	0.496	0.465	0.439	
126	1.383	G1	7.94																												

TABLE IX.—CONTINUED.

Rdg no.	Re _d	Grid	D _h , %	A _{x/d}	Gauge Frössling number																											
					2	3	4	5	6	7	8	9	10	11	12	13	14	15	16	17	18	19	20	21	22	23	24	25	26	27	28	
136	1.395	G2	7.43	0.177	0.692	0.592	0.620	0.652	0.701	0.737	0.774	0.829	0.865	0.936	1.022	1.070	1.106	1.100	1.050	0.984	0.928	0.872	0.825	0.777	0.736	0.710	0.675	0.644	0.607	0.614		
137	0.504	G2	7.05	0.177	0.639	0.532	0.589	0.613	0.605	0.664	0.705	0.739	0.788	0.820	0.885	0.951	0.984	0.996	0.961	0.924	0.869	0.823	0.773	0.737	0.699	0.666	0.625	0.601	0.561	0.539		
138	2.253	G2	4.87	0.231	0.612	0.605	0.630	0.654	0.661	0.710	0.745	0.782	0.843	0.844	0.946	1.021	1.072	1.089	1.079	1.029	0.940	0.908	0.851	0.807	0.766	0.725	0.692	0.663	0.640	0.612	0.612	
139	1.384	G2	4.98	0.231	0.537	0.539	0.579	0.608	0.612	0.663	0.702	0.742	0.796	0.897	0.969	1.008	1.029	1.011	0.976	0.916	0.873	0.819	0.776	0.734	0.692	0.658	0.629	0.596	0.556	0.520	0.524	
140	0.507	G2	4.68	0.231	0.504	0.515	0.560	0.584	0.577	0.639	0.674	0.711	0.759	0.767	0.847	0.915	0.929	0.942	0.940	0.909	0.860	0.815	0.771	0.736	0.699	0.663	0.627	0.595	0.572	0.523	0.524	
141	0.507	G2	5.49	0.208	0.509	0.520	0.562	0.562	0.593	0.588	0.647	0.689	0.716	0.775	0.788	0.863	0.926	0.944	0.953	0.957	0.925	0.873	0.837	0.786	0.752	0.708	0.674	0.637	0.607	0.583	0.546	0.539
142	1.395	G2	5.82	0.208	0.559	0.567	0.608	0.631	0.638	0.686	0.729	0.763	0.827	0.859	0.933	1.003	1.048	1.049	1.058	1.058	1.014	0.960	0.907	0.850	0.805	0.764	0.719	0.683	0.655	0.628	0.587	0.587
143	2.247	G2	5.71	0.208	0.658	0.650	0.668	0.680	0.688	0.731	0.768	0.801	0.852	0.895	0.959	1.046	1.095	1.128	1.120	1.042	0.993	0.940	0.877	0.835	0.792	0.753	0.726	0.694	0.677	0.648	0.662	
144	2.249	G2	8.62	0.160	0.777	0.747	0.755	0.759	0.751	0.792	0.820	0.847	0.897	0.938	1.010	1.106	1.174	1.236	1.243	1.175	1.091	1.027	0.959	0.916	0.866	0.831	0.802	0.779	0.764	0.746	0.771	
145	1.393	G2	8.88	0.160	0.643	0.648	0.668	0.696	0.740	0.779	0.817	0.864	0.901	0.981	1.073	1.126	1.174	1.182	1.127	1.054	0.991	0.920	0.881	0.830	0.786	0.752	0.723	0.694	0.659	0.645		
146	0.506	G2	8.27	0.180	0.555	0.555	0.598	0.626	0.619	0.684	0.718	0.757	0.805	0.836	0.909	0.987	1.016	1.042	1.045	1.010	0.956	0.916	0.853	0.817	0.769	0.728	0.688	0.658	0.622	0.572	0.587	
148	2.248	G3	4.87	0.110	0.635	0.627	0.650	0.670	0.673	0.720	0.756	0.794	0.848	0.896	0.962	1.047	1.093	1.132	1.104	1.038	0.969	0.915	0.849	0.810	0.767	0.728	0.701	0.670	0.648	0.623	0.631	
149	1.395	G3	4.45	0.110	0.564	0.567	0.604	0.636	0.638	0.691	0.731	0.777	0.826	0.879	0.944	1.021	1.056	1.085	1.060	1.017	0.953	0.903	0.830	0.801	0.744	0.711	0.678	0.649	0.604	0.583	0.572	
150	0.619	G3	4.16	0.110	0.518	0.521	0.581	0.591	0.601	0.651	0.695	0.740	0.779	0.819	0.877	0.950	0.965	0.970	0.967	0.924	0.876	0.834	0.775	0.749	0.703	0.667	0.644	0.607	0.573	0.536	0.531	
151	0.610	G3	2.68	0.143	0.494	0.496	0.540	0.553	0.567	0.616	0.661	0.695	0.739	0.769	0.825	0.894	0.899	0.915	0.906	0.875	0.827	0.788	0.739	0.717	0.667	0.634	0.612	0.583	0.512	0.503		
152	1.396	G3	2.88	0.143	0.524	0.538	0.576	0.605	0.612	0.668	0.708	0.745	0.795	0.840	0.903	0.971	1.009	1.019	1.002	0.950	0.909	0.855	0.805	0.759	0.729	0.679	0.648	0.623	0.588	0.552	0.540	
153	2.248	G3	3.26	0.143	0.556	0.557	0.593	0.624	0.626	0.685	0.721	0.752	0.810	0.856	0.921	0.994	1.035	1.047	1.037	0.988	0.928	0.880	0.821	0.778	0.736	0.694	0.653	0.634	0.600	0.570	0.548	
154	2.247	G3	2.88	0.162	0.562	0.561	0.586	0.610	0.622	0.673	0.711	0.749	0.804	0.849	0.909	0.976	1.011	1.034	1.013	0.972	0.912	0.865	0.811	0.767	0.724	0.684	0.650	0.625	0.588	0.561		
155	1.394	G3	2.34	0.162	0.514	0.519	0.563	0.591	0.602	0.652	0.694	0.735	0.784	0.824	0.879	0.954	0.971	0.995	0.975	0.942	0.888	0.845	0.788	0.753	0.712	0.665	0.640	0.605	0.570	0.533		
156	0.503	G3	2.17	0.162	0.479	0.483	0.520	0.556	0.546	0.597	0.646	0.667	0.710	0.750	0.795	0.875	0.917	0.959	0.979	0.957	0.904	0.857	0.816	0.770	0.729	0.689	0.657	0.629	0.498	0.504		
157	0.502	G3	6.78	0.082	0.554	0.561	0.606	0.633	0.632	0.681	0.721	0.752	0.810	0.856	0.921	0.994	1.035	1.047	1.037	0.988	0.928	0.880	0.821	0.778	0.736	0.694	0.653	0.634	0.601	0.561	0.562	
158	1.388	G3	7.24	0.082	0.638	0.644	0.681	0.704	0.701	0.758	0.789	0.833	0.886	0.937	1.012	1.111	1.193	1.255	1.234	1.150	1.053	0.980	0.901	0.857	0.804	0.767	0.733	0.708	0.676	0.648		
159	2.247	G3	7.65	0.082	0.801	0.748	0.770	0.775	0.758	0.805	0.836	0.870	0.916	0.965	1.036	1.081	1.128	1.156	1.127	1.081	1.027	1.071	1.035	0.935	0.894	0.848	0.810	0.782	0.742	0.707		
161	2.212	G3	7.65	0.082	0.807	0.773	0.772	0.776	0.814	0.849	0.879	0.935	0.996	1.045	1.085	1.134	1.164	1.256	1.316	1.293	1.186	1.129	1.091	0.935	0.907	0.852	0.820	0.792	0.754	0.717		
164	1.375	G3	7.24	0.082	0.653	0.648	0.683	0.700	0.713	0.757	0.803	0.838	0.886	0.940	1.028	1.131	1.216	1.259	1.290	1.146	1.148	1.067	0.967	0.903	0.860	0.807	0.770	0.743	0.709	0.665		
185	0.368	G3	6.78	0.082	0.556	0.558	0.616	0.626	0.642	0.642	0.703	0.744	0.779	0.822	0.891	0.937	1.025	1.061	1.083	1.057	1.025	0.944	0.893	0.837	0.796	0.751	0.705	0.686	0.639	0.607	0.569	
207	2.216	G3	7.65	0.082	0.795	0.757	0.759	0.760	0.752	0.794	0.832	0.850	0.913	0.948	1.042	1.136	1.227	1.286	1.261	1.149	1.149	1.095	0.996	0.922	0.882	0.804	0.765	0.729	0.700	0.678		
208	1.359	G3	7.24	0.082	0.661	0.644	0.661	0.711	0.694	0.750	0.808	0.842	0.900	0.954	1.031	1.130	1.209	1.258	1.236	1.153	1.059	0.983	0.903	0.859	0.825	0.782	0.747	0.714	0.677	0.657		
209	0.499	G3	6.78	0.082	0.573	0.624	0.645	0.668	0.717	0.765	0.794	0.854	0.897	0.971	1.061	1.102	1.135	1.120	1.045	1.005	0.934	0.842	0.826	0.782	0.750	0.729	0.700	0.662	0.629	0.591		
214	0.517	G3	6.78	0.082	0.588	0.577	0.632	0.657	0.687	0.721	0.760	0.804	0.854	0.914	0.979	1.045	1.124	1.151	1.140	1.086	1.017	0.944	0.871	0.831	0.775	0.735	0.701	0.665	0.637	0.598		
215	0.689	G3	6.78	0.082	0.602	0.597	0.643	0.660	0.687	0.731	0.774	0.826	0.874	0.924	0.998	1.048	1.147	1.179	1.173	1.118	1.030	0.963	0.886	0.855	0.792	0.751	0.715	0.682	0.644	0.613	0.507	
216	0.992	G3	7.24	0.082	0.633	0.619	0.673	0.691	0.709	0.755	0.801	0.839	0.894	0.950	1.027	1.115	1.190	1.237	1.230	1.162	1.069	1.000	0.914	0.876	0.815	0.770	0.736	0.706	0.671	0.638		
217	1.374	G3	7.24	0.082	0.670	0.655	0.697	0.715	0.728	0.771	0.813	0.859	0.912	0.970	1.043	1.150	1.243	1.294	1.276	1.193	1.093	1.024	0.924	0.886	0.836	0.789	0.759	0.730	0.697	0.671	0.633</td	

TABLE IX.—CONTINUED.

Rdg no.	Grid	Re _d	Tu %	Λ_x/d	Gauge																											
					2	3	4	5	6	7	8	9	10	11	12	13	14	15	16	17	18	19	20	21	22	23	24	25	26	27	28	
Frouding number																																
161	1.375	G4	4.19	0.066	0.551	0.555	0.607	0.630	0.638	0.693	0.739	0.774	0.837	0.892	0.952	1.040	1.076	1.095	1.081	1.037	0.970	0.909	0.844	0.798	0.750	0.706	0.671	0.638	0.604	0.565	0.561	
162	0.512	G4	3.77	0.066	0.515	0.513	0.565	0.586	0.586	0.653	0.700	0.726	0.784	0.835	0.897	0.962	1.016	1.029	1.030	0.978	0.917	0.867	0.788	0.758	0.708	0.667	0.630	0.618	0.557	0.531	0.529	
164	0.505	G4	5.37	0.061	0.558	0.563	0.613	0.637	0.638	0.706	0.736	0.771	0.822	0.861	0.928	1.016	1.073	1.155	1.202	1.168	1.086	1.003	0.910	0.856	0.781	0.731	0.696	0.652	0.608	0.567	0.557	
165	1.393	G4	6.01	0.051	0.635	0.628	0.664	0.694	0.698	0.753	0.786	0.822	0.882	0.922	1.007	1.099	1.184	1.254	1.277	1.210	1.124	1.044	0.948	0.894	0.823	0.782	0.739	0.699	0.656	0.642	0.529	
166	2.246	G4	6.01	0.051	0.757	0.717	0.733	0.736	0.740	0.783	0.812	0.856	0.941	1.025	1.120	1.218	1.317	1.337	1.255	1.159	1.069	0.977	0.916	0.859	0.813	0.783	0.746	0.724	0.721	0.71	0.756	
167	2.245	G4	2.49	0.099	0.533	0.534	0.572	0.599	0.617	0.668	0.705	0.745	0.801	0.808	0.913	0.987	1.021	1.035	1.031	0.982	0.926	0.875	0.812	0.774	0.721	0.682	0.652	0.613	0.581	0.564	0.541	
168	1.375	G4	2.40	0.099	0.507	0.514	0.557	0.584	0.594	0.651	0.692	0.727	0.781	0.820	0.895	0.959	0.992	1.010	0.989	0.951	0.890	0.852	0.787	0.754	0.698	0.660	0.635	0.591	0.559	0.518		
169	0.503	G4	2.19	0.099	0.493	0.490	0.540	0.565	0.581	0.624	0.680	0.686	0.741	0.780	0.840	0.915	0.930	0.940	0.933	0.889	0.820	0.792	0.743	0.707	0.662	0.628	0.597	0.566	0.541	0.504		
170	0.508	G4	1.63	0.123	0.484	0.484	0.529	0.557	0.552	0.616	0.651	0.680	0.738	0.774	0.835	0.907	0.923	0.920	0.872	0.810	0.785	0.744	0.686	0.644	0.604	0.574	0.529	0.504	0.491			
171	1.392	G4	1.77	0.123	0.496	0.506	0.544	0.579	0.583	0.640	0.677	0.716	0.772	0.815	0.861	0.946	0.972	0.979	0.967	0.918	0.860	0.825	0.775	0.719	0.644	0.618	0.576	0.548	0.509			
172	2.242	G4	1.86	0.123	0.513	0.521	0.555	0.582	0.599	0.659	0.734	0.788	0.842	0.909	0.978	1.017	1.021	1.003	0.951	0.886	0.840	0.780	0.734	0.694	0.653	0.623	0.591	0.540	0.520			
186	0.379	G4	5.37	0.051	0.544	0.532	0.601	0.620	0.628	0.678	0.716	0.755	0.792	0.852	0.904	0.968	1.056	1.122	1.162	1.149	1.079	0.977	0.867	0.828	0.767	0.713	0.673	0.626	0.594	0.551	0.545	
187	1.379	G4	6.01	0.051	0.623	0.611	0.663	0.679	0.687	0.737	0.782	0.814	0.867	0.926	0.964	1.091	1.184	1.271	1.278	1.220	1.136	1.042	0.881	0.822	0.759	0.731	0.690	0.658	0.627	0.525		
188	1.371	G4	6.01	0.051	0.619	0.612	0.654	0.673	0.685	0.735	0.775	0.812	0.860	0.919	0.990	1.085	1.176	1.246	1.266	1.211	1.116	1.031	0.939	0.876	0.816	0.764	0.729	0.687	0.654	0.621	0.518	
189	1.372	G4	6.01	0.051	0.618	0.615	0.654	0.677	0.681	0.734	0.778	0.813	0.860	0.917	0.969	1.084	1.175	1.257	1.265	1.207	1.122	1.027	0.939	0.879	0.814	0.764	0.725	0.687	0.655	0.624	0.521	
190	0.499	G4	5.37	0.051	0.544	0.532	0.601	0.620	0.628	0.678	0.716	0.755	0.792	0.852	0.904	0.968	1.056	1.158	1.189	1.163	1.079	0.950	0.896	0.833	0.768	0.718	0.679	0.634	0.597	0.560	0.548	
191	0.503	G4	2.19	0.099	0.504	0.500	0.555	0.587	0.576	0.644	0.684	0.716	0.768	0.836	0.869	0.971	1.008	1.015	0.977	0.940	0.873	0.817	0.756	0.730	0.683	0.644	0.615	0.587	0.554	0.522	0.515	
192	1.374	G4	2.40	0.099	0.528	0.532	0.576	0.600	0.618	0.669	0.716	0.753	0.812	0.860	0.926	1.016	1.045	1.065	1.045	1.002	0.939	0.874	0.815	0.777	0.722	0.684	0.646	0.614	0.583	0.542		
193	2.210	G4	2.49	0.099	0.549	0.549	0.583	0.622	0.636	0.685	0.733	0.774	0.826	0.906	0.971	1.058	1.107	1.126	1.100	1.034	0.970	0.894	0.832	0.785	0.736	0.694	0.661	0.627	0.599	0.576	0.545	
195	2.209	G4	6.01	0.051	0.723	0.700	0.718	0.734	0.742	0.787	0.823	0.872	0.921	0.979	1.059	1.162	1.253	1.318	1.265	1.161	1.066	0.997	0.932	0.883	0.838	0.793	0.766	0.738	0.717	0.695	0.675	
196	1.381	G4	6.01	0.051	0.619	0.618	0.660	0.689	0.700	0.749	0.804	0.841	0.878	0.914	0.964	1.029	1.121	1.181	1.208	1.180	1.103	1.038	0.978	0.915	0.849	0.819	0.750	0.711	0.667	0.638	0.628	
197	0.497	G4	5.37	0.051	0.568	0.571	0.614	0.648	0.653	0.719	0.765	0.811	0.864	0.920	0.976	1.063	1.097	1.109	1.093	1.047	1.003	0.935	0.875	0.830	0.781	0.731	0.699	0.658	0.621	0.578	0.542	
198	0.501	G4	5.37	0.051	0.568	0.562	0.610	0.649	0.650	0.721	0.766	0.802	0.859	0.917	0.976	1.057	1.090	1.115	1.101	1.040	1.013	0.945	0.880	0.837	0.784	0.734	0.699	0.660	0.629	0.578	0.542	
199	1.377	G4	6.01	0.051	0.626	0.622	0.664	0.691	0.707	0.761	0.805	0.841	0.900	0.958	1.032	1.112	1.178	1.205	1.177	1.118	1.048	1.003	0.935	0.891	0.843	0.793	0.758	0.717	0.687	0.653	0.649	
200	2.222	G4	6.01	0.051	0.721	0.691	0.729	0.730	0.772	0.814	0.851	0.902	0.958	1.030	1.111	1.181	1.226	1.264	1.233	1.161	1.127	1.047	0.972	0.908	0.840	0.799	0.757	0.710	0.683	0.651	0.626	0.578
201	2.216	G4	4.24	0.066	0.610	0.599	0.627	0.653	0.664	0.707	0.757	0.789	0.848	0.914	0.983	1.072	1.132	1.161	1.171	1.127	1.047	0.975	0.908	0.846	0.780	0.741	0.702	0.672	0.634	0.574	0.547	
202	1.364	G4	4.18	0.066	0.556	0.558	0.601	0.633	0.648	0.697	0.746	0.784	0.853	0.905	0.982	1.061	1.109	1.129	1.199	1.099	1.036	0.972	0.901	0.836	0.761	0.724	0.687	0.643	0.607	0.574	0.547	
203	0.505	G4	3.77	0.066	0.534	0.541	0.583	0.620	0.623	0.680	0.730	0.752	0.812	0.870	0.922	0.985	0.999	1.017	0.987	0.952	0.917	0.867	0.808	0.786	0.733	0.690	0.655	0.621	0.581	0.551		
204	0.507	G4	2.51	0.089	0.504	0.504	0.548	0.574	0.578	0.638	0.680	0.704	0.750	0.801	0.849	0.909	0.937	0.970	0.928	0.894	0.832	0.760	0.739	0.690	0.649	0.619	0.582	0.550	0.520			
205	1.374	G4	2.76	0.089	0.528	0.535	0.573	0.603	0.611	0.668	0.717	0.750	0.814	0.857	0.924	0.991	1.024	1.036	1.008	0.960	0.909	0.856	0.834	0.791	0.751	0.715	0.683	0.651	0.626	0.602		
206	2.216	G4	2.85	0.089	0.543	0.544	0.580	0.606	0.613	0.670	0.718	0.759	0.813	0.864	0.934	1.001	1.049	1.060	1.034	0.975	0.920	0.863	0.799	0.759	0.719	0.674	0.643	0.610	0.581	0.554		
219	2.225	G4	3.37	0.079	0.598	0.596	0.630	0.657	0.676	0.721	0.767	0.806	0.863	0.926	0.988	1.076	1.123	1.153	1.123	1.058	0.983	0.924	0.860	0.821	0.772	0.731	0.698	0.669	0.634	0.607		
220	1.365	G4	3.30	0.079	0.553	0.565	0.603	0.651</td																								

TABLE IX.—CONCLUDED.

Rdg no.	Re _d	Grid	Tu,	Λ_x/d	Cause Frossling number																											
					2	3	4	5	6	7	8	9	10	11	12	13	14	15	16	17	18	19	20	21	22	23	24	25	26	27	28	
238	0.528	G4	2.51	0.089	0.521	0.523	0.571	0.590	0.602	0.658	0.706	0.725	0.783	0.824	0.873	0.933	0.949	0.964	0.952	0.924	0.884	0.847	0.791	0.770	0.723	0.676	0.648	0.613	0.577	0.552	0.534	
239	0.526	G4	2.21	0.098	0.507	0.508	0.557	0.57	0.582	0.638	0.699	0.758	0.806	0.851	0.916	0.938	0.945	0.933	0.906	0.858	0.812	0.763	0.737	0.701	0.652	0.624	0.595	0.559	0.530	0.516		
240	1.371	G4	2.42	0.098	0.529	0.541	0.577	0.610	0.624	0.67	0.719	0.757	0.804	0.860	0.923	0.997	1.035	1.053	1.038	1.007	0.943	0.892	0.828	0.788	0.742	0.694	0.664	0.626	0.591	0.562	0.550	
241	1.205	G4	2.5	0.098	0.582	0.586	0.591	0.620	0.637	0.683	0.727	0.761	0.817	0.876	0.937	1.013	1.052	1.078	1.067	1.022	0.966	0.904	0.842	0.803	0.750	0.702	0.676	0.634	0.606	0.579	0.567	
173	2.268	G5	1.63	0.069	0.608	0.617	0.646	0.677	0.688	0.748	0.781	0.816	0.875	0.922	0.990	1.065	1.108	1.131	1.112	1.060	1.000	0.952	0.891	0.851	0.802	0.762	0.730	0.689	0.660	0.633	0.618	
174	1.380	G5	1.77	0.078	0.579	0.583	0.627	0.651	0.670	0.730	0.771	0.801	0.866	0.913	0.979	1.047	1.083	1.097	1.097	1.086	1.038	0.980	0.940	0.877	0.840	0.787	0.745	0.714	0.674	0.635	0.618	
175	0.498	G5	2.08	0.103	0.540	0.542	0.591	0.627	0.622	0.693	0.732	0.760	0.827	0.842	0.925	0.988	1.036	1.036	1.029	1.016	0.976	0.921	0.887	0.821	0.800	0.748	0.703	0.685	0.636	0.604	0.570	0.563
176	0.481	G5	3.40	0.099	0.596	0.598	0.652	0.684	0.689	0.762	0.809	0.835	0.914	0.956	1.022	1.102	1.122	1.141	1.133	1.090	1.026	0.978	0.908	0.871	0.814	0.765	0.739	0.689	0.652	0.615	0.602	
177	1.384	G5	2.62	0.065	0.617	0.620	0.670	0.705	0.719	0.782	0.822	0.862	0.927	0.975	1.038	1.123	1.168	1.190	1.182	1.124	1	0.943	0.901	0.835	0.797	0.755	0.717	0.676	0.645	0.630		
178	2.262	G5	2.45	0.063	0.672	0.671	0.705	0.727	0.744	0.803	0.843	0.885	0.945	0.995	1.064	1.148	1.197	1.229	1.210	1.151	1.082	1.028	0.961	0.917	0.863	0.818	0.783	0.743	0.710	0.684	0.678	
179	2.262	G5	1.09	0.077	0.510	0.523	0.556	0.582	0.600	0.650	0.689	0.723	0.770	0.825	0.879	0.945	0.981	0.985	0.977	0.939	0.886	0.844	0.787	0.748	0.702	0.666	0.634	0.596	0.563	0.538	0.526	
180	1.372	G5	1.20	0.092	0.503	0.500	0.548	0.573	0.583	0.641	0.677	0.706	0.760	0.805	0.861	0.930	0.960	0.965	0.962	0.962	0.915	0.872	0.828	0.775	0.738	0.692	0.654	0.628	0.590	0.552	0.515	
181	0.498	G5	1.28	0.108	0.477	0.470	0.523	0.545	0.543	0.631	0.631	0.662	0.711	0.745	0.799	0.862	0.871	0.881	0.839	0.795	0.762	0.717	0.682	0.646	0.602	0.588	0.551	0.528	0.485	0.491		

REPORT DOCUMENTATION PAGE

Form Approved
OMB No. 0704-0188

Public reporting burden for this collection of information is estimated to average 1 hour per response, including the time for reviewing instructions, searching existing data sources, gathering and maintaining the data needed, and completing and reviewing the collection of information. Send comments regarding this burden estimate or any other aspect of this collection of information, including suggestions for reducing this burden, to Washington Headquarters Services, Directorate for Information Operations and Reports, 1215 Jefferson Davis Highway, Suite 1204, Arlington, VA 22202-4302, and to the Office of Management and Budget, Paperwork Reduction Project (0704-0188), Washington, DC 20503.

1. AGENCY USE ONLY (Leave blank)			2. REPORT DATE December 1994		3. REPORT TYPE AND DATES COVERED Technical Paper		
4. TITLE AND SUBTITLE Influence of Turbulence Parameters, Reynolds Number, and Body Shape on Stagnation-Region Heat Transfer			5. FUNDING NUMBERS WU-505-62-52				
6. AUTHOR(S) G. James Van Fossen, Robert J. Simoneau, and Chan Y. Ching			8. PERFORMING ORGANIZATION REPORT NUMBER E-8882				
7. PERFORMING ORGANIZATION NAME(S) AND ADDRESS(ES) National Aeronautics and Space Administration Lewis Research Center Cleveland, Ohio 44135-3191			10. SPONSORING/MONITORING AGENCY REPORT NUMBER NASA TP-3487				
9. SPONSORING/MONITORING AGENCY NAME(S) AND ADDRESS(ES) National Aeronautics and Space Administration Washington, D.C. 20546-0001							
11. SUPPLEMENTARY NOTES G. James Van Fossen and Robert J. Simoneau, NASA Lewis Research Center; Chan Y. Ching, Syracuse University, Syracuse, New York 13244 (work funded by NASA Grant NAG3-621). Responsible person, G. James Van Fossen, organization code 2630, (216) 433-5892.							
12a. DISTRIBUTION/AVAILABILITY STATEMENT Unclassified - Unlimited Subject Category 34				12b. DISTRIBUTION CODE			
13. ABSTRACT (Maximum 200 words) The purpose of the present work was threefold: (1) to determine if a free-stream turbulence length scale existed that would cause the greatest augmentation in stagnation-region heat transfer over laminar levels; (2) to investigate the effect of velocity gradient on stagnation-region heat transfer augmentation by free-stream turbulence; and (3) to develop a prediction tool for stagnation heat transfer in the presence of free-stream turbulence. Heat transfer was measured in the stagnation region of four models with elliptical leading edges that had ratios of major to minor axes of 1:1, 1.5:1, 2.25:1, and 3:1. Five turbulence-generating grids were fabricated; four were square mesh, biplane grids made from square bars. The fifth grid was an array of fine parallel wires that were perpendicular to the model spanwise direction. Heat transfer data were taken at Reynolds numbers ranging from 37 000 to 228 000. Turbulence intensities were in the range of 1.1 to 15.9 percent while the ratio of integral length scale to leading-edge diameter ranged from 0.05 to 0.30. Stagnation-point velocity gradient was varied by nearly 50 percent. Stagnation-region heat transfer augmentation was found to increase with decreasing length scale but no optimum length scale was found. Heat transfer augmentation due to turbulence was found to be unaffected by the velocity gradient near the leading edge. A correlation was developed that fit heat transfer data for the square-bar grids to within ± 4 percent.							
14. SUBJECT TERMS Heat transfer; Turbulence; Stagnation flow					15. NUMBER OF PAGES 48		
					16. PRICE CODE A03		
17. SECURITY CLASSIFICATION OF REPORT Unclassified		18. SECURITY CLASSIFICATION OF THIS PAGE Unclassified		19. SECURITY CLASSIFICATION OF ABSTRACT Unclassified		20. LIMITATION OF ABSTRACT	

